RUPRECHT-KARLS-UNIVERSITÄT HEIDELBERG

Karsten Hoechstetter

Magnetic source imaging of tactile evoked activity in the human secondary somatosensory cortex

Dissertation

HD-KIP-01-13

KIRCHHOFF-INSTITUT FÜR PHYSIK

INAUGURAL–DISSERTATION
zur
Erlangung der Doktorwürde
der
Naturwissenschaftlich-Mathematischen
Gesamtfakultät
der
Ruprecht-Karls-Universität
Heidelberg

vorgelegt von
Dipl.-Phys. Karsten Hoechstetter
aus Münchberg
Tag der mündlichen Prüfung: 4. Juli 2001

Magnetische Quellenanalyse taktil evozierter Aktivität im sekundären somatosensorischen Kortex des Menschen

Gutachter: Prof. Dr. Karlheinz Meier
Prof. Dr. Michael Scherg

Dissertation
submitted to the
Combined Faculties for the Natural Sciences and for Mathematics
of the Rupertus Carola University of
Heidelberg, Germany
for the degree of
Doctor of Natural Sciences

Magnetic source imaging of tactile evoked activity in the human secondary somatosensory cortex

presented by
Diplom-Physicist Karsten Hoechstetter
born in Münchberg

Heidelberg, July 4th, 2001

Referees: Prof. Dr. Karlheinz Meier
Prof. Dr. Michael Scherg

Magnetische Quellenanalyse taktil evozierter Aktivität im sekundären somatosensorischen Kortex des Menschen. In der vorliegenden Arbeit wurde die Antwort des menschlichen Gehirns auf taktile Fingerstimulation mittels Magnetoenzephalographie (MEG) untersucht. Zur Darstellung des zeitlichen Aktivitätsverlaufs im primären (SI) und sekundären (SII) somatosensorischen Kortex wurde räumlich-zeitliche Quellenmodellierung angewandt. Hauptuntersuchungsobjekt war SII. Zur Auswertung von Daten verschiedener Versuchspersonen wurde eine Kombination aus sequentiellem Dipol-Fit und dem Setzen von Quellen aus standardisierten Kernspinbildern entwickelt und in drei Studien angewandt. Zunächst wurden simultane Ableitungen von Elektroenzephalogramm (EEG) und MEG durchgeführt. Sie offenbarten die Existenz zweier Aktivitätsgeneratoren im SII-Areal. Aufgrund der geringeren Durchsetzung mit Hintergrundaktivität erwies sich das MEG im Vergleich zum EEG als das geeignetere Mittel zur Abbildung von SII-Aktivität. In einer zweiten Studie wurde gezeigt, dass Lenkung der Aufmerksamkeit auf den Reizort bzw. die Reizintensität die SII-Aktivität bei einer Latenz von etwa 80 ms um 52 % bzw. 64 % erhöht. Dieser Effekt wurde zum Teil durch eine Verlangsamung der Amplitudenabnahme mit zunehmender Stimulationsdauer hervorgerufen. Eine dritte Studie zur Verarbeitung simultaner Stimulation zweier Finger ergab signifikante suppressive Interaktion der Reize in SII sowohl bei Stimulation von Fingern einer Hand als auch bei Reizung beider Hände. Während bilateraler Stimulation schienen sich beide Hemisphären auf die Verarbeitung des contralateralen Reizes zu spezialisieren und den ipsilateralen Stimulus zu unterdrücken.

Magnetic source imaging of tactile evoked activity in the human secondary somatosensory cortex. In this work the response of the human brain to tactile finger stimulation was studied by means of magnetoencephalography (MEG). Spatio-temporal source imaging was applied to map the temporal evolution of activity in the primary (SI) and secondary (SII) somatosensory cortex with focus directed to SII. A method combining sequential dipole fitting and source seeding from standardized magnetic resonance images was developed for the analysis of data obtained from several subjects and applied in three different studies. First, a combined measurement of electroencephalogram (EEG) and MEG revealed two distinct generators of activity in the vicinity of SII. MEG was less contaminated with background brain activity and, therefore, proved more appropriate to image SII activity than EEG. In the second study, attention to stimulus location and intensity was shown to enhance SII activity around 80 ms by 52 % and 64 %, respectively. This effect was partly due to decelerated response decrement with persisting stimulation. The third study on simultanous stimulation of two fingers revealed significant suppressive interaction in SII of stimuli presented to one or two hands. During bilateral stimulation, both hemispheres appeared to specialize in the processing of the contralateral input and to suppress ipsilateral input.

Meinen Eltern

Contents

List of Figures

List of Tables

Introduction

Magnetoencephalography (MEG) provides a powerful tool for the study of activity in the human brain. It relies on the measurement of magnetic fields outside the head generated by neuroelectric currents inside the brain. Effective application of this idea was possible only after the invention of superconducting quantum interference devices (SQUIDS) in the late 1960s [154] that allow high-precision measurements of small magnetic fields. During the last decades, device design quickly developed from the first single-SQUID measurements in 1972 [26] to modern whole-head magnetometers with up to 306 detection channels [97].

Given the distribution of neuronal currents inside the brain, standard electrodynamics can be applied to calculate the extracranial magnetic fields generated by them. In the analysis of MEG data one must proceed in the opposite direction and estimate the current distribution from the measured magnetic fields. In order to obtain solutions for this 'inverse problem', physical models need to be applied. A common approach in MEG is to model the head as a conducting sphere and represent active brain regions by equivalent current dipoles. Fitting algorithms can then optimize location and orientation of these current sources inside the brain. Accordingly, the time course of neuronal activity that best explains the measured data is mapped by time-varying dipole moments.

Aside from its non-invasiveness and the fairly good spatial resolution, the major advantage of MEG over other functional imaging methods is its high temporal resolution on the order of milliseconds. By detecting the magnetic responses following the application of external stimuli, information about spatial and temporal details of the processing of sensory input can be obtained. The feasibility of MEG to monitor the auditory [79], visual [53] and somatosensory system [54] has been demonstrated. In this work tactile pressure pulses were delivered to the fingers and the magnetic field in response to this stimulus was detected. The focus of interest in this thesis was the secondary somatosensory cortex (SII), one of the brain regions that are activated by such somatosensory stimuli.

The first cortical stage of somatosensory processing is the primary somatosensory cortex, SI. This area in the postcentral gyrus is activated by tactile pressure stimuli as well as

vibration or electric pulses. SI has been extensively studied in humans by intracranial [4, 118] and extracranial imaging methods [12, 77, 140]. The existence of a second brain area processing somatosensory stimuli in humans was first documented by Penfield and Rasmussen in 1950 [119]. This region in the upper bank of the Sylvian Fissure was termed the secondary somatosensory cortex SII. In the following decades its role was shown to reach beyond the mere detection of incoming stimuli. Rather, SII appears to represent the first associative stage of somatosensory processing. As opposed to SI, many neurons in SII have bilateral receptive fields [93], thus combining information of both sides of the body. Accordingly, SII has been assigned an active role in the integration of the two body halves and in the maintenance of the body scheme [35, 59]. The importance of SII is also evident from its participation in pain perception [61], sensorimotor integration [38] and tactile learning [43].

Due to its essential role in these complex and associative skills, detailed imaging of activity in SII promises insight into general mechanisms of human cortical processing. From a medical point of view, the involvement of SII in complex somatosensory processing merits detailed investigation. Comparison of SII activation in healthy subjects and patients revealed altered SII responses as a correlate of phantom limb sensations [59] or impaired tactile skills. The involvement of SII in pain perception demands further research on that area in search of correlates of perturbed pain perception in acute and chronic pain patients.

The recognition of the need to image the function of SII was followed by studies applying modern different imaging techniques. Positron emission tomography (PET) [22] and functional magnetic resonance images (fMRI) [34] provide good spatial accuracy in locating SII and quantitative measures for the averaged activity over time. These methods rely on changes in the regional cerebral blood flow that evolve as a physiological consequence of the enhanced neuronal activity with time constants $> 100\,\mathrm{ms}$. Therefore the temporal resolution of these methods is rather poor. Noninvasive analysis of the time course of SII activity is possible only by methods that measure neuronal electrical activity directly, for example by electroencephalography (EEG) [5] or MEG. Measurement of evoked fields from SII was first demonstrated by Hari *et al.* in 1983 [58].

The goal of the present work was to apply optimized magnetic source imaging to identify multiple components in SII and to characterize their functional properties with high temporal resolution. In order to evoke cortical activity, tactile pressure pulses were delivered to the fingers. This is in contrast to most previous reports employing electric stimulation. Pressure pulses correspond better to everyday tactile experience and therefore represent a more realistic imitation of natural stimulation.

Chapter 1 gives a brief summary of the physical, physiological, anatomical, technical and

mathematical background that is indispensable for efficient and reliable analysis of MEG data. In chapter 2 an appropriate imaging technique for SII activity is determined and a modeling method developed for the group analysis of data obtained from several subjects. The developed technique is applied in a combined EEG/MEG study that is presented in chapter 3. Different generators of activity in the SII region are identified and their latency and orientation determined using spatio-temporal source analysis. Specific properties of EEG and MEG are compared and the advantages of MEG for imaging activity in SII are demonstrated. Voluntarily induced alteration of SII activity is investigated in chapter 4, where the influence of attention on SII activity is analyzed. The differential effects of attention to stimulus location and intensity on component amplitudes and latencies are determined and compared with each other. To examine the mechanisms underlying the attention-induced changes of SII-activity, the effect of response decrement over stimulation time and its dependence on the state of attention is examined. The suggested role of SII in the integration of different body parts is the basis for the study presented in chapter 5. Here the interaction of simultaneous input to different fingers is analyzed in order to examine the processing of input from multiple sites.

This work has been funded by the "Pain Research Programme" of the University Hospital of Heidelberg, Germany. Parts of this thesis have been published in references [64], [65] and [66].

Chapter 1

Fundamentals

Efficient exploitation of the potential of magnetoencephalography (MEG) requires knowledge of the underlying microscopic biological processes, the physical laws governing the genesis of the extracranial magnetic fields, the functionality of the technical devices used for signal recording, the mathematical fundamentals of the different data analysis methods and the specific properties of the physiological system under investigation. In order to provide a basis for the understanding of the studies presented in this thesis, this chapter presents a brief overview of these topics. More detailed information can be found in the references cited in each section.

1.1 Microscopic generators of neuroelectromagnetic activity

The basic information-processing units in the human brain are neurons. These cells specialize in the reception, processing and transmission of information in the form of potential differences produced by concentration gradients of charged ions. The structure of a typical cortical neuron is shown in Fig. 1.1. Threadlike extensions, the dendrites, receive stimuli from other cells. The cell body or soma contains the nucleus and the metabolic machinery of the cell. A single long fiber, the axon, transmits electric impulses to other cells.

The cell is surrounded by a membrane. It contains protein molecules that actively pump ions into or out of the cell. In the rest state, the resulting currents are balanced by diffusive and ohmic currents for each ion type and lead to a concentration gradient between intra- and extracellular space. The main ions involved in these processes are K^+, Na^+ and Cl^-.

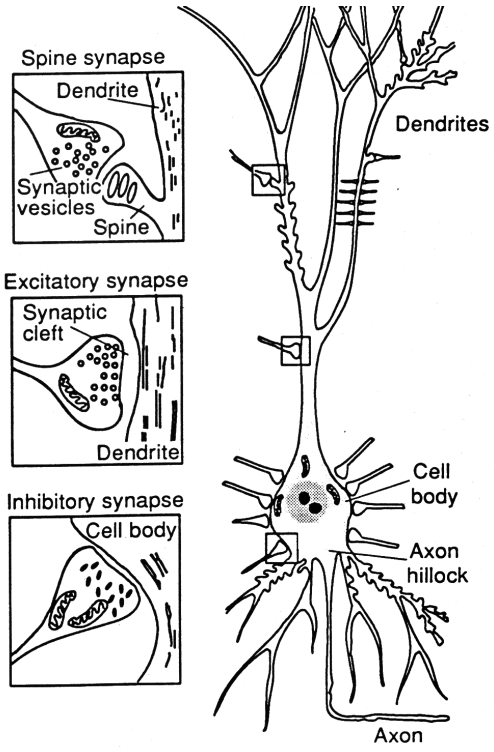

Figure 1.1: *Schematic view of a cortical neuron with different types of synapses. (from [50])*

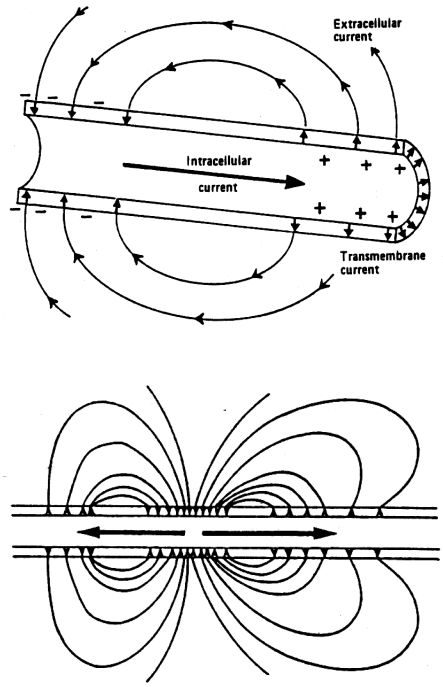

Figure 1.2: *Intra- and extracellular current flow associated with the conduction of postsynaptic potentials (top) and action potentials (bottom).*

According to the Nernst equation applied to the corresponding concentrations of these ion types [47], a transmembrane potential of about -70 mV results in equilibrium, called the cell's rest potential.

The permeability of the cell membrane changes at the synapses when the presynaptic cell releases transmitter molecules into the synaptic cleft that activate selective ion channels in the membrane. The result is a depolarization (excitatory postsynaptic potential, EPSP) or a hyperpolarization (inhibitory postsynaptic potential, IPSP) of the cell. While most excitatory synapses occur at the dendrites, many inhibitory synapses can be found at the soma (Fig. 1.1). Fig. 1.2, top, shows the current flow inside a dendrite segment. It results from activation of an excitatory synapse that causes a slow influx of Na^+ into the cell. The mutual repulsion of the positive ions inside the cell leads to an intracellular axial current (predominantly K^+ ions), whose net direction is determined by the shape of the dendrite. In case of excitatory synapses at the periphery of the dendrites, this current is directed towards the soma. The resulting increasing positive charge inside

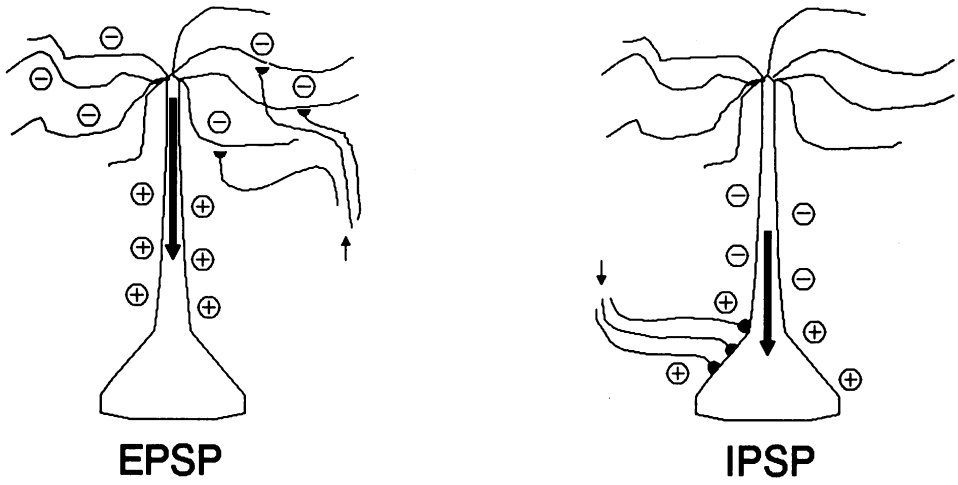

Figure 1.3: *Dipolar field distribution of excitatory (left) and inhibitory (right) postsynaptic potentials. (from[127])*

the cell leads to a repulsion of the extracellular positive charges that tend to move back towards the negative charge near the synapse (extracellular current, Fig. 1.2, top). Within the neuron, the potentials induced by all active synapses sum up, resulting in a net postsynaptic potential that builds up and decays on the order of tens of milliseconds. The corresponding currents can be considered quasistatic (for a detailed derivation see section 1.2). Hence current continuity ensures the net equality of extra- and intracellular current [153]. For inhibitory synapses analogous considerations hold. Fig. 1.3 illustrates the resulting dipolar field and current distribution for both cases.

When the summed PSPs of all synapses of a neuron reach a critical threshold of about -40 mV at the axon hillock (Fig. 1.1), an action potential is initiated in the cell's axon. The membrane permeability for Na^+ increases. Like in the case of the postsynaptic response, the accumulating positive charges produce an intracellular axial current of K^+ defining the depolarization front of the action potential. Subsequently, the slower K^+ channels of the axon begin to open, permitting an outward flow of these ions. The resulting reverse intracellular current defines the repolarization front of the current. Fig. 1.2, bottom, illustrates the resulting current quadrupole including the corresponding reverse extracellular currents.

The magnetic field and electrical potential produced by the current and charge distributions of an active single neuron is by orders of magnitude too low to be detected outside the head by means of MEG or electroencephalography (EEG). It is only the summation of simultaneous activity of neuronal assemblies that accounts for detectable signals. Here the special arrangement of the pyramidal neurons in the cortex is of essential importance. As illustrated in Fig. 1.4, these neurons tend to be aligned in parallel to each

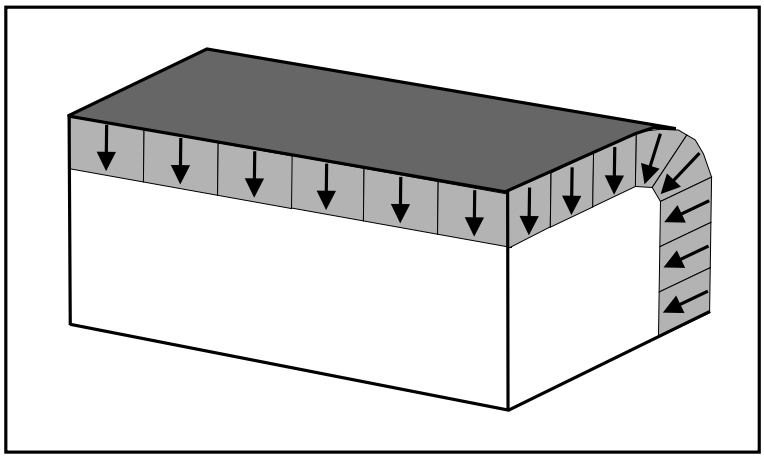

Figure 1.4: *Schematic view of the alignment of the pyramidal cells in the cortex.*

other within a layer of the cortex termed the gray matter due to its shaded appearance in the anatomical substrate. The orientation of the cells is perpendicular to the cortex surface. Thus the net current flow to be considered on a mesoscopic scale is about the sum of the currents in all neurons. By this summation the net produced magnetic field can reach a magnitude that makes it detectable outside the human head.

When comparing the effects of action potentials and postsynaptic potentials, two considerations are important. First, the dipolar field produced by the PSP decreases with distance as $1/r^2$, more slowly than the $1/r^3$-dependent quadrupolar field of an action potential. Second, temporal overlapping of the activities of different neurons is a prerequisite for the summation of their effects. While a typical PSP lasts for tens of milliseconds, the duration of an axonal action potential is on the order of 1 ms, making temporal synchronisation much less common. Thus cortical MEG and EEG signals reflect almost exclusively the activity produced by the postsynaptic current flow with its approximately dipolar distribution. The predominance of the dipolar components of the intracellular currents in generating the external magnetic field was recently verified experimentally [115]. However, at the wrist MEG measurements have been performed also on action potentials conducting somatosensory information [55].

1.2 Physics of extracranial electromagnetic fields

When the neural electric current generators and the electric conductivity σ at any point inside the head are known, expressions for the resulting extracranial electric and magnetic fields, $\vec{E}$ and $\vec{B}$, can be calculated. Important specific properties of EEG and MEG can be understood on the basis of the derivations of the corresponding fields.

Starting point are Maxwell's equations:

$$\nabla \cdot \vec{E} = \rho/\epsilon_0 \qquad (1.1) \qquad \nabla \cdot \vec{B} = 0 \qquad (1.2)$$

$$\nabla \times \vec{E} = -\frac{\partial \vec{B}}{\partial t} \qquad (1.3) \qquad \nabla \times \vec{B} = \mu_0 \left(\vec{J} + \epsilon_0 \frac{\partial \vec{E}}{\partial t} \right) \qquad (1.4)$$

In equation 1.4 use has been made of the fact that the magnetic permeability μ of tissue inside the head equals that of free space, μ_0. ϵ_0 is the permittivity of vacuum, ρ the charge density and $\vec{J}$ the total current density in the passive nonmagnetic medium:

$$\vec{J} = \sigma \vec{E} + \frac{\partial \vec{P}}{\partial t} \qquad (1.5)$$

with the polarization $\vec{P} = (\epsilon - \epsilon_0)\vec{E}$.

The above equations can be simplified further by noting that the time derivatives in equations 1.3 and 1.4 can be neglected. The resulting equations represent the *quasistatic approximation* of Maxwell's equations. To see this one considers fields of the form

$$\vec{E} = \vec{E}_0(\vec{r}) e^{i2\pi f t} \qquad (1.6)$$

$$\vec{B} = \vec{B}_0(\vec{r}) e^{i2\pi f t} \qquad (1.7)$$

with typical frequencies of neuroelectromagnetism $f \leq 100\,\mathrm{Hz}$. With equations 1.5 and 1.6, equation 1.4 becomes

$$\nabla \times \vec{B} = \mu_0 \left[\sigma \vec{E} + \epsilon \frac{\partial \vec{E}}{\partial t} \right]. \qquad (1.8)$$

Assuming uniform σ and ϵ and inserting typical values $\sigma = 0.3\,\frac{1}{\Omega \mathrm{m}}$ and $\epsilon = 10^5\,\epsilon_0$, one finds $2\pi f \epsilon/\sigma \leq 10^{-3} \ll 1$, which justifies the neglection of the time dependence of the electric field in equation 1.4.

To show that the contribution of $\frac{\partial \vec{B}}{\partial t}$ to $\vec{E}$ is small, equation 1.4 is inserted into 1.3:

$$\nabla \times \nabla \times \vec{E} = -\mu_0 \frac{\partial}{\partial t} \left(\sigma \vec{E} + \epsilon \frac{\partial \vec{E}}{\partial t} \right) = -i2\pi f \mu_0 \left(\sigma + i2\pi f \epsilon \right) \vec{E}. \qquad (1.9)$$

The solution for $\vec{E}$ as obtained from this equation has typical spatial changes on the characteristic length scale

$$\lambda_c = \left| 2\pi f \mu_0 \sigma \left(1 + i2\pi f \frac{\epsilon}{\sigma} \right) \right|^{-\frac{1}{2}} = 65\ \mathrm{m}. \qquad (1.10)$$

Since this is much larger than the diameter of the head, the contribution of $\frac{\partial \vec{B}}{\partial t}$ to $\vec{E}$ is small. Hence $\vec{E}$ can be approximated as curl-free and the time-derivative in equation 1.2 can be neglected [50]. Therefore, a scalar potential V of the electric field can be defined such that

$$\vec{E} = -\nabla V. \tag{1.11}$$

The current density $\vec{J}(\vec{r})$ produced by the neuronal activity can be divided into two components: the passive volume or return current $\vec{J}^v(\vec{r})$ in the medium and the localized primary current $\vec{J}^p(\vec{r})$ inside or in the close vicinity of the cell.

$$\vec{J}(\vec{r}) = \vec{J}^p(\vec{r}) + \vec{J}^v(\vec{r}) = \vec{J}^p(\vec{r}) - \sigma(\vec{r})\nabla V(\vec{r}), \tag{1.12}$$

where $\sigma(\vec{r})$ is the macroscopic conductivity of the medium.

With equation 1.12 the magnetic field outside the head produced by the current density $\vec{J}(\vec{r})$ can be calculated from the Ampère-Laplace law for the quasistatic approximation,

$$\vec{B}(\vec{r}) = \frac{\mu_0}{4\pi} \int \frac{\vec{J}(\vec{r}\,') \times \vec{R}}{R^3}\, dv' = \frac{\mu_0}{4\pi} \int \left(\vec{J}^p - \sigma \nabla' V\right) \times \frac{\vec{R}}{R^3}\, dv', \tag{1.13}$$

where $\vec{R} = \vec{r} - \vec{r}\,'$. By use of simple mathematical identities this can be transformed into

$$\vec{B}(\vec{r}) = \frac{\mu_0}{4\pi} \int \left(\vec{J}^p + V \nabla' \sigma\right) \times \frac{\vec{R}}{R^3}\, dv'. \tag{1.14}$$

Thus in general both $\vec{J}^p$ and $\sigma\vec{E}$ contribute to the magnetic field. In equation 1.14 the return currents are represented by $V\nabla\sigma$, a fictitious current without physical meaning. This notion illustrates that if the conductivity in the medium is homogeneous, $\nabla\sigma = 0$ and the return currents do not contribute to the extracranial magnetic field at all.

The calculation of $\vec{B}(\vec{r})$ by means of equation 1.14 is straightforward once the potential V is known. It can be easily obtained by taking the divergence of equation 1.12 and noting that $\nabla \cdot \vec{J} = 0$. One obtains

$$\nabla \cdot (\sigma \nabla V) = \nabla \cdot \vec{J}^p, \tag{1.15}$$

which in many cases can be solved for V analytically with proper boundary conditions [50].

In the special case of a conductor that consists of *piecewise homogeneous parts* G_i, $i = 1, \ldots, m$, with conductivities σ_i, the second term in equation 1.13 can be written as sum of integrals over the corresponding surfaces S_{ij} between G_i and G_j. This is shown by writing equation 1.13 as

$$\vec{B}(\vec{r}) = \vec{B}_0(\vec{r}) - \frac{\mu_0}{4\pi} \sum_{i=1}^{m} \sigma_i \int_{G_i} \nabla' V \times \frac{\vec{R}}{R^3}\, dv', \tag{1.16}$$

where $\vec{B}_0(\vec{r})$ is the magnetic field produced by the primary current alone:

$$\vec{B}_0(\vec{r}) = \frac{\mu_0}{4\pi} \int_G \vec{J}^p(\vec{r}\,') \times \frac{\vec{R}}{R^3}\, dv'. \tag{1.17}$$

With use of vector identities, equation 1.16 can be transformed into

$$\vec{B}(\vec{r}) = \vec{B}_0(\vec{r}) + \frac{\mu_0}{4\pi} {\sum_{ij}}' (\sigma_i - \sigma_j) \int_{S_{ij}} V(\vec{r}\,') \frac{\vec{R}}{R^3} \times d\vec{S}'_{ij}, \tag{1.18}$$

where the primed sum indicates summation over all boundaries [50].

If the conductor consists of *homogeneous spherical shells*, a model commonly applied to the human head in MEG, the contribution of the volume currents to the radial field component $B_r = \vec{B}(\vec{r}) \cdot \vec{e}_r$ vanishes, since

$$\vec{R} \times \vec{n}(\vec{r}\,') \cdot \vec{e}_r = (\vec{r} - \vec{r}\,') \times \frac{\vec{r}\,'}{|\vec{r}\,'|} \cdot \frac{\vec{r}}{|\vec{r}|} = 0. \tag{1.19}$$

$\vec{n}(\vec{r}\,')$ is a vector perpendicular to the boundary ∂G_i pointing outwards from G_i. If now, in accordance with the microscopic considerations made in section 1.1, the localized primary current is modeled as a current dipole $\vec{Q}$ at $\vec{r}_Q$,

$$\vec{J}^p(\vec{r}) = \vec{Q}\, \delta(\vec{r} - \vec{r}_Q), \tag{1.20}$$

the radial component of the magnetic field can be written as

$$B_r = \frac{\mu_0}{4\pi} \int \vec{J}^p(\vec{r}\,') \times \frac{\vec{R}}{R^3} \cdot \vec{e}_r\, dv' = -\frac{\mu_0}{4\pi} \frac{\vec{Q} \times \vec{r}_Q \cdot \vec{e}_r}{|\vec{r} - \vec{r}_Q|^3}. \tag{1.21}$$

Since $\nabla \times \vec{B} = 0$ outside the head, $\vec{B}$ can be assigned a magnetic scalar potential U such that $\vec{B} = \mu_0 \nabla U$. Since $\nabla \cdot \vec{B} = 0$, U is uniquely determined by its normal derivative on the conductor surface and by the requirement to vanish at infinity. On a sphere, $\partial U / \partial r = -B_r / \mu_0$, which can be integrated to yield

$$U(\vec{r}) = \frac{1}{\mu_0} \int_{t=1}^{\infty} B_r(t\vec{r})\, dt. \tag{1.22}$$

Therefore the whole magnetic field can be computed without the knowledge of the conductivity profile $\sigma(\vec{r})$ inside the spherically symmetric conductor. Analytic solutions for $\vec{B}(\vec{r})$ using equation 1.22 are given in references [75] and [125]. Another important property of neuromagnetic fields is seen from equation 1.21: B_r vanishes if the primary current is radial. According to equation 1.22 this implies $U(\vec{r}) = 0$ and therefore also $\vec{B}(\vec{r}) = 0$. MEG therefore is mainly sensitive to primary current components tangential to the head surface.

1.3 The inverse problem

Equations 1.14 and 1.15 show that both $\vec{B}$ and $\vec{E}$ depend linearly on the primary current $\vec{J}^p$. Thus the output b_i of one magnetometer can be written as

$$b_i = \int \vec{L}_i(\vec{r}) \cdot \vec{J}^p(\vec{r})\, dv, \tag{1.23}$$

where the vector field $\vec{L}_i$ is called the lead field that describes the sensitivity distribution of the ith magnetometer. It can be calculated from the equations derived in section 1.2. Under realistic conditions, the recorded fields b_i contain small contributions from the environmental magnetic fields and electronic channel noise aside from the signals generated by the neuronal currents $\vec{J}^p$. A common way to model $\vec{J}^p$ is to assume a set of discrete current dipoles $\vec{Q}_k$ at $\vec{r}_k$ according to equation 1.20, with fixed orientations and time-varying activity. If the output of m magnetometers is sampled at t discrete time points, equation 1.23 becomes the matrix equation [110, 133]

$$b_{ij} = L_{ik} \cdot Q_{kj}. \tag{1.24}$$

Here $\tilde{b}$ is a $(m \times t)$-matrix with B_{ij} denoting the field at the ith magnetometer at time point j, Q_{kj} is the dipole moment of dipole k at that time point. The elements L_{ik} form the Lead Field matrix. They indicate the sensitivity of magnetometer i to the activity of dipole k and therefore depend on its location and orientation. By applying the pseudo-inverse L^{-1} to both sides of the equation, the time course of the source activities can be calculated from the measured magnetic field. Data analysis is usually performed by a fitting algorithm that iteratively varies the source locations and orientations in order to find a configuration that best explains the measured data. As a criterion often the p-norm of the difference between the measured field $\tilde{b}$ and the field explained by the model, $\tilde{b}'$, is applied:

$$\delta = \left\| \tilde{b} - \tilde{b}' \right\|_p = \left\| \tilde{b} - \tilde{L}\tilde{Q} \right\|_p = \left\| \tilde{b} - \tilde{L}\tilde{L}^{-1}\tilde{b} \right\|_p = \left\| \left(\tilde{I} - \tilde{L}\tilde{L}^{-1} \right) \tilde{b} \right\|_p, \tag{1.25}$$

with $\tilde{I}$ the identity matrix. If, as in the present work, the L_2-norm is applied ($p = 2$), δ^2 is the residual variance.

Brain activity can be modeled with dipoles in two principally different ways that are illustrated in Fig. 1.5. A *distributed source model* assumes primary current dipoles densely spaced along the brain's gray matter (Fig. 1.5, A). The orientation of the dipoles can be chosen perpendicular to the brain surface, corresponding to the anatomic facts described in section 1.1. In this case, the number of dipoles in the model ($\sim 10^4$) exceeds the number of sensors (up to 306 in current MEG systems). Hence one has to deal with an

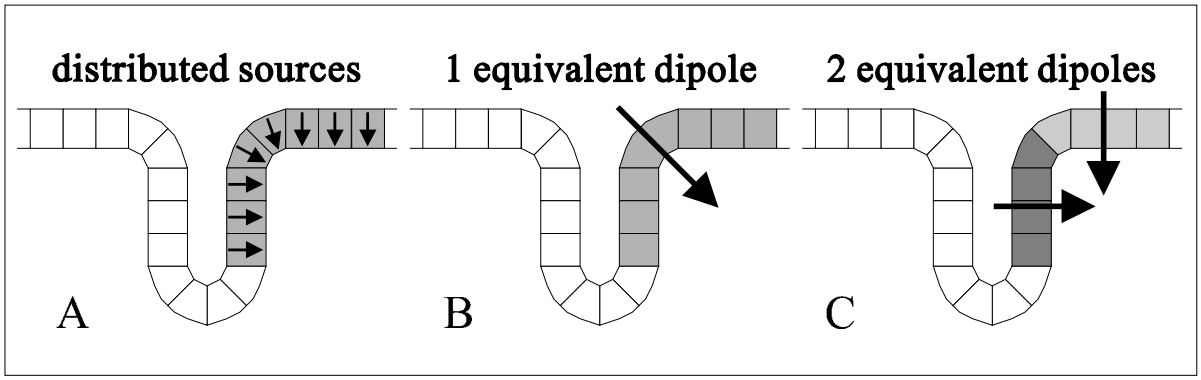

Figure 1.5: *Modeling of cortical brain activity by equivalent current dipoles. (from [129])*

underdetermined problem and needs to place constraints in order to find the solution considered most likely. One possibility is to choose the solution with minimum norm of the summed dipole activities (the so called "Minimum norm solution", cf. section 2.3.3).

Another way of modeling the data is the use of *discrete equivalent dipoles* (Fig. 1.5 B, C). This method is based on the assumption that during specific brain processes only small discrete brain regions are active. Each of these patches can be modeled by one or a few single *equivalent dipoles*, resulting in a model consisting of much less sources than measurement sensors and hence representing an overdetermined problem. Brain areas in close vicinity with simultaneous activity but different orientations can be modeled by a *regional source*, a construct of two (or three in the case of EEG) dipoles with orthogonal orientations describing the local source current in any direction (Fig. 1.5 C) [110, 130, 133]. However, the current distribution inside the head can not be retrieved uniquely from the electromagnetic field measured extracranially with any model [63]. Therefore it is necessary to place constraints on the allowed source configurations, e. g. by using physiological and anatomical knowledge about the system under investigation.

1.4 Magnetoencephalography – methods and devices

1.4.1 Data acquisition

All MEG measurements presented here were performed with a Neuromag-122™ whole head magnetoencephalograph [1]. The subject sits with the head placed inside a helmet-shaped device, the dewar, in which 122 supraconducting coils are positioned. The resulting distance between the head surface and the sensors thus is $\lesssim 5\,\mathrm{cm}$ (Fig 1.8). The sensors are planar gradiometers rather than magnetometers, since due to the figure-of-8

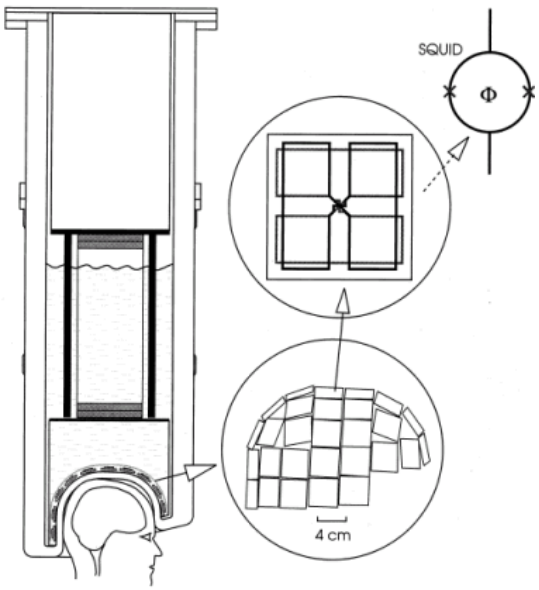

Figure 1.6: *Schematic view of an MEG system with incorporated SQUIDs.*

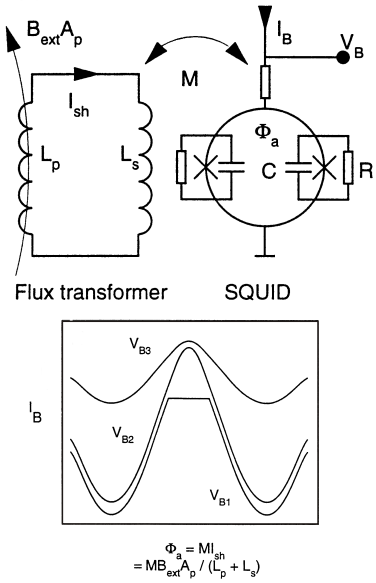

Figure 1.7: *Circuit diagram of the voltage biased SQUID electronics.*

shape of these coils (Fig. 1.6) the induced voltage V is proportional to one component of the planar gradient of the magnetic field component perpendicular to the head surface in the xy-plane, $\begin{pmatrix}\partial/\partial_x \\ \partial/\partial_y\end{pmatrix} B_z \equiv \nabla_2 B_z$. The planar gradient of the magnetic field has a more focal distribution above the dipolar primary current inside the head than B_z or its axial gradient in z-direction. This facilitates visual data inspection. The rather homogeneous field produced by distant noise sources is effectively cancelled by gradiometers. On the other hand, due to the faster decay of the field gradient with distance than that of the field itself, the sensitivity of gradiometers to deep sources is weaker when compared to magnetometers. In the Neuromag-122™ system, the sensors are mounted on 61 chips, each containing two pickup-coils. The chip is positioned approximately in a plane parallel to the dewar surface and the orientations of the two twisted coils are perpendicular to each other. The coil with its axis pointing towards the vertex is termed the "radial", the other the "circular" sensor of the chip. The sum of the squared signals detected by the two coils thus equals the square of the planar gradient $\nabla_2 B_z$ in the xy-plane.

A secondary coil transforms the voltage induced in each pickup coil back into a secondary magnetic field that is detected by a voltage biased SQUID (Super Conducting Quantum Interference Device) (cf. Fig. 1.7). With a properly chosen value of the bias voltage V_B, the current I_B flowing through the SQUID is a periodic function of the secondary magnetic field Φ_a penetrating the SQUID loop (cf. Fig. 1.7, bottom, for different values of the bias voltage V_B). The periodicity is one flux quantum ($\Phi_0 = h/2e = 2.07 \cdot 10^{-15}$ Vs). This allows

for an accuracy of each sensor ≤ 1 fT/cm, which is necessary to detect the neuromagnetic activity which is a few orders of magnitude smaller than the geomagnetic noise. In order to prevent this and other noise fields from technical devices and other environmental factors to disturb the detected signals, all measurements were carried out inside a magnetically shielded room (Imedco, Switzerland). The output of the 122 gradiometers was sampled by an A/D-converter and stored for subsequent off-line analysis.

1.4.2 Matching the coordinate systems

The different steps of data analysis require matching of four independent coordinate systems.

1. The location and orientation of the gradiometer coils are given in dewar-fixed *device coordinates*.

2. The left and right preauricular point (LPA / RPA) and the nasion (N) of the subject's head define the *head coordinate system*. Its relation to the device coordinates depend on the subject's position inside the dewar.

3. MEG modeling is performed within a *unit sphere* approximating the brain as a homogeneous sphere with radius 1 as described in section 1.2.

4. In order to relate the modeled MEG sources to anatomical locations within the individual brain, these coordinates need to be matched with magnetic resonance images (MRI) given in *MR coordinates*.

The relationship of these reference systems is established as follows [31]:

- **Head – Device:** Before each measurement, four conducting coils (Head Position Indicators, HPI) are attached to the subject's head. The three-dimensional positions of these coils relative to the three reference points (LPA, RPA, N) are determined by a Polhemus-3D-Isotrak digitizer (Fig. 1.9). When the subject is seated under the dewar and the head already rests in the position that is pertained throughout the measurement, a triangular current is sent through these coils. The generated magnetic field is detected by the MEG sensors, and the location of the coils with respect to the gradiometer sensors, i. e. in device coordinates, can be calculated from the resulting signals.

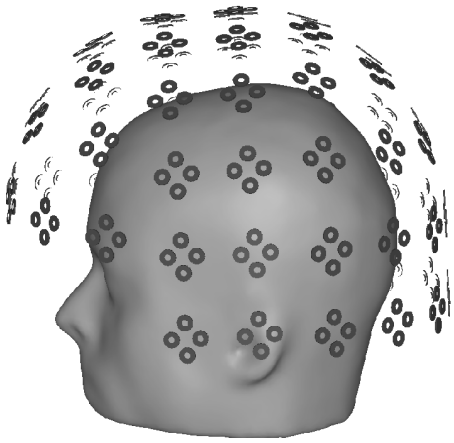

Figure 1.8: *Sensor positions relative to the head*

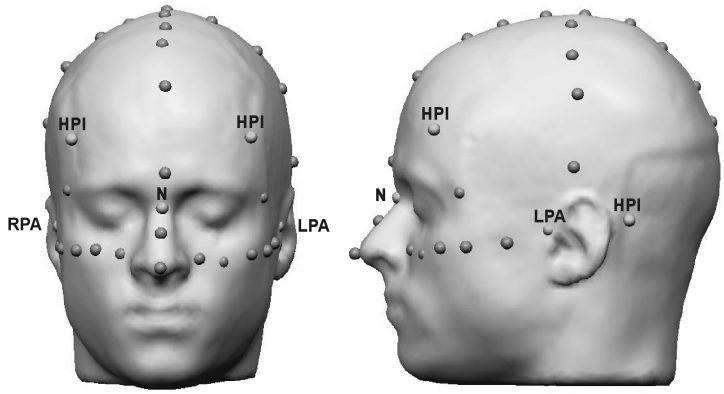

Figure 1.9: *Locations of the digitized head points as used for MEG measurements.*

- **Head – MR:** The transformation between these coordinate systems is established by fitting the 3D-coordinates of the fiducials, the HPI coils and 32 additional reference points on the subject's head to the surface reconstructed from the anatomical 3D MR image [31]. This is shown in Fig. 1.9.

- **Head – Unit sphere:** When a three-dimensional MR data set of the subject is at hand, the posterior commissure (PC) is used as an anatomical landmark to define the center of the model unit sphere. For that purpose, the MR data set is rotated and resampled to align one axis with the line that connects anterior and posterior commissure using the BrainVoyager™ 2000 software (Brain Innovation, Maastricht). In the current work, the point 5 mm anterior and 5 mm superior to PC was taken as center of the unit sphere (Fig. 1.10). The known transformation between head and MR coordinates is used to save its position in the head coordinate system. Subsequently the radius of the sphere is determined by a least squares fit of the sphere surface to the digitized head surface points (excluding the nose). If no MR data set exists, the sphere midpoint and radius are both determined from fits to these points. The resulting model sphere is visualized for one subject in Fig. 1.10. It illustrates the difficulties inherent in using one sphere to model the whole head: while parts of the frontal cortex are located outside, the sphere exceeds the cortex over the temporal lobes. These deficits, however, must be viewed under consideration of the fact that in MEG the sphere dimensions only serve for restricting the volume in which modeled brain activity can occur. The fitted location of sources inside the sphere will not be changed by enlarging the sphere diameter. Rather the important parameter is the sphere midpoint, defining the notion of "radial" neuromagnetic currents that can not be modeled.

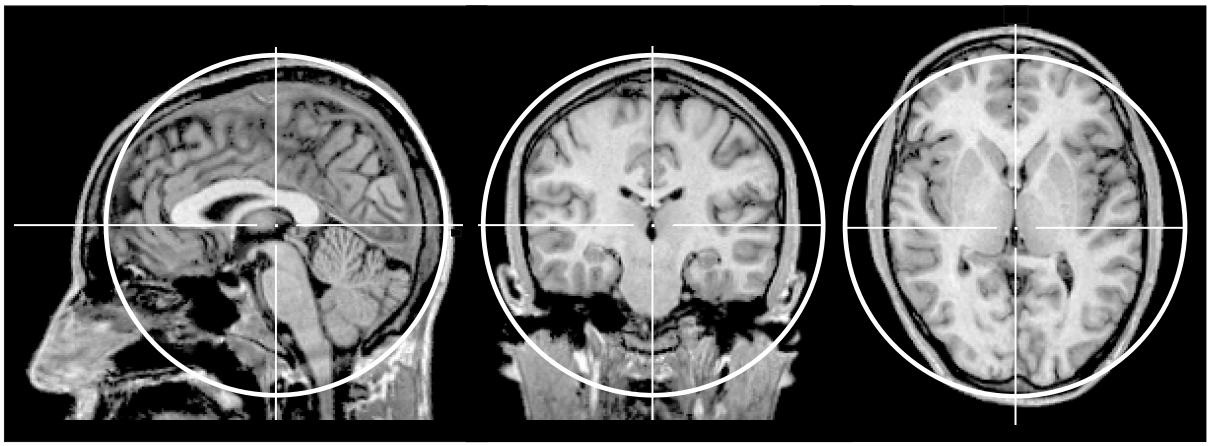

Figure 1.10: *Fit of the model sphere to the head surface.*

More details on the data analysis that partly depend on the specific properties of the applied paradigm will be given in the chapters describing the corresponding studies.

1.4.3 Stimulation

In the studies presented here, subjects received tactile stimulation to one or two fingers during the measurement in order to generate somatosensory evoked magnetic fields (SEF). This was performed using commercially available finger stimulator clips (BTI, Aachen) as shown in Fig. 1.11. The clip was clamped to the subject's finger such that the inner part of the finger rested on a rubber membrane of about $0.5\,\mathrm{mm}^2$ cross-section. The membrane formed one boundary of a cavity that was connected to a compressed air supply (pressure 6 bar) outside the magnetically shielded room via a thin tube of polyurethane. An interposed valve allowed for the transmission of short air pressure pulses. It could be triggered with a personal computer via TTL signals. A sharp pressure pulse produced by a short opening of the valve ($t = 25\,\mathrm{ms}$) arrived slightly broadened temporally at the end of the tube and displaced the membrane at the finger clip. This in turn caused an indentation of the skin at the subject's finger and thereby produced a tactile sensation.

Fig. 1.12 depicts the time course of the air pressure pulse at the end of the polyurethane tube. The curve was recorded with a piezo pressure sensor attached to the tube instead of the finger clip. $t=0$ represents the trigger time. Due to the tube length of about 2 m, the pulse arrived with a delay of 32 ms. The pressure reached its maximum about 45 ms after the trigger onset. Thus when averaging the measured data offline, the delay of 32 ms was taken into account in order to obtain the correct latencies, assuming that the skin indentation starts nearly simultaneously with the arrival of the pressure pulse inside the

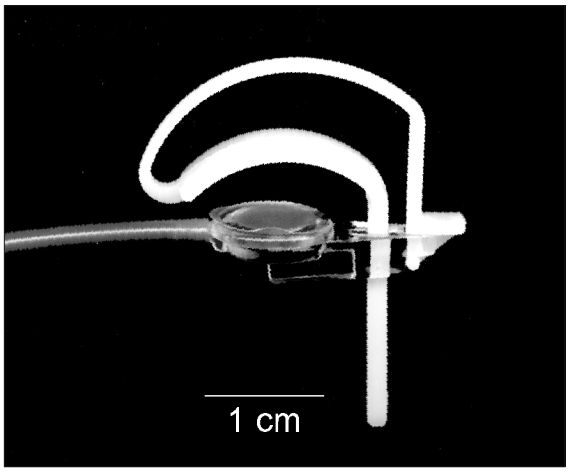

Figure 1.11: *BTI finger clip used for tactile stimulation.*

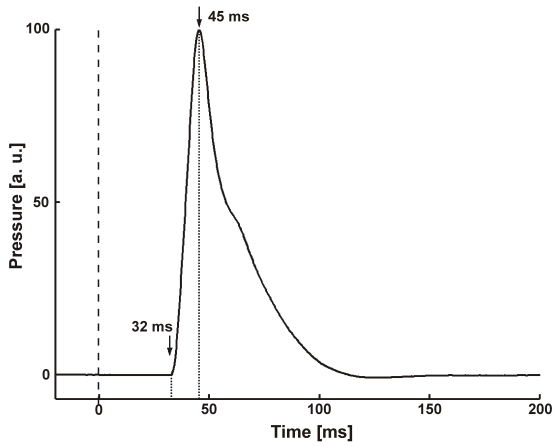

Figure 1.12: *Time evolution of an air pressure pulse.*

clip cavity. Since the clip is designed such that the finger tightly rests on the membrane, this assumption is justified. The depth of skin indentation is on the order of 1 mm, varying from subject to subject, depending mainly on the individual skin constitution. The arrival of the air pressure pulse inside the finger clip cavity is accompanied by a short noticeable sound. In order to prevent auditory evoked brain responses, this sound was masked by white noise, which was produced by small transducers located under the gantry chair and delivered to the subject's ear via polyurethane tubes and foam ear plugs. Loudness was individually adjusted to a level that was sufficient to prevent the subject from noticing the sound produced by the clips.

In literature, somatosensory evoked fields (SEF) and potentials (SEP) have often been generated by delivering electric stimuli to the median nerve at the subject's wrist [15, 62, 105, 109]. This nerve collects fibers from thumb, index and middle finger. Therefore electric stimulation has the advantage of producing very precise timing and synchronisation and evoking comparatively strong brain activity, but it evokes sensations that are rather unspecific in location. Electric pulses are rather unnatural stimuli and are perceived unfamiliar and unpleasant by many subjects. As opposed to that, finger clips solely stimulate mechanoreceptors in the skin and evoke a quite natural sensation that usually is not regarded as unpleasant.

1.5 The somatosensory system

As mentioned in section 1.3, paradigm design and analysis strategies for neuromagnetic measurements strongly depend on the stimulated modality, e. g. visual, auditory or somatosensory. In this chapter a short review of the specific properties of the somatosensory system is given. The generation of tactile evoked cortical activity is described in its different steps to provide a basis for the understanding of the emerging magnetic field pattern evoked by tactile pressure stimulation.

1.5.1 Skin receptors mediating tactile sensations

Mechanoreceptors are responsible for the transformation of tactile stimuli into neuronal activity. In the glabrous skin of the human fingers four different receptors types with different response properties can be distinguished. They are categorized into slowly adapting (SA) and rapidly adapting (RA) receptors. The slowly adapting Merkel receptors and Ruffini corpuscles respond continuously to an enduring stimulus, while the Meissner and the Pacinian corpuscles predominantly respond to rapidly changing skin indentation like vibration or the onset of an enduring stimulus. Fig. 1.13 shows their location within the different skin layers. Meissner corpuscles and Merkel receptors are located rather close to the skin surface and have very small receptive fields on the order of $1\,\mathrm{mm}^2$. As opposed to that, most of the deeper Pacinian and Ruffini corpuscles respond to stimuli within an area up to the size of a whole finger [102].

Hence the short indentation of the skin produced by the membrane of the finger clips activates all of these receptors, mainly however rapidly adapting Meissner and Pacinian corpuscles. This still results in a sharp neuroelectric signal, since the conduction velocities of the action potentials in the corresponding axons are all in the Aβ range ($\sim 40\,\frac{\mathrm{m}}{\mathrm{s}}$) [102, 52]. This fact prevents a temporal smearing of the compound transmitted signal.

1.5.2 Afferent Pathways

Mechanoreceptors represent the first stage of the afferent somatosensory pathway. Subsequent synapses to second and higher order neurons in the spinal chord, the brain stem, the thalamus and the cortex serve as relay stations for the serially organized signal transmission from the periphery to the cortical gray matter. However, as illustrated in Fig. 1.14, this process has a parallel component as well, because there are two pathways transmitting somatosensory information which separate in the spinal chord. Most of the somatosensory evoked information is transmitted via the dorsal column–medial lemniscal system.

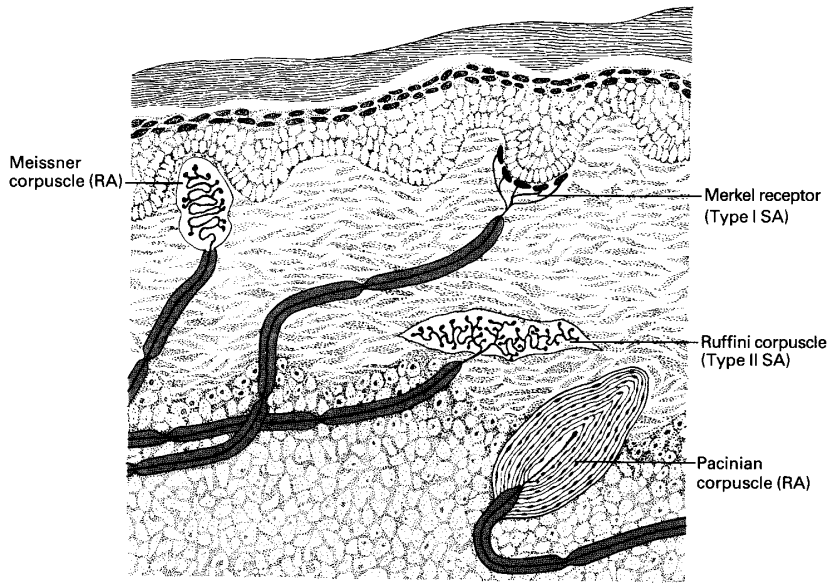

Figure 1.13: *Location of the four morphologically distinct types of mechanoreceptors in glabrous skin. A rough subdivision can be made into slowly (SA) and rapidly (RA) adapting receptors. (from [102])*

Here input from one body side crosses over to the contralateral hemisphere in the brain stem before proceeding to the thalamus and the cortex. To a much lesser extent signals are conducted in the anterolateral system, whose main purpose is the transmission of pain and temperature information. In this pathway the crossing over to the contralateral hemisphere takes place already on the level of the spinal chord [102].

Fig. 1.14 shows the thalamus to be the last relay station before the information reaches the cortex. The thalamus is an important branching point of somatosensory information, and more than one cortical region is served with input from that stage. These different regions are described briefly in the next section.

1.5.3 Cortical structures and intracortical pathways

The primary somatosensory cortex

The first cortical activity following tactile stimulation (about 20 ms after the stimulus presentation) is evoked in the postcentral gyrus contralateral to the stimulation site directly via thalamic connections (cf. Fig. 1.14). This region is the primary or first somatosensory cortex (SI). Its location is depicted in Fig. 1.15. Input to different body sites activates different regions in SI, leading to a distinct representation of the contralateral half of the

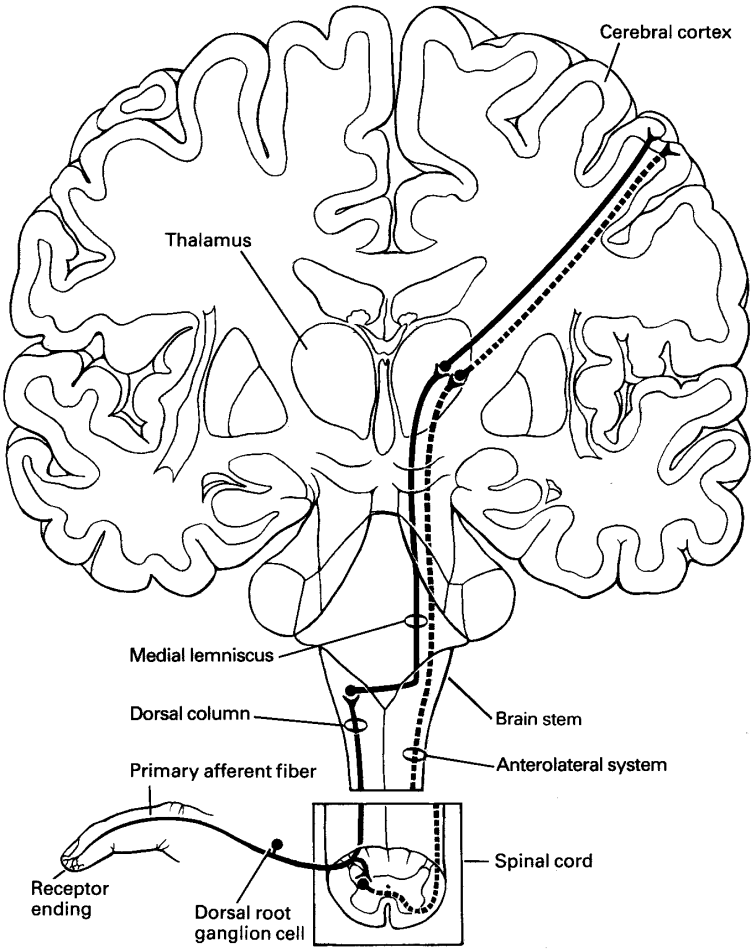

Figure 1.14: *The two parallel ascending pathways of the somatosensory system. The main pathway is termed the dorsal column-medial limniscal system (solid line). To a much lesser extent, tactile sensations are mediated by the anterolateral system (broken line). (from [102])*

body in the postcentral gyrus [118]. This body representation is termed "homunculus" and is shown in Fig. 1.16. It has been replicated in MEG studies that employed dipole source analysis [13, 77, 114, 141]. The size of the cortical area corresponding to one body region is about proportional to the number of mechanoreceptors in that region. The large size of the hand area in SI is a correlate of the high receptor density in the fingers and the importance of the fingers for tactile perception of the environment. SI is subdivided into four cytoarchitectonically distinct regions, Brodmann's areas 1, 2, 3a and 3b [11] (cf. Fig. 1.15), each of which is important for slightly different aspects of somatosensory information processing. In MEG measurements primarily the tangentially orientated activity in region 3b is recorded.

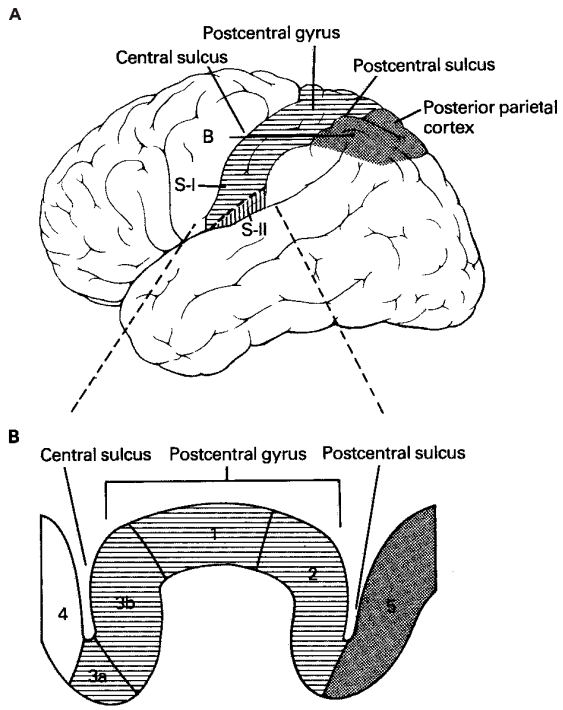

Figure 1.15: *Views of the location of the somatosensory cortices and the posterior parietal association cortex. (taken from [101])*

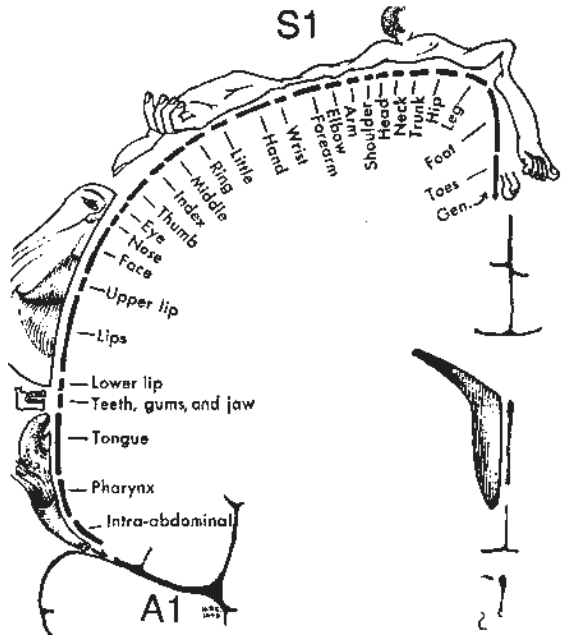

Figure 1.16: *The somatosensory homunculus in the postcentral gyrus (primary somatosensory cortex).*

The secondary somatosensory cortex

A second cortical region activated by tactile stimuli is the secondary somatosensory cortex (SII). It is situated lateral and inferior to SI in the upper bank of the Sylvian Fissure, the Parietal Operculum (Fig. 1.15). This location corresponds to the preinsular portion of Brodmann's area 2 [11]. As opposed to SI, SII is activated bilaterally after unilateral body stimulation [3, 60, 138]. There is an ongoing debate whether the somatosensory cortex is hierarchically organized and SII is activated mainly via SI. The secondary somatosensory cortex may be an important part in a tactile processing pathway that proceeds from SI to the limbic system [113]. Meanwhile it has been shown that apart from these connections from SI, contralateral SII receives also direct input via the ventral posterior nucleus of the thalamus [83, 85]. Ipsilateral SII receives afferent input from the ventral postero-inferior nucleus of the thalamus [17, 85] as well as interhemispheric signals from contralateral SI and SII via transcallosal fiber connections [34, 84, 117].

SII is considered the first associative stage in the processing of somatosensory information. Its function presumably reaches beyond the mere detection of somatosensory stimuli and its activity is related to early cognitive processing. Single cell recordings in monkeys

revealed the involvement of SII in tactile learning [43] and texture discrimination [81]. SII was also shown to play an important role in sensorimotor integration [38, 72]. Altered SII responses in patients with phantom limb phenomena suggested an involvement of this brain area in the maintenance of the body scheme [35, 59]. In addition, SII seems to be essentially involved in the perception of pain as evidenced among others by SEF studies [61, 89, 94]. Magnetic fields generated in SII have also been elicited by visceral oesophagal stimulation [135].

The first observation of SII activity with MEG measurements has been reported in 1983, later than that of SI [58, 62, 143]. The main reason is the smaller magnetic field produced outside the head due to the deeper location of SII in the head when compared to SI. SII responses occur later than those of SI, in a time range of about $50 - 200$ ms [49, 62].

A somatotopic organization in SII has been demonstrated in intracranial recordings [124] as well as in magnetoencephalography (MEG) experiments [50, 56, 100]. However, receptive fields of SII neurons tend to be much larger and more overlapping than those of SI neurons [93, 124, 151]. This leads to a less distinct body representation in SII as compared to that in SI.

The Posterior Parietal Cortex

A third region receiving somatosensory input is the posterior parietal cortex (PPC), located posterior to SI and comprising Brodmann's area 5 and parts of area 7. One of its functions as an associative area is the processing of sensory and motor information and the integration of the different somatosensory submodalities that is necessary for perception [19, 101]. The PPC area also seems to provide information about the coordinates of different body parts with respect to the surrounding space [112]. In SEF studies, activity around 70–110 ms has been reported from this region [36, 40].

Chapter 2

MEG signals from SII – determining the appropriate modeling technique

2.1 Motivation

An optimal data analysis that exploits all possibilities offered by modern whole head systems is an essential part of each MEG study. While providing fairly good spatial information [96], the excellent temporal resolution of EEG and MEG data on the order of milliseconds is not reached by any other noninvasive functional imaging method. Therefore the methods applied for data analysis must be capable of imaging location and temporal evolution of the brain activity simultaneously. Direct imaging of the data acquired by the recording channels, possibly including preprocessing steps, is one way of visualizing the brain responses. Another is to make use of the physical background presented in chapter 1 to apply inverse modeling and map the underlying cortical activity. Different approaches have been developed for that purpose. The physical background and different approaches for the solution of the inverse problem have been discussed in chapter 1, where the concepts of distributed versus discrete sources have been introduced. It remains to be shown how their specific physical and mathematical properties take effect in the analysis of real data.

Which modeling approach is most appropriate for imaging evoked brain activity depends on the goal of the study and to a large extent on the stimulation paradigm and the specific properties of the brain system under investigation. For tactile stimulation of the somatosensory system, the physiological facts have been stated in section 1.5. The investigations presented in this chapter aim at an evaluation of different existing imaging techniques with respect to their capability to visualize tactile evoked activity in the

secondary somatosensory cortex. The main criterion is therefore the ability to separate the bilateral activity in SII from that of SI and to provide a quantitative measure for the time course of the underlying neuronal currents. At the end of the chapter the gained insights are used to develop an analysis method suitable for the analysis of group data with data obtained from different subjects. Thereby the basis is provided for the studies described in the following chapters.

2.2 Materials and Methods

2.2.1 Stimulation paradigm

The advantages and disadvantages of the different MEG analysis techniques are demonstrated by means of a sample data set with a high number of averages and therefore good signal-to-noise ratio. The subject was a healthy, 35-year-old, left-handed female volunteer. Stimuli were presented to the left index finger at a constant interstimulus interval (ISI) of 1.03 s. An oddball paradigm was applied. Standard stimuli with 80% frequency were delivered to the second phalanx, deviants to the first phalanx at a pseudo-random order. The stimulation was presented for 16 minutes. During the measurement, the volunteer was asked to fixate a point at the wall of the measurement cabin. In order to direct the subject's attention towards the stimulus, she was given the task to count deviants silently during the measurement. She correctly counted all 193 stimuli that were actually presented, indicating sufficient discriminability of the stimuli and good compliance of the volunteer.

2.2.2 Data recording and analysis

Data was bandpass-filtered between 0.03 Hz and 200 Hz during recording and sampled at a rate of 769 Hz. An epoch of 100 ms pre- and 1000 ms post-stimulus was averaged under consideration of the delay of 32 ms between trigger and stimulus onset. Silent or excessively noisy channels were excluded from averaging. Only artifact-free epochs were used. The artifact scan was performed automatically by setting threshold values for signal amplitudes (1000 fT/cm) and gradients (800 fT/cm difference between two neighboring sample points) in each channel. Epochs during which at least one channel exceeded one of these thresholds were rejected. During the average process, a baseline correction was performed by subtracting the mean value of the data in the pre-stimulus interval in each channel. The remaining 695 epochs of the stimulation of the second phalanx were averaged for further analysis. For imaging and mapping, data was digitally filtered

offline. In order to prevent artificial latency shifts due to filtering [33, 99, 126], zero-phase-shift filters were used. They perform an implicit forward and backward filtering of the data and thus compensate for the latency shifts of both filter types. To remove slow components, a 3 Hz (slope 6 dB/oct) low cutoff filter was used. The cutoff of the low-pass filter was set to 70 Hz (slope 12 dB/oct). This value guaranteed a significant reduction of the fast noise components while not altering the comparatively slow short- and middle-latency components in the evoked activity between 30 and 200 ms. The first and rather fast cortical component of the SEF produced in SI after about 20 ms (the N20m peak [31, 87, 106]) was slightly weakened by this filter setting, but this component was not the focus of interest in the studies presented here.

2.3 Comparison of different imaging techniques for tactile evoked brain activity

2.3.1 Top view of the averaged data

The most obvious method of data visualization is to directly view the averaged signals of the 122 gradiometers. By using their positions inside the dewar, a view onto the sensor data from the top can be simulated as depicted in Fig. 2.1. For the sake of clearness, radial and circular sensors, located pairwise at the same coordinates, were separated from each other with circular sensors shown above the radial ones. From this view, the special characteristics of somatosensory evoked field gradients can be derived: unilateral stimulation of the left index finger led to a predominant activity over the right cortical hemisphere.

The most prominent signal occurred at a latency of about 40 ms at a location roughly above the right primary somatosensory cortex, SI, in the region of the central fissure (Fig. 2.1, top right). However, the widespread activity distribution over the right hemisphere did not allow for a decision whether all recorded activity originated from that brain region. Rather, knowledge of the underlying physiology (section 1.5.3) suggested another active brain region in that hemisphere, the contralateral secondary somatosensory cortex, SIIc. Its location roughly corresponds to the channel enlarged in the bottom right corner of Fig. 2.1. The overlap of SI and SIIc activities make it difficult to assign the observed components to one of these brain regions. It is even harder to determine whether there was a significant signal produced by the posterior parietal cortex, PPC. Though the channels located roughly above the suspected location of this area (cf. Fig. 1.15) recorded evoked activity, this might well correspond to fields evoked by SI. The assignment of recorded

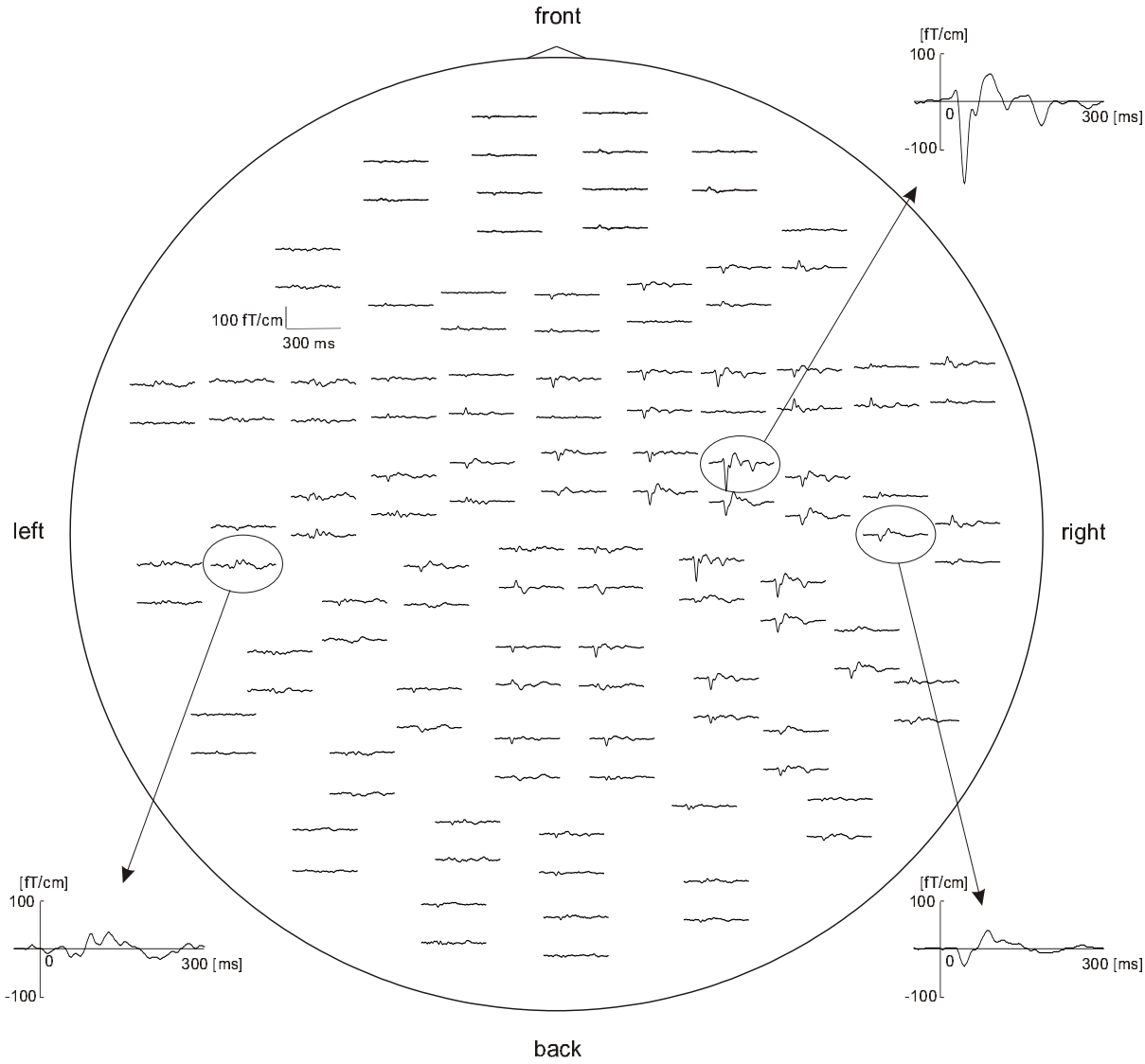

Figure 2.1: *Top view of the averaged MEG channel data.*

signal components to a specific brain region was easier at the ipsilateral hemisphere. The comparatively weak activity could be assigned to the ipsilateral secondary somatosensory cortex, SIIi, due to the fact that it is the only brain region receiving significant early input evoked by unilateral tactile stimuli (Fig. 2.1, bottom left).

The advantage of this visualization method is that it can be performed in realtime during the measurement and does not require any elaborate postprocessing steps. However, this is achieved at the expense of interpretability. An assignment of activity to specific brain regions is difficult to achieve exclusively on the basis of this method.

2.3.2 Surface maps

The top view of the averaged data recorded by the MEG sensors is difficult to interpret not only because of the overlapping activities of SI and SIIc, but also due to the mixture of unprocessed temporal and spatial information. Since radial and circular channels in pairs record field gradients from the same location, their information can be combined to image the total field activity in that spot. Spline interpolation can be used to visualize the spatial distribution of the data more clearly. Assignment of the recorded data to the corresponding head regions is facilitated by projecting the obtained information onto the surface of a standard head.

This projection is performed mathematically by solving the inverse problem for a model of several hundreds of dipoles inside the unit sphere and subsequent forward-calculation of B_z and its planar gradients $\nabla_2 B_z$ produced by the modeled activity. Thus this activity itself is not interpreted, the large amount of model sources is just chosen in order to account for all details of the recorded data. The resulting maps of B_z, and the absolute value $|\nabla_2 B_z|$ are shown in Fig. 2.2.

Because MEG mainly detects brain currents tangential to the head surface, the magnetic flux maps show the typical dipolar field distribution of such sources with symmetric areas of flux inflow (depicted in blue) and outflow (red). Zero flux B_z is produced at the source's vertical projection point to the surface. The distance of flux maximum and minimum is an indicator of source depth [129]. The exact location of the source below the $B_z = 0$ line is more easily obtained by taking the planar gradient of B_z. Its absolute value is at maximum directly above the dipolar source inside the head. Therefore, as can be seen in Fig. 2.2, gradient maps tend to be more focal and thereby facilitate visual source location. However, side maxima occur in $|\nabla_2 B_z|$ [50] that must not be misinterpreted as an indicator for additional sources. Consequently, B_z and its planar gradient should be viewed simultaneously for efficient data analysis. If several sources are active at one time, the corresponding distributions overlap and become difficult to interpret by mere visual inspection of the maps.

The time points chosen in Fig. 2.2 correspond to relative maxima in the global field power (GFP). It is the summed square of the activities of all recording channels scaled to 100 % at its maximum value. This measure is an indicator of the total activity inside the brain. Therefore maxima of the GFP tend to reflect significant activation of at least one cortical area. In Fig. 2.2 latencies of $23, 40, 61, 87, 118$ and 182 ms were chosen for visualization. The first significant activity occurred around 23 ms over the contralateral (right) hemisphere. The gradient map at 40 ms shows activity at the same location, corresponding roughly to the SI area. The flux distribution was exactly reversed compared to that at 23 ms, suggesting a change in polarity of this source. At 61 ms post-stimulus the

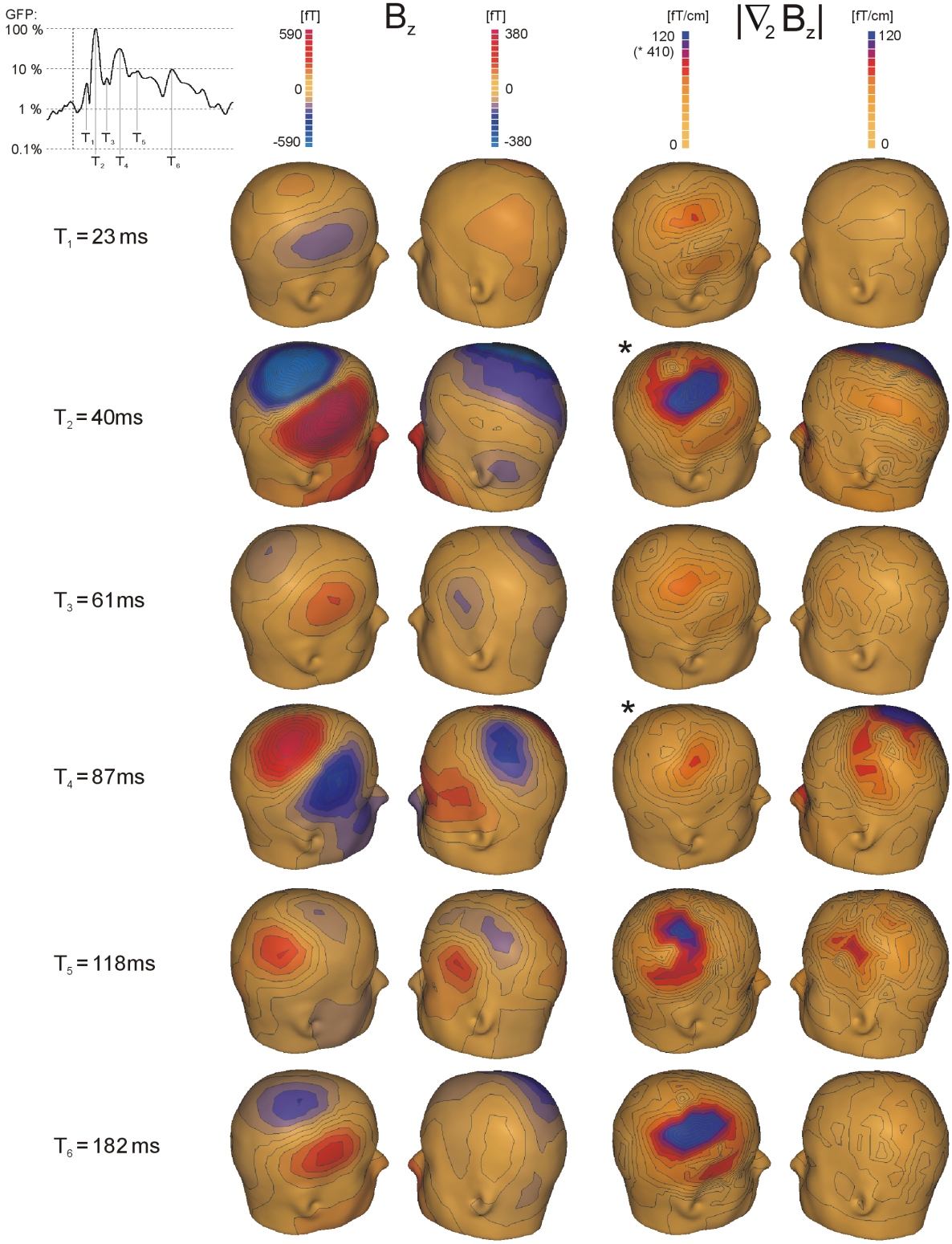

Figure 2.2: *Magnetic flux (left) and gradient (right) maps at peak latencies of the Global Field Power (GFP). Note the different scaling for left and right hemisphere.*

flux distribution contralaterally was slightly rotated with respect to $t = 40$ ms. Whether this was due to a change in orientation of SI activity or to a second active source nearby cannot be decided from the map. Although the gradient map shows a second maximum in an inferior location, this question can not be clarified with certainty at this point. Until this stage the ipsilateral signal was rather weak and diffuse. At 87 ms a clear shift in location and orientation of contralateral activity was observed that was mirrored over the ipsilateral hemisphere, indicating bilateral activation of SII. While the ipsilateral activity pattern was simply attenuated at 118 ms, contralaterally another significant change in orientation and location of the dipolar field occurred. Its origin might be the PPC area. However, it cannot be ruled out that activity in SI, possibly intermingled with a still active source in SII was reflected in this pattern. Finally at 182 ms ipsilateral activity vanished, while contralaterally a pattern very closely resembling that at 40 ms emerged, suggesting late activity in SI.

The example shows advantages and disadvantages of the projected maps of B_z and $|\nabla_2 B_z|$. Spatial information is more easily obtained than from the top view presented in the previous section. Temporal evolution of the patterns can be derived either by selection of specific time points as shown in Fig. 2.2 or by viewing a movie of the maps on the PC monitor. Reliable source localization can not be performed by visual inspection. This is true especially for the case of somatosensory evoked fields discussed here, since SI and SII activities overlap spatially and temporally, producing an intermingled field distribution. The very small distance of the vertical projections of their locations to the head surface makes it difficult to distinguish them even in the rather focal gradient map. The distance of SII to the head surface is much larger than that of SI. This causes SII activity to be picked up much less than that of SI (compare the maps at 40 ms and 87 ms). Therefore, in order to enable a better discrimination between these areas, mapping methods are required that directly depict source activity rather than their magnetic correlates in the sensor plane. Different approaches concerning this issue are the topic of the following sections.

2.3.3 Minimum norm techniques

The minimum norm technique uses a distributed source model as introduced in section 1.3. Instead of modelnig the individual gyration of the subject's gray matter, the version presented here (implemented in the BESA® 2000 software) is based on several hundreds of regional sources arranged on a sphere with a radius of 0.75 in unit sphere coordinates. No source fitting is performed, rather merely the individual dipole moments Q are calculated from equation 1.24. Since the number of recording channels is smaller than the number of sources, one has to deal with an underdetermined problem, which

necessitates the use of constraints as discussed in section 1.3. A common approach is to require the norm of the activities of all sources to be at minimum [9, 51, 103, 146]. Here the inverse model was solved under the constraint of a minimum L_2 norm, i. e. of all possible solutions the current distribution with the smallest Euclidian norm is selected [51]. The leadfield matrix (cf. equation 1.24) of each regional source was scaled with the reciprocal of its first singular value. This depth weighting prevents a smearing of the activity of focal deep sources that would occur without any additional constraints. For visualization, the resulting dipole moments were projected onto the surface of a standard averaged high-resolution brain created by the Montreal Neurological Institute. The brain surface was smoothed in order to not pretend an image accuracy on the order of the gyrus dimensions that is not provided by the method. In Figures 2.3 and 2.4 the activity was scaled such that the 100 % value represented the maximum value of source activity at each time point.

The resulting maps in Fig. 2.3 were calculated at the same time instants as those chosen in Fig. 2.2. The dominant activity over the contralateral hemisphere was observed at any time point. A discrimination between SI, SIIc and PPC was not possible, although the center of activity at 61 and 87 ms occurred to be significantly different from the earlier latencies. In accordance with the maps in Fig. 2.2, at 118 ms a posterior shift of the activity occurred that may be assigned to the PPC area. Significant ipsilateral brain currents appeared only between 61 and 118 ms (note the different scaling at these time points). However, the inherent blurring of the minimum norm signal precluded an unambiguous identification of the SII region.

Suggestions have been made how to reduce the smearing of focal activity that is inherent in the minimum norm approach. One method is to use L_p norms with $p < 2$ for choosing the desired solution of the inverse problem [9, 103, 146]. A different approach introduces an additional spatio-temporal weighting of the leadfield matrix prior to applying the minimum norm procedure. This weighting is based on the MUSIC algorithm (cf. section 2.3.4). Two ways of calculating the weighting factor are compared in Fig. 2.4. One is to reduce the data matrix to the subspace of its principal vectors. In the example the 6 vectors that account to more than 1 % to the data in the time interval of 65–150 ms were chosen. The square of the correlation of each regional source's leadfield to the data matrix (p^2) was used as the corresponding weighting factor [110]. Another method follows a suggestion by Dale and Sereno [28]. It makes use of the pseudo-inverse of the data covariance matrix and thus avoids the necessity to choose a dimension of the signal subspace. A reciprocal function based on a principal component analysis is used as weighting factor for each regional source. From Fig. 2.4 it is evident that the p^2-method focused the activity distribution slightly but did not lead to a significant separation of SI and SIIc at 87 ms. The method of Dale and Sereno provided very efficient focusing. How-

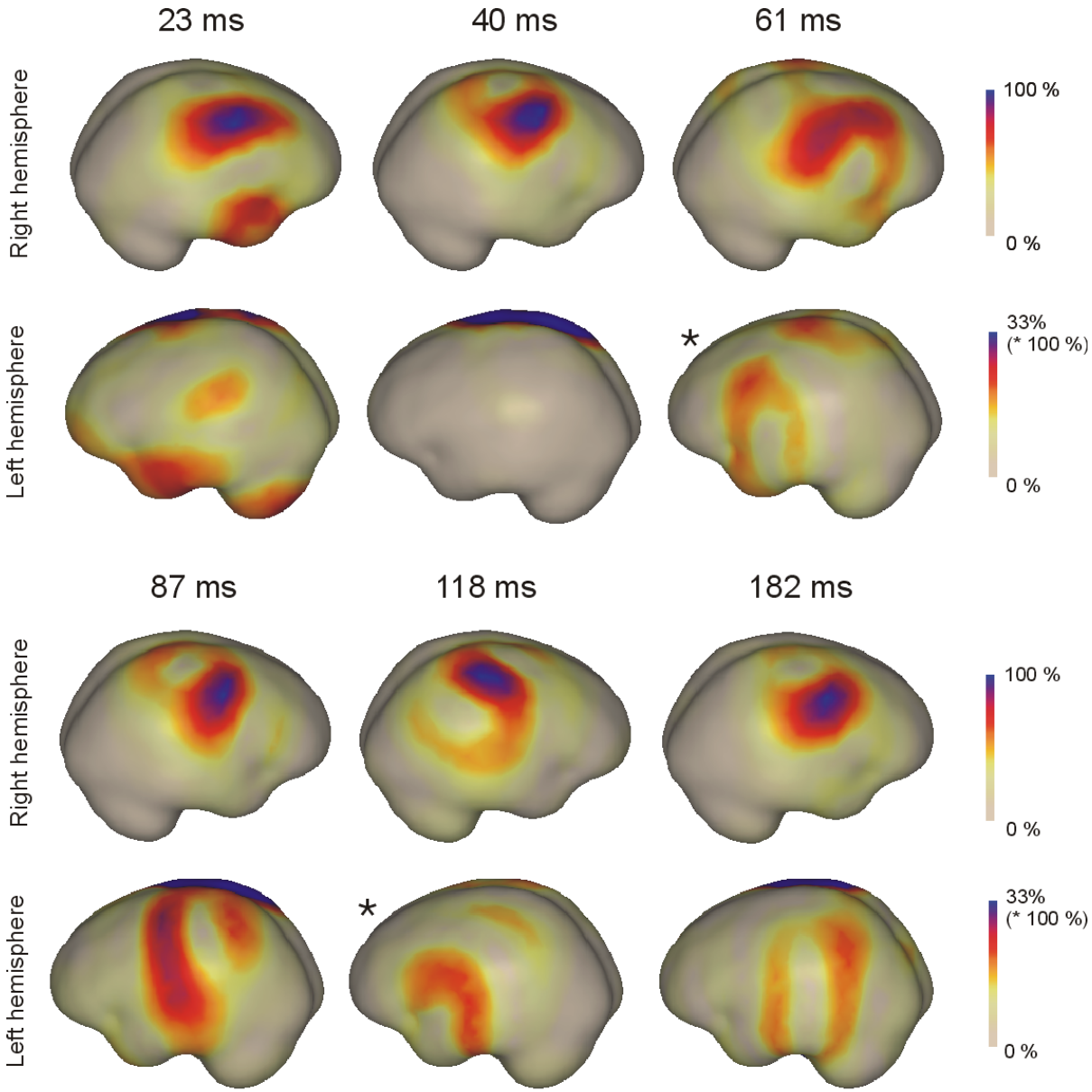

Figure 2.3: *Minimum norm images of the evoked brain activity at peak latencies of the Global Field Power. Note the different scaling for left and right hemisphere.*

ever, the resulting centers of activity did not correspond to SI and SIIc. Rather on the contralateral side two foci emerged. One of them can be assigned to SI, while the other suggested medial activity over the posterior parietal area. Ipsilateral activity, however, was well centered around SIIi after applying this weighting method. The differences in spatial extent of the source depended on the applied weighting method. This indicates that minimum norm techniques are not suitable for estimating the spatial extent of the

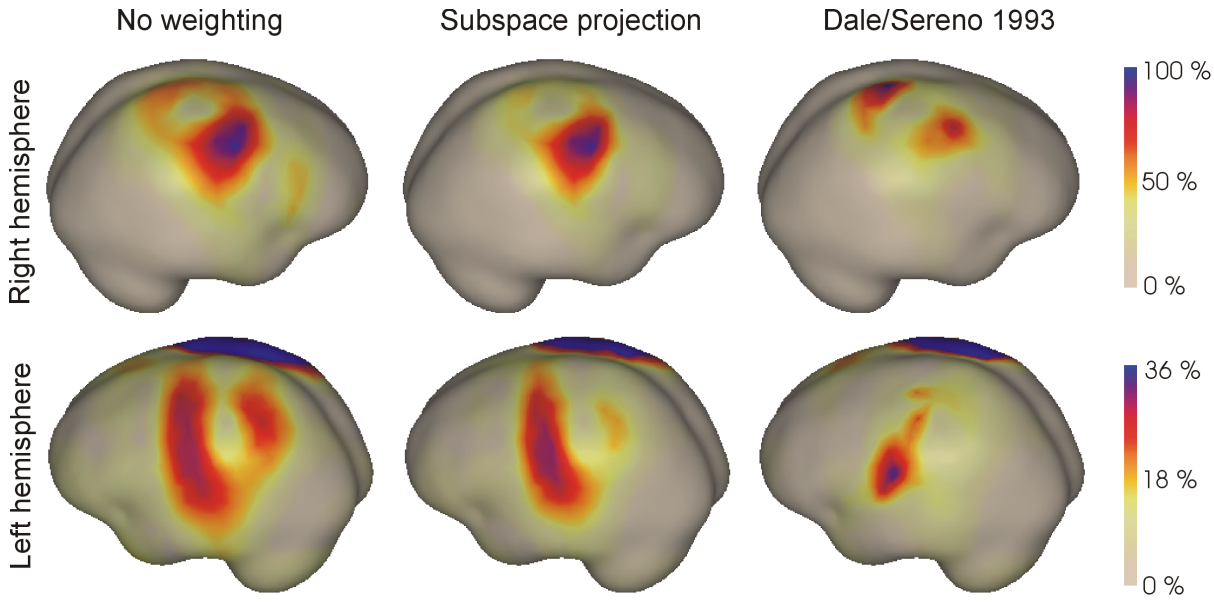

Figure 2.4: *Influence of spatio-temporal weighting by single dipole scans on minimum norm images of the evoked brain activity at* 87 *ms.*

active brain region, although this might be suggested by the direct visualization on the brain surface.

The example demonstrates that the distributed source model is not capable of separating activity in SI and SIIc. Contralateral activity is dominated by the shallow SI source, while SIIc, located in the Sylvian Fissure, projects to an area on the brain surface very close to SI. Consequently, spatial blurring of the current distribution that is inherent in the method leads to a large overlap. A quantitative evaluation of the activity in the different cortical areas is precluded by this substantial smearing that strongly depends on the applied weighting method. These ambiguities contradict the claim for an objective data analysis. Accordingly the goal to reach a solution of the inverse problem without use of pre-assumptions about the activity distribution can not be reached by this method. Fortunately, the knowledge about the specific properties of the somatosensory system (section 1.5) can be exploited by the employment of discrete source models as will be demonstrated in the following sections.

2.3.4 RAP MUSIC

The Multiple Signal Classification (MUSIC) algorithm [111] is based on a decomposition of the data space (defined by the matrix $\tilde{b}$ in equation 1.24) into the principal components of its covariance matrix. The assumption is that the evoked activity is contained in the

components with large principal value, while the remaining components mainly contain channel noise. Therefore noise filtering can be achieved by reducing the data space to the signal subspace spanned by a few major principal vectors. A regional source is moved along a predefined grid within the unit sphere and the correlation p of its topography (defined by the leadfield, cf. equation 1.23) to the signal subspace computed. The location with the highest p value is considered optimal. The Recursively Applied and Projected (RAP) version [110] allows for a modeling of several sources with no mutual spatial and temporal correlation. It is possible to model two active sources with highly temporally synchronous activity, e. g. bilateral sources in the auditory cortex. If a predefined correlation threshold cannot be reached with one regional source, the scan is repeated with two sources that are assigned to the same topography. The method of sequential brain source imaging [130] is applied that subtracts from the signal subspace the projection of the source topography into that space. If desired, another regional source scan is performed on the remaining subspace.

The left panel of Fig. 2.5 shows the main principal vectors of the data covariance matrix in our example in the time interval of 20–200 ms. Only the five components contributing to more than 1 % to the data were considered to contain evoked activity and defined to span the signal subspace. Using anatomical knowledge (cf. section 1.5) three or four active sources could be expected (SI, SIIc, SIIi and possibly PPC), of which SIIc and SIIi might evolve strongly correlated in time. Therefore two sets of parameters were chosen: in Fig. 2.5a, the algorithm scanned for three single dipolar topographies, while in Fig. 2.5b a correlation threshold of 90 % was required, and if not reached a two-dipolar topography was assumed. The resulting source waveforms looked very similar. The first activated source represented SI with a localization corresponding to the contralateral central sulcus. The second source found by the algorithm in both cases corresponded to SIIi and was located in good agreement with known anatomy. The main difference between the two approaches was seen for the third topography. The one-dipolar scan assigned it to a region medial and posterior to SI, corresponding roughly to the PPC area. When a two-dipolar topography was allowed, however, two sources were found (circled in Fig. 2.5b), located in the area of SIIc and inferior to SI.

The discrete source modeling of RAP MUSIC gave the advantage to obtain discrete source waveforms that did not interfere with each other, i. e. the compound signals recorded by the individual channels (Fig. 2.1) could be separated into source waveforms that were uncorrelated to each other. However, the assignment of these temporal evolutions to brain areas was ambiguous for the third component. The fact that several sources were active in the contralateral hemisphere seemed to cause interactions that could not be resolved unambiguously. The reason are two fundamental properties of the MUSIC algorithm that are not appropriate for modeling somatosensory evoked brain activity:

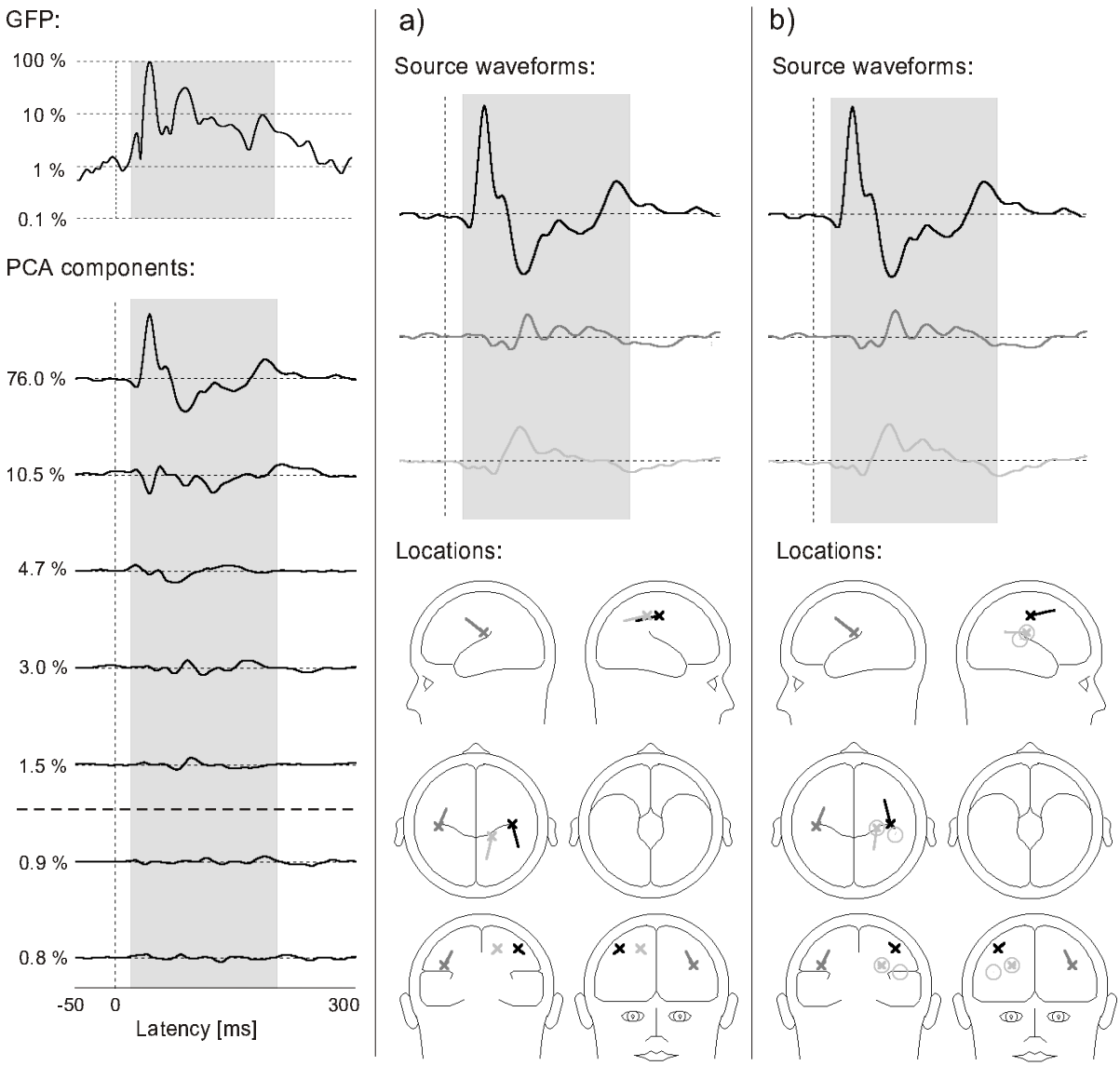

Figure 2.5: *A model consisting of three spatial components as obtained from the RAP MUSIC algorithm with sequential brain source imaging. Shaded areas indicate the time interval used for calculation of the principle component analysis (PCA). a) Model consisting of three single-dipolar topographies. b) Model consisting of two single-dipolar and one two-dipolar topography.*

- A basic assumption is the temporal and spatial orthogonality of the source activities that is inherent in the principal component decomposition. This is not necessarily true for neuromagnetic activity. In the case of tactile evoked fields, considerable spatial correlation between the contralateral topographies can occur that prevents a valid separation of these areas. In addition, the temporal activity patterns of the two SII areas are closely correlated to each other. However, they are not highly

synchronous either (as is the case e. g. for auditory evoked brain currents in the left and right auditory cortex). Therefore even a two-dipolar topography can not solve the problem.

- In RAP MUSIC, one epoch has to be selected over which the principal component analysis is to be calculated. This does not account for the different activation periods of the active brain areas. An optimal mapping method should make use of this fact as well. This concept is realized in sequential dipole fits that are demonstrated in the following section.

2.3.5 Sequential dipole fitting

In response to peripheral stimulation usually distinct circumscribed brain regions are activated at different latencies. The concept of sequential dipole fitting [128, 130, 131, 132, 133] takes into account these facts. Source activities are separated by modeling each source as discrete equivalent current dipole or regional source as described in section 1.3. Sources can be assigned individual fit intervals and are fitted consecutively. A common approach is to search for the earliest activated source first, then fix its location and orientation while searching for additional sources in later time intervals. The method employs the Genetic [46] or the Simplex algorithm [122] to determine dipole locations and orientations inside the model sphere that minimize the residual variance (equation 1.25) within the chosen time window.

Phantom experiments with artificial current sources were conducted in order to test for the location accuracy of this method. Approximately dipolar magnetic field patterns were generated by sinusoidal currents sent through conducting wire segments of 7 mm length. They were placed under the dewar with known distances to each other that ranged from 2 to 15 cm. Equivalent current dipoles were fitted to the measured MEG data using the Simplex algorithm. The determined distances between the fitted dipoles deviated by less than 1 % from the actual values, which documented the accuracy of the fit algorithm.

Figure 2.6 illustrates the application of sequential dipole fits on somatosensory evoked data. The global field power (GFP) was used as an aid for the choice of the fit intervals. First the epoch between 20 and 53 ms was selected to fit one dipole. This resulted in the source in SI with components at 23 and 42 ms that accounted for the first two peaks in the GFP. These components are known from literature and termed N20m and P40m [87]. The second major peak in the GFP was analyzed by choosing 70–100 ms as next fit interval. Since SI might still be active in this time interval, the corresponding dipole was left active during the fit but fixed in position and orientation. Two additional sources were searched for by the fitting algorithm. Due to local minima, the output of the

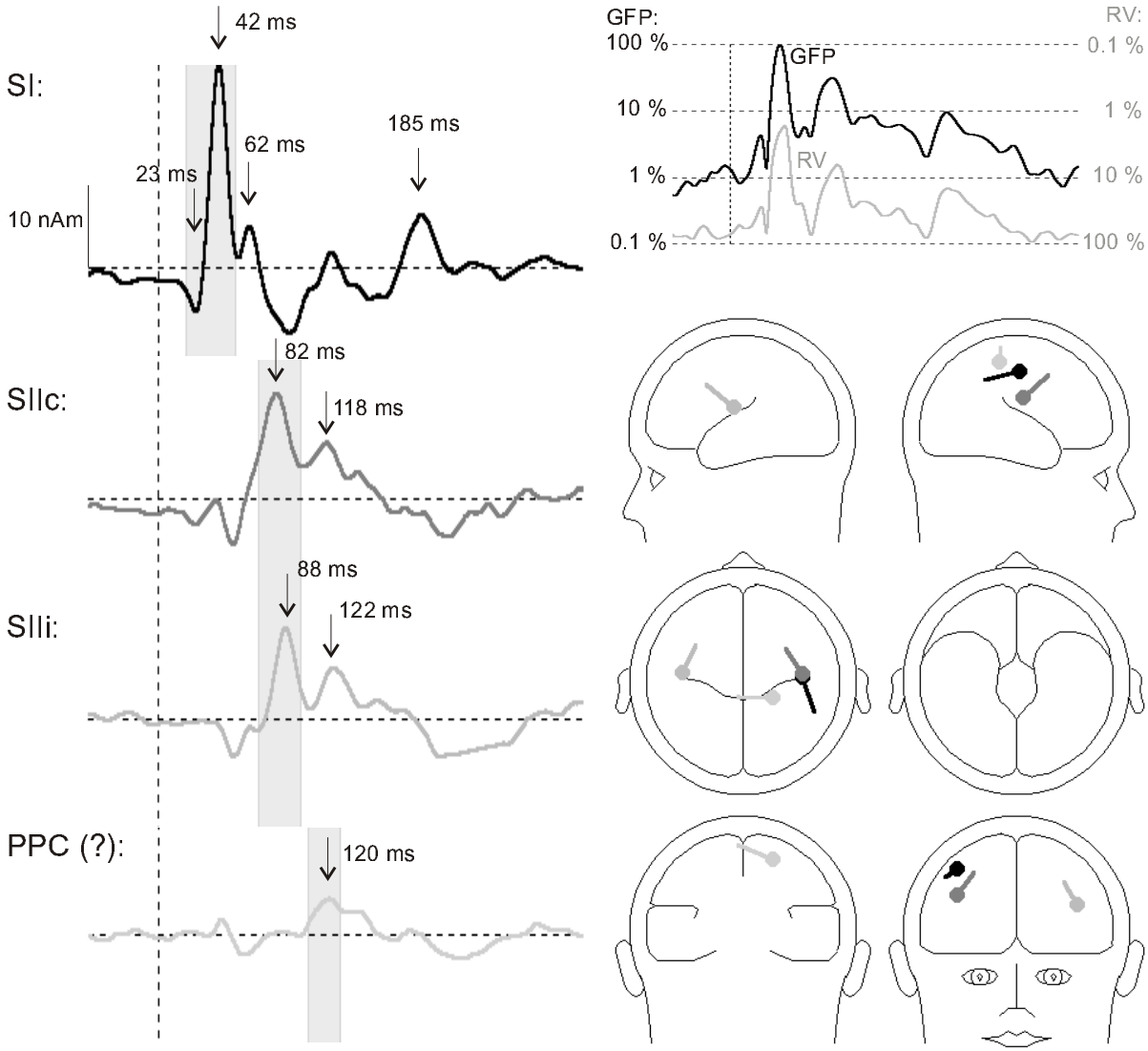

Figure 2.6: *A model consisting of four equivalent dipoles as obtained from a sequential dipole fit. Shaded areas mark the time interval chosen for localization of the corresponding source.*

algorithm, especially of the Simplex applied here, may depend on the starting point for the dipole search when two sources or more are fitted simultaneously. According to the knowledge of the physiological properties of the somatosensory system (section 1.5) and the information obtained from the imaging methods described in the previous chapters, two temporal dipoles were set bilaterally as initial configuration. The result of the fitting routine were bilateral sources with nearly symmetric locations and orientations. They correspond to the SII region in each hemisphere. The source waveforms in Fig. 2.6 show the close temporal correlation of the activity distribution in the two SII areas. The fact that SIIc components occurred 6 and 4 ms earlier than the corresponding ipsilateral peaks

(cf. Fig. 2.6) is characteristic for the SII areas [60, 138]. As a measure for the quality of the obtained model, the residual variance (RV) wan be plotted in one diagram with the global field power. If a logarithmic scale for the GFP and an inverse logarithmic scale for the RV is chosen like in Fig. 2.6, a good explanation of the data has its correlate in a nearly parallel time course of the two curves. Sensor signals in intervals with low GFP are determined by noise and consequently the corresponding residual variance is large. The obtained three dipole model explained the data very well according to this criterion. The overall residual variance in the time window from 0 to 200 ms was 17.1 % with a minimum of 1.9 % at 45 ms. An attempt to account for left unexplained signal between 105 and 127 ms resulted in a fourth dipole, corresponding to the PPC area. However, its activity was weaker than that of the other sources and its temporal evolution did not agree with previously reported PPC activity [36]. If only SII activity is to be examined, it is not essential to model this source, since its existence does not alter the source waveforms of SIIc and SIIi significantly.

The obtained model produced a clear separation of the brain activities evoked by tactile finger stimulation. This was due to the lack of mathematical assumptions like spatial and temporal orthogonality of the source topographies, but instead exploitation of physiological knowledge by defining individual fitting epochs and initial locations for the dipole fits. Fit quality and source separability vary between subjects and also depend on data quality. SII source localization fails in some data sets due to low signal and individual differences in brain gyration — subjects with substantial radial components in SII do not produce strong extracranial magnetic fields from that region. Sometimes better results are obtained when SIIc and SIIi are fitted consecutively with fit intervals of 65–90 ms (SIIc) and 75–100 ms (SIIi), for example. However, a dipole fit can be considered stable only when source location and orientation are not sensitive towards small changes in the selected fit interval. The judgment of the quality of an obtained source model thus depends to some extent on subjective criteria defined by the experimenter. In the studies presented in the following chapters, neither the PPC source nor a previously reported source in the mesial frontal cortex [39] was found consistently over subjects and therefore a model of three dipoles was sufficient to account for the measured data.

2.4 A mapping strategy for the analysis of group data

For the analysis of somatosensory evoked fields, the spatial location accuracy of sequential dipole fits must be considered superior to the other techniques that have been presented above. Nevertheless, statistical errors between measurements as well as systematic errors

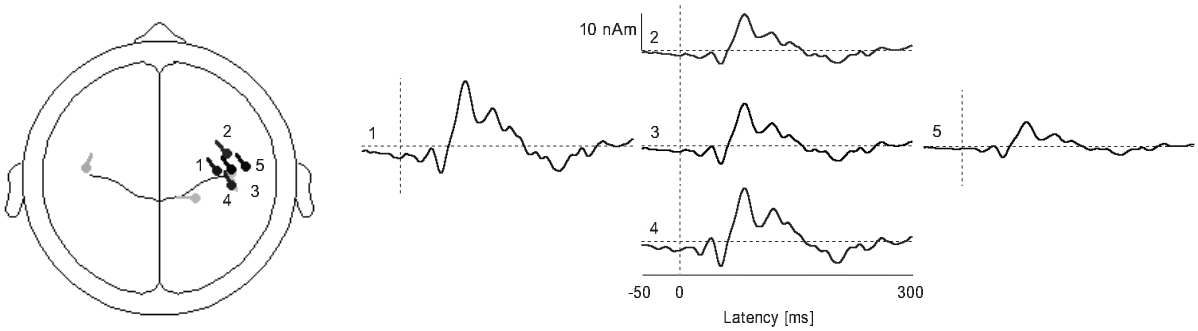

Figure 2.7: *Effect of source location on the source waveform. Amplitudes mapped onto deep sources are larger than those of shallow sources.*

occur (e. g. due to the simplification of a spherical head model, Fig. 1.10). The power of MEG therefore is primarily its superior temporal resolution of cortical activity. Hence in the analysis of data obtained from several subjects under equal stimulation conditions the prior goal usually is to obtain a mean temporal evolution of the activity of a certain brain region rather than to get information about the exact location inside the brain. This is achieved by taking the grand average of the corresponding source waveforms over all subjects and performing a suitable statistics to obtain an error estimate. One is faced with two main problems of this approach:

- An error in dipole location can affect the amplitude of the corresponding source waveform considerably. This effect is illustrated in Fig. 2.7, where the SIIc source was shifted by 1 cm radially and tangentially with respect to its fitted position. Whereas morphology and peak latencies of the corresponding source waveforms were not changed significantly, the amplitudes are very sensitive to source depth. This effect must be compensated for before taking the grand average in order to prevent overrating of waveforms that resulted from deep source localization.
- Due to noisy data it might be impossible to obtain a stable dipole fit for the SII regions in some subjects, even though the corresponding data sets do contain signals from that region.

A solution for both problems is reached by combining the fitting results with a seeding technique that makes use of the individual MR images. The method employs a transformation of the individual MR data sets into the standardized Talairach coordinate system [142]. It is based on a division of each individual brain into twelve cuboid compartments defined by the anterior, posterior, superior, inferior, left- and rightmost point of the gray brain matter and the anterior and posterior commissure. Each compartment is stretched or compressed to match standard dimensions defined in the brain atlas by

Talairach and Tournoux [142]. The resulting Talairach coordinates of a specific brain area (in this case the secondary somatosensory cortex) are roughly the same for all healthy subjects, independent of the size and shape of the individual brain. By applying this transformation using the BrainVoyager™ 2000 software, a method for analyzing group data can proceed as follows.

1. For each data set an attempt is made to fit the locations of SIIi and SIIc as described in section 2.3.5.
2. If a stable fit solution for an SII source can be obtained, the transformations between unit sphere and MR coordinates and between the MR and Talairach coordinate systems are applied to determine the Talairach coordinates of the dipole location.
3. The mean Talairach coordinates of the fitted dipoles over all subjects are calculated. These locations serve as reference coordinates for all subjects.
4. The inverse transformations are applied to place a dipole at this mean Talairach coordinates in each individual, including the subjects for which a fit of the location could not be performed.
5. The orientation of each SII dipole is fitted to the individual data in a time interval that comprises the maximum activity in SII (e. g. 65–90 ms for SIIc and 75–100 ms for SIIi).
6. The resulting source waveforms can now be averaged and used for further statistics.

Fig. 2.8 illustrates the effect of this method when applied to ten measurements with different subjects using the same paradigm (cf. section 2.2.1). In three subjects stable fits of dipoles representing SIIc could not be obtained. After seeding dipoles to the mean fitted Talairach position, even in these subjects waveforms could be mapped that were consistent in morphology with the typical SII activity as shown in Fig. 2.6.

The introduced procedure makes use of the fit results as much as possible. By taking their mean Talairach coordinates, statistical errors that manifest themselves in varying localization are corrected, while possible systematic errors inherent in the fitting routines are accounted for. This implies that the resulting mean SII location might well be slightly off the anatomical correct position, for example as a consequence of the simplified head model (cf. Fig. 1.10). This has to be accepted in order to map realistic source waveforms. An exclusive seeding technique that places dipoles from the individual MRI at the anatomically correct position in the parietal operculum would possibly lead to distorted source waveforms. For the same reason functional magnetic resonance images

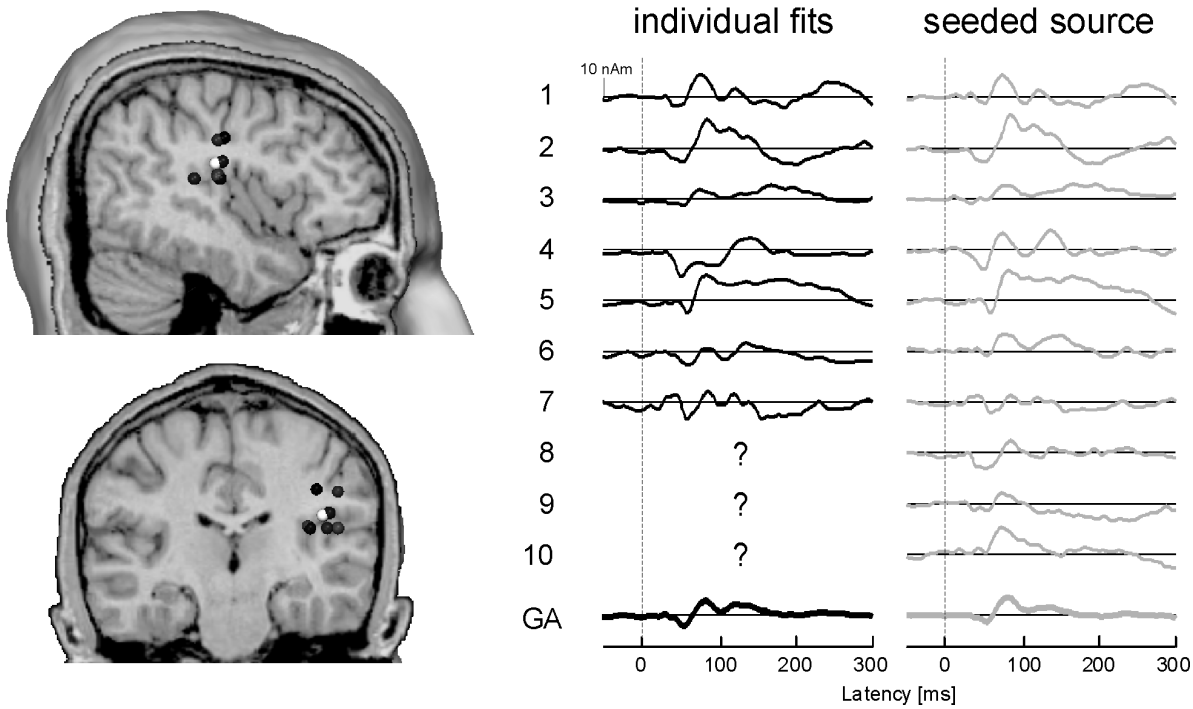

Figure 2.8: *Illustration of the combined fitting and seeding technique. In seven of ten subjects stable fits for SIIc could be obtained. Shown in black are the locations (left) and the corresponding source waveforms (middle). Seeding sources at the mean fitted Talairach position (gray) allows for mapping source waveforms in all ten subjects (right). The corresponding grand average waveforms (GA) are shown in the bottom.*

(fMRI) can only serve as approximate indicator for expected MEG dipole locations. In a recent study comparing MEG and fMRI localization, mean distances between the foci of activity determined with both methods were 7 mm for SIIc and 22 mm for SIIi, repectively [91]. These differences were partly also due to the fact that fMRI detects changes in blood oxygenation level that do not necessary take place at the same location as the neuronal activity. In addition, several regions in the parietal operculum might be active that contribute differently to MEG and fMRI signals [5]. This issue is investigated in the following chapter.

2.5 Conclusion

All different modeling techniques presented above have special properties that make them appropriate for certain types of cortical activity patterns. Data produced by only one dipolar source, for example epileptic spike activity, can well be mapped with minimum

norm approaches. RAP MUSIC is capable of mapping spatially and temporally uncorrelated brain activity. The case of somatosensory evoked fields is less simple. Three dipoles need to be modeled which are spatially and temporally correlated with a latency lag between SIIc and SIIi. Sequential dipole fits represent the appropriate approach to deal with these circumstances. This technique manages to map source waveforms with minimum mutual interference. However, other approaches still can give clues to where and when a certain brain region can be expected to be active. The time intervals for the sequential fits can be chosen under consideration of this information. Systematic and statistical errors inherent in all mapping methods make it necessary to direct the focus of interest to the temporal information rather than exact localization. Therefore, the seed of sources from individual MR images should always be based on fit results in order to account for systematic errors that might occur due to simplifying assumptions underlying the MEG model. The approach presented in section 2.4 demonstrates the application of this maxim to the analysis of data from different subjects.

Chapter 3

Comparison of MEG and EEG

3.1 Introduction

The considerations concerning the solution of the inverse problem (section 1.3, chapter 2) hold for both magneto- (MEG) and electroencephalography (EEG). Whereas in magnetoencephalography magnetic fields or field gradients outside the head are detected, electroencephalography records the electric voltage distribution on the scalp surface. Dipolar source modeling applied on the data should in principle lead to equal localizations. However, this must be reconsidered under the light of the different generator mechanisms. While the volume currents J_v (equation 1.12) have only a minor contribution to the extracranial magnetic field, they are essential for the generation of the scalp potential distribution. Therefore in EEG data analysis the different values of the electric conductivity σ of the brain tissues, the cerebral spinal fluid and the skull have to be considered and modeled appropriately. The consequence is a greater sensitivity of EEG source localization to inaccuracies of the underlying head model. This is the main reason for localization errors in EEG. Currently attempts are made to reduce this deficiency of EEG source localization by the development of more accurate realistic head models. The quality of MEG verus EEG localization accuracy has been an object of debate between advocates of both methods in the past decade [27, 57, 96, 104, 152].

A second important difference between MEG and EEG has been derived in section 1.2. MEG is dominated by neuronal currents in brain fissures that are oriented tangentially to the head surface. EEG signals, on the contrary, predominantly reflect radial cortical activity. This fact likely accounts for discrepancies of reported latencies of SII activity. Literature data range from 80–90 ms [87, 100, 106, 150] to 130 ms [41, 45, 109, 147], and some reports note the existence of two components [3, 5, 139].

In this chapter the brain response to tactile stimuli was recorded using MEG and EEG simultaneously. The study was performed in order to pursue the following questions:

1. How do the two methods differ with respect to their ability to localize the secondary somatosensory cortex and to map SII activity?
2. Are there different generators of activity in SII and how is their relative contribution to the signals recorded by EEG and MEG?

The consistency of the results with the common theory of EEG and MEG models is evaluated. Conclusions are drawn for the suitability of both methods to image activity in SII.[1]

3.2 Materials and methods

3.2.1 Stimulation paradigm

The study was performed with 16 healthy subjects. The tactile stimulation paradigm was the same as that used for the sample data set in chapter 2 with pressure pulses delivered to the first (20 %) and second (80 %) phalanx of the index finger in pseudo-random order. The interstimulus interval was 1.03 s. Each subject participated in one measurement consisting of five blocks of ten minutes duration each: in the first and the fifth block stimuli were delivered to the index of one hand, in the second and fourth to the other hand. An auditory stimulation was presented in the third block. It was not subject of this investigation. In order to direct attention towards the stimulus, subjects were instructed to silently count the deviant stimuli to the first phalanx.

3.2.2 Data recording and source modeling

EEG electrodes were fixed to the subject's head using an EEG cap by Falk Minow. Commercially available electrode paste was applied to provide a resistance smaller than 5 kΩ between electrode and skin. 61 electrodes on the scalp surface and two earlobe-electrodes were used for EEG recording. The electrodes were approximately evenly distributed across the scalp. The exact positions were digitized before each measurement. Fig. 3.1

[1] This study was performed in cooperation with the group of Prof. R.-D. Treede, Institut für Physiologie und Pathophsiologie, University of Mainz, and funded partly by the Deutsche Forschungsgemeinschaft (DFG).

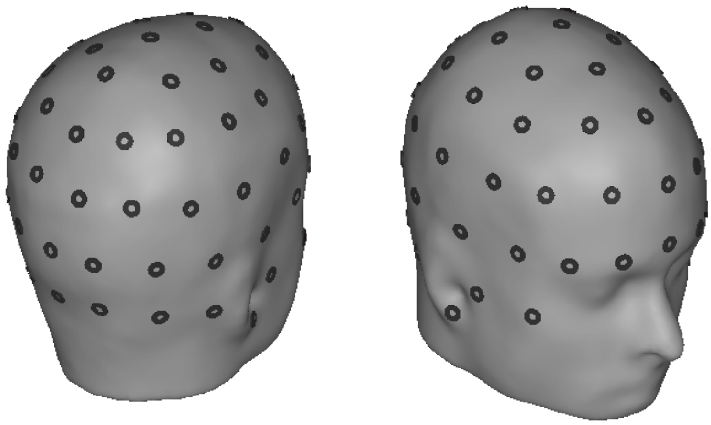

Figure 3.1: *Electrode positions of the 61 channel cap for one subject.*

shows the electrode locations of one subject. In addition, an electrocardiogram (ECG) was recorded in order to identify heartbeat artifacts. During the measurement the subject sat under the dewar with the electrode cap fastened, so that EEG and MEG could be recorded simultaneously.

Data was bandpass-filtered between 0.03 Hz and 160 Hz during recording and sampled at a rate of 500 Hz. An epoch of 300 ms pre- and 1000 ms post-stimulus was averaged. Epochs with amplitudes larger than 1000 fT/cm (MEG) and 100 μV (EEG) or gradients exceeding 800 fT/cm per sample (MEG) and 75 μV per sample (EEG), respectively, as well as silent or excessively noisy channels were excluded from averaging. A baseline correction was performed using the 100 ms pre-stimulus period. For further analysis only the 10 measurement sets with the least number of bad channels and the highest signal-to-noise ratio were used. Of the 10 remaining subjects seven were male, nine right-handed, their age was 22.6 ± 1.1. Only data from stimulation of the second phalanx was evaluated because of the larger number of averaged trials (402.4 ± 32.9 left and 404.4 ± 33.8 right) compared to the first phalanx. Subsequently data was digitally filtered offline between 3 Hz (zero-phase, 6 dB/oct) and 70 Hz (zero-phase, 12 dB/oct).

For EEG data analysis each subject's head was modeled as a sphere with a radius equal to that used for MEG modeling. As opposed to MEG, EEG data depends on the distribution of the electric conductivity σ inside the head (equation 1.15). Therefore the different values of σ for brain tissue, cerebral spinal fluid, skull and scalp were approximated by dividing the sphere into four shells with relative conductivities $\sigma_r = 0.33$ (brain), $\sigma_r = 1.00$ (cerebral spinal fluid, thickness 1 mm), $\sigma_r = 0.0042$ (skull, thickness 7 mm) and $\sigma_r = 0.33$ (scalp, thickness 6 mm) [7].

Discrete sequential source analysis was performed to obtain models independently for EEG and MEG data. MEG source modeling was applied to each individual data subset.

A common reference model used for final MEG data evaluation was determined according to the procedure for the analysis of group data as described in section 2.4. Because Magnetic Resonance Images were not available for the subjects of this study, unit sphere coordinates were chosen instead of Talairach coordinates to provide a reference coordinate system that was approximately independent of the individual head shape. To obtain a reference model for the EEG data, grand averages were calculated. For each subject and each stimulation site the measurement with the least number of excluded EEG channels was selected. Of the remaining 10 data subsets for each stimulation site, averaged signals were calculated for each channel. Electrodes that were not included in all measurements were excluded from this process. Mean electrode positions were calculated from the digitized 3D coordinates. The EEG reference model was obtained by fitting sources to this fictitious data set for both stimulation sites.

3.2.3 Statistical analysis

For comparison of the source waveforms obtained from discrete sequential source fits (cf. section 2.3.5), individual source waveforms were averaged. 90 % confidence intervals were determined using the Bootstrap-BC_a method [32] with 1000 randomly drawn bootstrap samples of the data (MATLAB® 6.0). This method allowed for calculation of confidence intervals without any prior assumptions about the distribution of the individual waveforms, e. g. a Gaussian distribution. Latencies of the grand average source waveforms were determined after interpolating 10 additional time points in each 2 ms sample interval using cubic splines (MATLAB® 6.0). Individual peak amplitudes and latencies were determined. For each subject the average values of the two measurements with equal stimulation sites were calculated. A multivariate analysis of variance (MANOVA, GLM procedure, SAS® 6.12) was performed on these values to test for effects of the factors stimulation side (left versus right) and hemisphere (ipsi- versus contralateral) for each recording method. Differences between EEG and MEG were analyzed by a two-tailed Student's t-test for correlated observations.

3.3 Results and discussion

3.3.1 Spatio-temporal source analysis

In order to compare the source waveforms obtained from EEG and MEG data, it was necessary to employ comparable source models. However, the different properties of EEG and MEG as described above had to be taken into account. Fig. 3.2 shows the data of

one subject evoked by right index stimulation and illustrates the main differences in somatosensory evoked EEG and MEG source modeling. The left diagrams depict the Global Field Power (GFP) of the recorded data. Both curves show a significant peak around 40 ms, known to be generated mainly in SI. The second component around 80 ms is also visible in both recordings. Its overall power relative to the 40 ms component was higher in the MEG Global Field Power. This is the latency of maximum SII activity in MEG recordings (cf. section 2.3.5). However, also SI was still active at this time point. The most striking difference between the two graphs is the absence of the dominant EEG component around 134 ms in the MEG data. The latency agrees with literature reports on SII latencies in EEG measurements [45, 147]. In the following, these two SII components corresponding to the peaks in the GFP of the EEG data are termed P80 and P130, respectively.

In the middle and right panels of Fig. 3.2, models obtained from fits to the GFP peaks are shown. The example demonstrates specific properties of both recording methods. In the EEG example, an equivalent dipole representing SI was obtained by choosing a fit interval of 16–50 ms (dipole 1). An attempt to model the P80 component with two independent dipoles failed, resulting in unstable source configurations that are implausible on the basis of the physiological facts. Therefore a symmetry constraint was imposed on dipoles 2 and 3 that enforced source localization in analogous positions in the two hemispheres. The selected fit interval was 60–100 ms. Subsequently these dipoles were deactivated in order to fit sources accounting for the P130 component (dipoles 4 and 5, fit interval 120–160 ms). The resulting model and the corresponding source waveforms illustrate the deficits of EEG data analysis: while localization of sources 2 and 3 roughly agreed with the known location of SII in the upper wall of the Sylvian Fissure, dipoles 4 and 5 were in bad agreement with physiology. In addition, localizations strongly depended on the exact fit interval and varied substantially between subjects. The reason could be derived from the obtained waveforms of the SII sources. The fitted components (P80 and P130, respectively) occurred embedded into a high background noise activity. α-rhythm (with a frequency of around 10 Hz) contributed to this background, but also other spontaneous brain activity. In some cases, these rhythms could have been accounted for by modeling them as regional sources or spatial components [8], however the results were not consistent between subjects. Moreover, such additional sources tended to interfere with the activity under investigation and thus themselves induced distorted source waveforms. The contamination of averaged data by such signals was much higher in EEG than in MEG, probably due to the predominantly radial orientation of the underlying generators. Therefore, the ability of EEG to image radial components turned out to be disadvantageous because too many active regions induced activity at the recording electrodes.

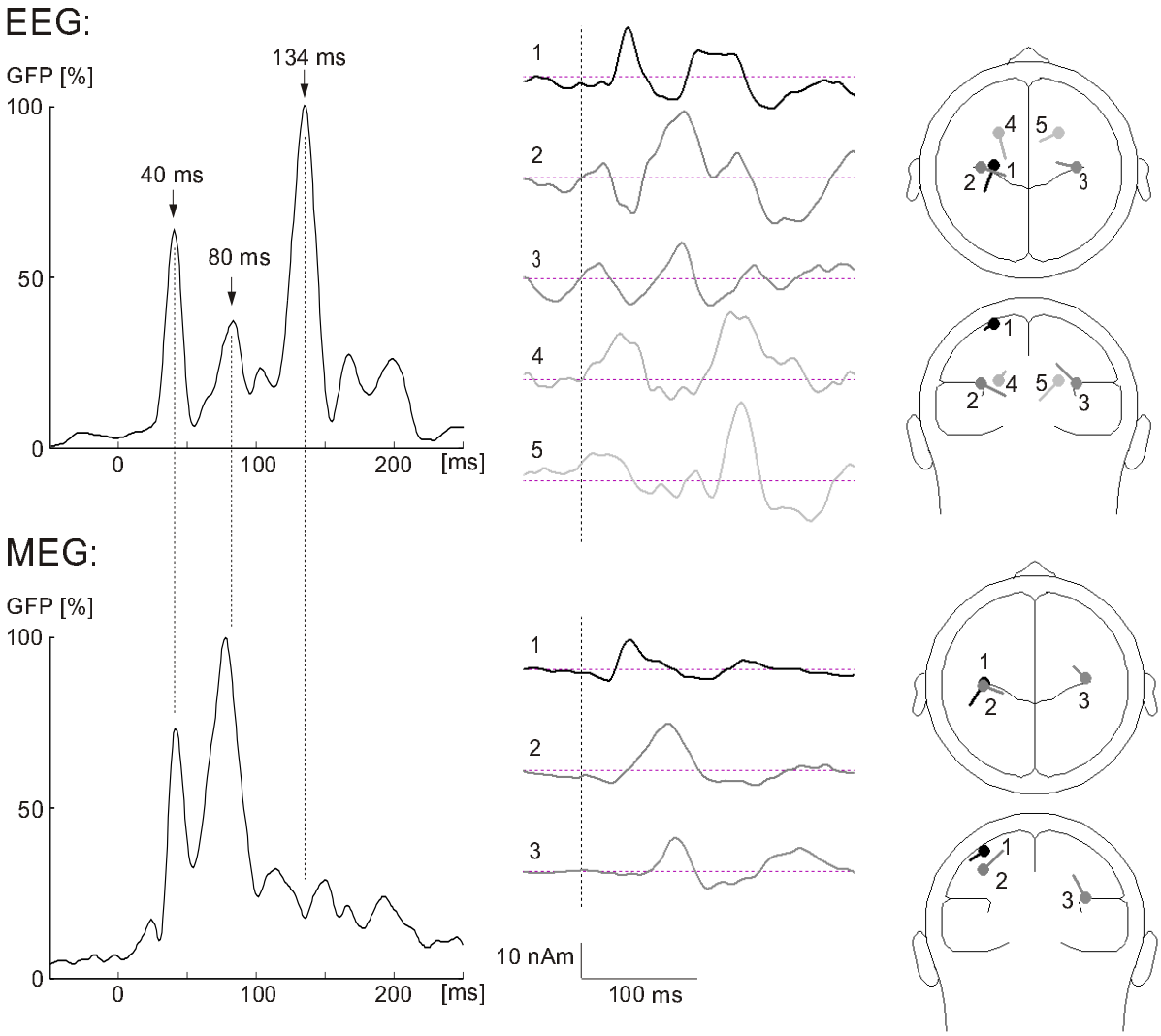

Figure 3.2: *Comparison of EEG (top) and MEG (bottom) source analysis in one subject.*

As opposed to EEG, MEG data could be analyzed with a sequential fit of three independent dipoles as described in section 2.3.5, although the dipole representing contralateral SII localized slightly too high in this subject, probably due to interference with the SI activity in the same hemisphere. The corresponding waveforms were nearly undisturbed by background noise and the SII components around 80 ms clearly dominated the evoked response.

Table 3.1 lists the number of subjects for which a stable dipole fit to SII could be established in at least one of the two measurements for each stimulation side. Even when imposing a symmetry constraint on the two SII dipoles, localization of SII was possible in not more than 5 out of 10 subjects. The numbers refer to fit attempts to either the

	Stimulation left			Stimulation right		
	SIIc	SIIi	SII sym.	SIIc	SIIi	SII sym.
EEG	1	2	4	3	4	5
MEG	9	10	10	9	8	10

Table 3.1: *Number of subjects for which stable fits for SII could be obtained individually (SIIc and SIIi) or with imposed symmetry constraint (SII sym.). The numbers document the superiority of MEG in localizing SII.*

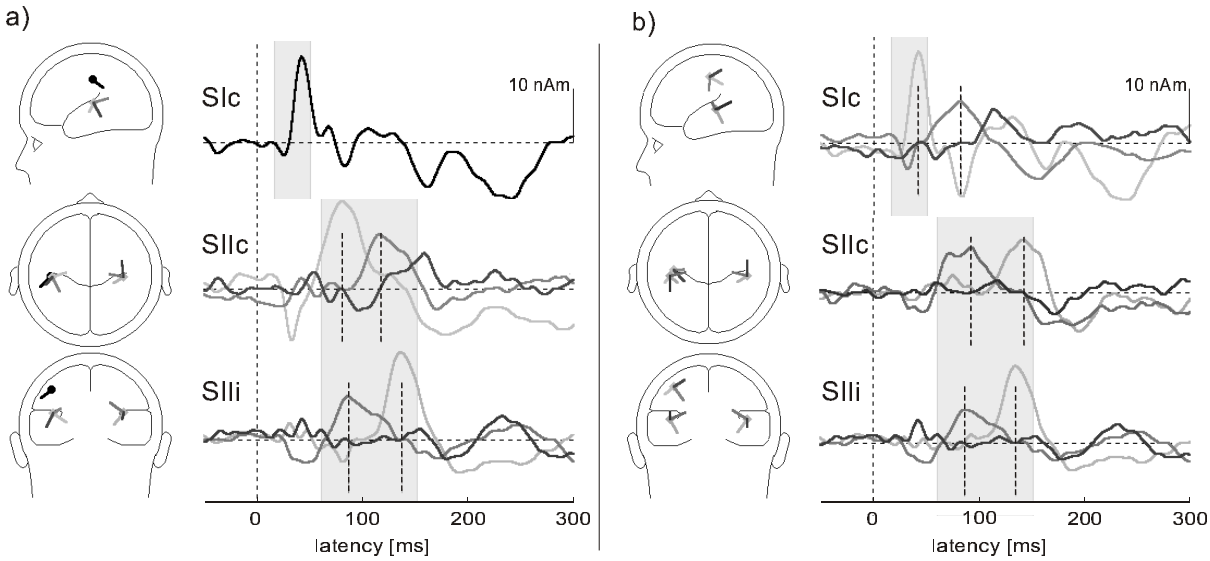

Figure 3.3: *Grand average EEG response to the stimulation of the right index with a) SI modeled as equivalent dipole and b) SI modeled as regional source. Waveforms of the 3 orthogonal components of each regional source are overplotted. Latencies and amplitudes of the SIIc waveform are significantly affected by the model strategy. Latencies of the maxima of the source waveforms are marked by dashed lines. Shaded areas mark the time interval that was chosen for localization of the corresponding source.*

early SII peak around 80 ms or the late component around 130 ms. Robust MEG solutions could be obtained in nearly all subjects, even when fitting SII individually in each hemisphere.

The inconsistency and instability of the individual EEG models made it impossible to determine a reliable reference model from the individual data fits. Therefore the grand average data was employed to determine the appropriate model. In order to examine components in SII with possibly different orientation, a regional source (cf. section 1.3) was chosen to model this region in each hemisphere. It is known that also SI activity contains radial as well as tangential activity [4, 147], resulting from activation of areas 1,

		Stimulation left			Stimulation right		
		x	y	z	x	y	z
SI	EEG:	0.41	0.09	0.58	−0.49	0.03	0.55
	MEG:	0.48	0.06	0.60	−0.50	0.03	0.56
SII	EEG:	±0.47	0.01	0.25	±0.43	−0.02	0.27
	MEG:	±0.43	0.09	0.31	±0.48	0.04	0.33

Table 3.2: *Unit sphere coordinates of the EEG and MEG sources.*

2, 3a and 3b (cf. Fig. 1.15 B). Fig. 3.3 illustrates the effect of SI modeling on SII waveforms using the grand average EEG following right index stimulation. SI was modeled as single equivalent dipole (a) and as a regional source (b). The waveform of contralateral SII was considerably affected by the SI model strategy, while SIIi in the opposite hemisphere was nearly unaffected. In Fig. 3.3 a, SIIc showed an early component around 25 ms that was not present when SI was modeled as regional source (Fig. 3.3 b). This component likely represented the early N20 component in SI and hence was falsely attributed to SIIc in Fig. 3.3 a. However, also the late components in SIIc were sensitive to the model. With SI modeled as single dipole, P80 and P130 were clearly discernible in SIIc, and their latencies were shorter than the corresponding SIIi components by 11 ms on average (indicated by the dashed lines). A regional source in SI significantly reduced the P80 component in SIIc and led to a latency shift of both P80 and P130. Now SIIc seemed to be activated later when compared to SIIi. From intra– and extracranial recordings it is known that the contralateral response precedes the corresponding ipsilateral components [37, 41, 65].Therefore it was concluded that for these late components a single equivalent dipole in SI was more appropriate to provide realistic mapping of SII activity. The shallower SI source tended to take over activity from the deeper SIIc source. In general, the more sources are modeled, the more likely mutual interference occurs. This problem affects EEG more than MEG data, since due its sensitivity to radial components more sources (3 components of a regional source as opposed to 2 in MEG) are needed to cover the complete orientation information from SII. It became evident from this example that ambiguities remained in the modeling of tactile evoked potentials that could not be resolved completely.

As a consequence of these results, models for further data analysis were chosen as follows.

- **EEG:** One dipole (representing SI, fit interval 16–50 ms) and two bilateral symmetrical regional sources (SII, 60–150 ms) were fitted to the EEG grand averages of the data of left and right index stimulation. The obtained model (in unit sphere coordinates) was then used to map the source waveforms in each individual measurement.

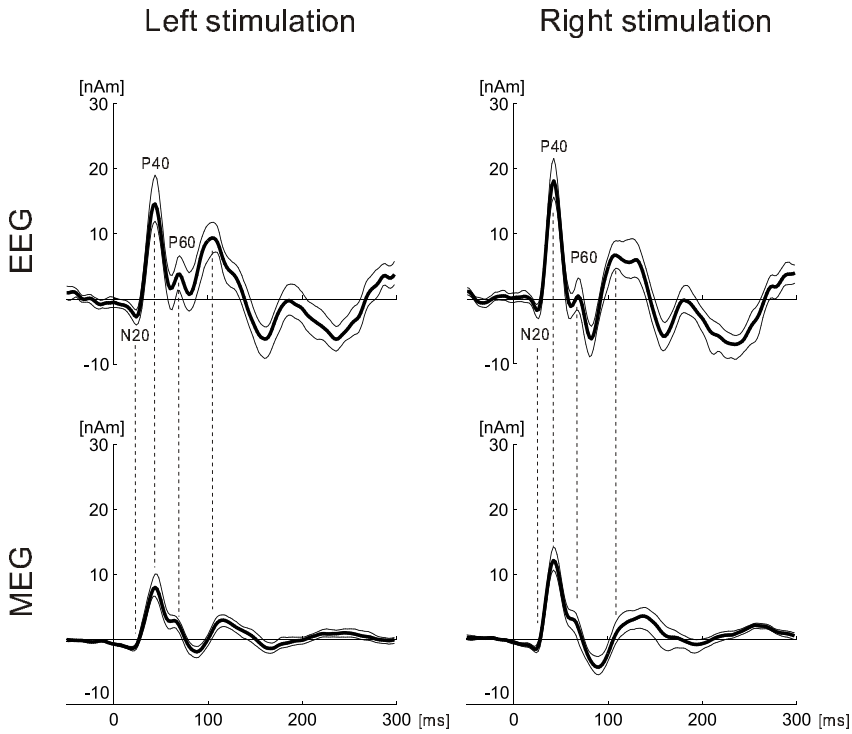

Figure 3.4: *Grand average of the SI source waveforms. Thin lines indicate the 90 % confidence interval.*

- **MEG:** In order to provide comparability with the EEG model, SII sources were constrained to be symmetrical in the MEG model as well. The same epochs as those used in EEG were chosen for fits to the individual data sets. The average unit sphere coordinates obtained from these fits were calculated. The individual source waveforms obtained with the resulting averaged model were used for final analysis.

Source locations of the final models are given in Table 3.2. The coordinates are comparable for EEG and MEG with the exception of a slightly larger z-coordinate (i. e. a more superior location) of the MEG SII sources when compared to their EEG counterparts.

3.3.2 EEG versus MEG components

Primary somatosensory cortex

Fig. 3.4 illustrates the grand average SI source waveforms. Both for left and right stimulation EEG and MEG waveforms showed very similar time courses in the early latency range. The activity around 20 ms was more prominent in the EEG recordings, probably

due to the contribution of a radially oriented source in area 1 [16]. The dominant component was the P40 with a clear hemispheric asymmetry. In MEG the response was 36 % larger after stimulation of the right index than after stimulation of the opposite finger ($t(9) = 4.472$, $p < 0.01$). In EEG the difference was 14 % and did not reach statistical significance ($t(9) = 1.32$, $p > 0.05$). EEG P40 amplitudes were on average 57 % larger than their MEG counterparts ($t(19) = 5.115$, $p < 0.001$). In the latency range between 50 and 200 ms waveform morphologies still resembled each other, but peak latencies did not coincide. EEG data contained more components and showed higher inter-subject variability compared to MEG, which led to larger confidence intervals. The larger number of components as well as the higher EEG waveform amplitudes over the whole time range can be attributed to the low sensitivity of MEG towards radial neural currents.

Secondary somatosensory cortex

The grand average of the individual SII source waveforms was calculated and the power P determined from the n components Q_i of each regional source according to the formula $P = (\sum_{i=1}^{n} Q_i^2)^{1/2}$ with $n = 2$ for MEG and $n = 3$ for EEG. The results are shown in Fig. 3.5. Mean amplitudes and latencies of the prominent peaks are listed in Table 3.3. All EEG power curves were dominated by two peaks with latencies around 80 and 130 ms. The early peak in the contralateral hemisphere likely resulted from SI activity that was not modeled by the SI dipole as discussed in section 3.3.1. In the MEG recordings, a small SII peak around 50 ms was followed by a dominant component around 80 ms. Also later activity between 120 and 150 ms was discernible.

EEG and MEG latencies were comparable for the component around 80 ms in the ipsilateral hemisphere (mean difference 0.8 ms, $t(17) = 0.81$, $p > 0.05$). However, contralateral SII latencies were on average 10.5 % shorter in MEG ($t(17) = 2.25$, $p < 0.05$). This was due to a significant latency lag of 9.7 ms in the grand average between SIIc and SIIi in the MEG data ($F(1, 9) = 7.52$, $p < 0.05$). Amplitudes of this component were 73 % larger contralaterally in MEG ($F(1, 9) = 49.29$, $p < 0.001$) and 54 % in EEG ($F(1, 6) = 0.07$, $p > 0.05$). The late components peaked significantly earlier in EEG than in MEG (11.5 ms ipsilaterally, $t(14) = 2.79$, $p < 0.01$ and 15.2 ms contralaterally, $t(13) = 1.59$, $p > 0.05$) with peaks around 130 ms (EEG) and 145 ms (MEG), respectively (compare Table 3.3). For these components, statistical analysis revealed no significant difference in latency or amplitude between SIIc and SIIi. The MEG components are termed P80m and P145m in the following, which takes into account the latency difference of the late components between EEG and MEG.

Whether the P80/P80m and P130/P145m peaks in the power curves of the two recording method belonged to separate SII components or possibly to one biphasic component was

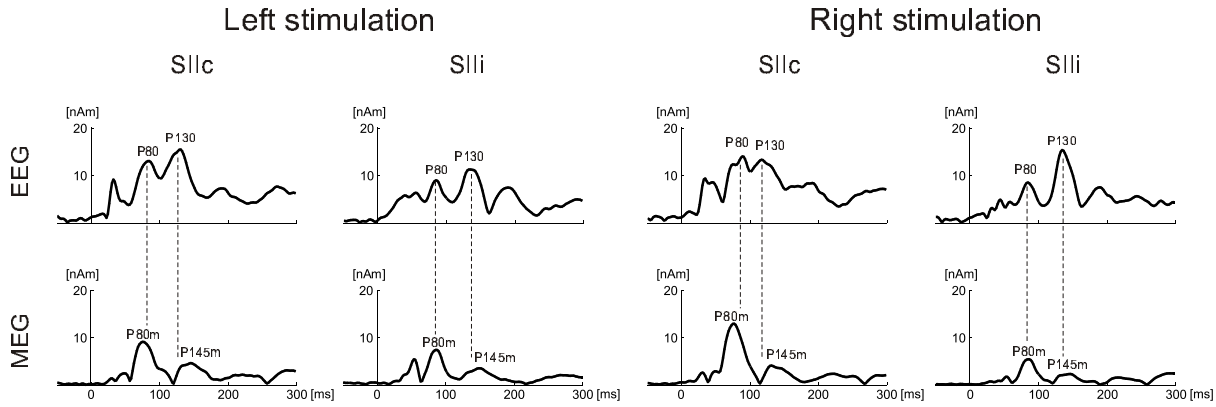

Figure 3.5: *Power of the grand average of the SII regional sources.*

		Amplitude [nAm]				**Latency [ms]**			
		Left stim.		Right stim.		Left stim.		Right stim.	
		SIIc	SIIi	SIIc	SIIi	SIIc	SIIi	SIIc	SIIi
EEG	P80:	13.1	9.0	14.1	8.6	83.3	84.7	88.8	84.0
	P130:	15.5	11.3	13.4	15.4	129.5	133.1	116.6	134.5
MEG	P80m:	9.1	7.4	13.0	5.4	75.3	85.0	75.7	85.3
	P145m:	4.6	3.5	4.1	2.3	147.4	145.0	130.1	145.6

Table 3.3: *Amplitudes and latencies of the main SII components taken from the power of the grand averages.*

investigated by analyzing their orientations using the following procedure:

1. At the latencies of the P80/P80m and P130/P145m peaks in the power diagrams (Fig. 3.5) the net orientation of the activity in each regional source was determined by taking the vector sum of the orthogonal source components. The assumption was that at these time points the activity overlap of the possibly different generator sources of the two components is small and hence the obtained orientation vectors represented the orientations of the two generator areas.

2. The two unit vectors pointing in the determined directions (in the case of EEG supplemented by the vector perpendicular to the plane of the P80 and P130 vectors) were used as new oblique base of the 2–(MEG) or 3–(EEG) dimensional space spanned by the regional source components. This oblique coordinate transformation was performed offline. Thereby the signal at any time point could be described as sum of the activities of the two presumed generator sources in SII (plus the remaining activity in EEG).

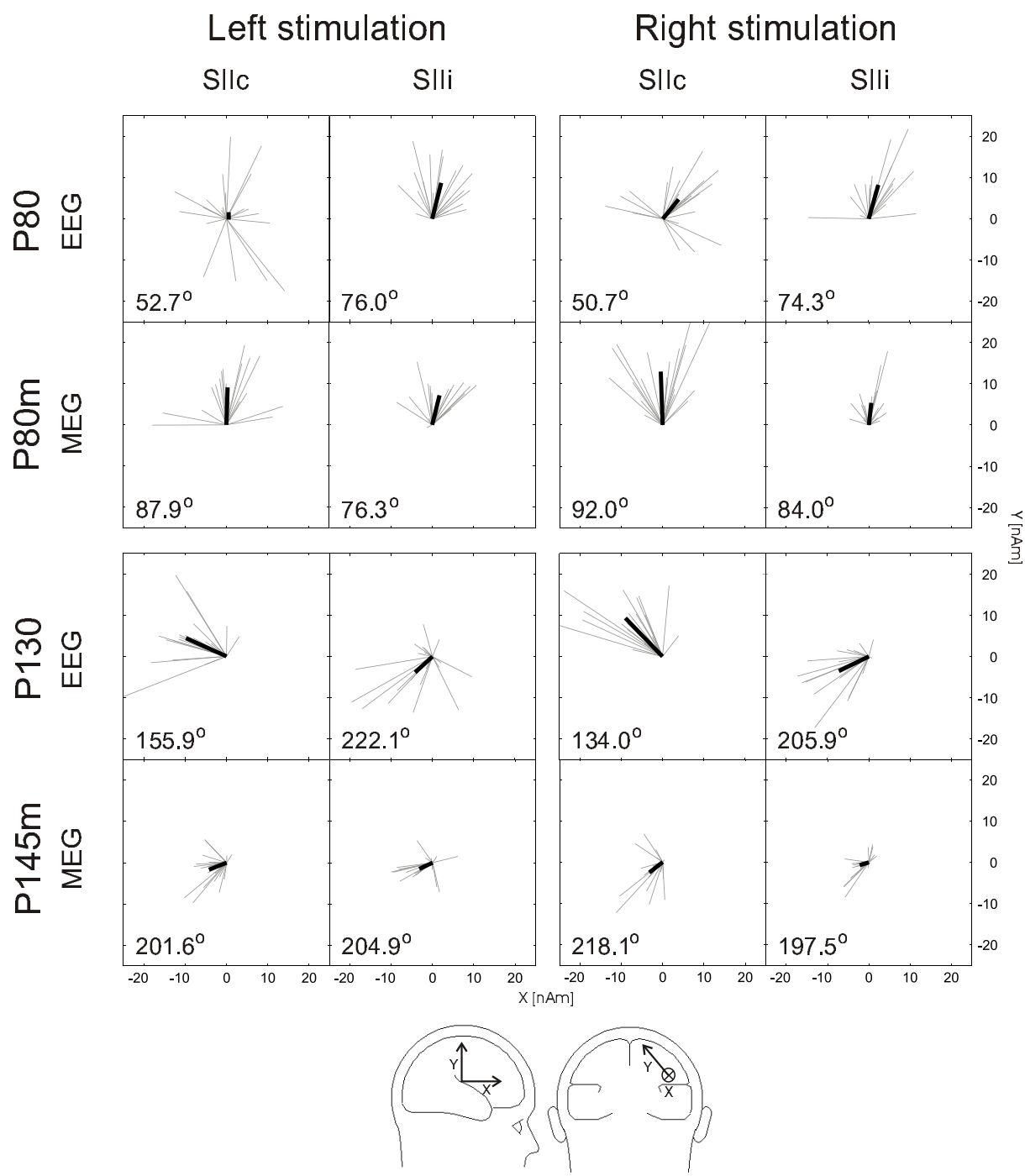

Figure 3.6: *Tangential projections of the P80/P80m and P130/P145m components at the corresponding grand average peak latencies. Gray lines refer to individual measurements, the thick black line represents the peak in the corresponding grand average waveform. Its angle with respect to the anteriorly pointing X-axis is given at the left bottom corner of each plot.*

Fig. 3.6 illustrates that the orientation of the two components were in fact different from each other. The orientations in the tangential plane are shown for each of the 20 individual data sets (thin gray lines) and for the grand average curve (thick black line). The net orientation of the P80/P80m component was towards the vertex with a small positive X-value (i. e. in the anterior direction). The corresponding in-plane angles were on average 85.0° (MEG) and 63.4° (EEG), respectively. Angles were determined with respect to the anteriorly pointing X-axis. Inter-individual differences were large only for the contralateral sources in EEG. This was probably due to the interference with other components in the contralateral hemisphere, predominantly generated in primary areas 1 and 2, that could not be perfectly separated by the simple 3-source model in EEG. Much less variability was seen in the MEG data because radial activity was not present. The good agreement of the orientation of the P80/P80m component in EEG and MEG suggested that the same source generator was mapped with the two methods.

The P130/P145m pointed on average in the anterior–posterior direction. MEG amplitudes at this latency were significantly smaller than their EEG counterparts (3.6 nAm versus 13.9 nAm, $p < 0.01$), but the clear difference in orientation when compared to the P80m made it obvious also a later generator was recorded in MEG as well. The two methods were in very good agreement with each other in the ipsilateral hemisphere, where the grand average orientation had a small negative Y-value. The average in-plane angels were 201.2° (MEG) and 214.0° (EEG), respectively. The result was similar for the contralateral sources in MEG (209.9°), but EEG components had positive Y-values contralaterally (145°) with only little inter-individual variability.

When comparing the angle to the tangential plane, differences between ipsi- and contralateral components in the EEG recordings became obvious as well. In Table 3.4 positive angles indicate an inward-pointing source current, 0° a perfectly tangential source. The small angles of the P80 in SIIi for left and right stimulation were to be expected, since the P80m was dominant in MEG recordings. On the other hand, the large angles for the contralateral component indicated a dominant radial orientation and did not agree with this expectation. All P130 peaks had tangential as well as radial contributions. SIIi values for left and right stimulation were both around 59°, whereas SIIc appeared to be more tangential.

The tangential orientation of ipsilateral P80 and the more radial P130 are in agreement with a study of Allison *et al.* [5]. The authors recorded transcortical potentials in the vicinity of SII in humans. They found evidence for two components generated in this region in response to median nerve stimulation. The authors recorded a P100/N100 complex with tangential orientation and speculated that it was presumably generated in the upper wall of the Sylvian Fissure. This is in agreement with the present finding of a tangential P80 with inferior–superior orientation in the tangential plane. In the study of

	Left stim.		Right stim.	
	SIIc	SIIi	SIIc	SIIi
P80	82.1°	−5.1°	64.4°	0.1°
P130	46.1°	59.8°	13.9°	58.4°

Table 3.4: *Angles or the EEG component orientation to the tangential plane.*

Allison *et al.* this component was followed by a later component around 125 ms that was probably generated in the lateral surface cortex above the Sylvian Fissure. It presumably corresponds to the P130 having a dominant radial orientation in the present study. The results of the spatio-temporal source analysis thus confirm these intracortical electrode recordings. In addition the present results suggest an explanation for localization differences between functional magnetic resonance images (fMRI) and MEG. In a recent report [91], fMRI centers of activity were 12 mm lateral and 6 mm superior to the fitted MEG dipoles on the average. Considering the current results, this would be reasonable if the area in the surface cortex above the Sylvian Fissure had a significant contribution to fMRI signals. Activity in this region is scarcely recorded in MEG signals, which are dominated by the more medially generated P80m.

The differences between ipsi- and contralateral source angles may be attributed to separate generators having different orientations. However, as discussed in section 3.3.1, interference of different contralateral areas, especially SI and SII, could not be ruled out. Therefore this partial mapping of SI activity onto the contralateral SII source waveforms appeared to account for the observed discrepancies. This interpretation becomes plausible especially when reports on bilateral receptive fields of SII neurons are considered [93, 151]. This fact suggests a considerable overlap of the cortical areas activated by ipsilateral and contralateral stimulation.

The difference in orientation of the two components in the tangential plane supported the interpretation of separate source generators and justified the projection procedure described above. The resulting projected source waveforms are shown in Fig. 3.7. The smooth MEG waveforms were less contaminated by noise and showed less intersubject variability as indicated by the smaller 90 % confidence intervals. MEG and EEG source waveforms both confirmed reports of a larger P80 amplitude contralaterally than ipsilaterally [18, 65, 138]. In the MEG data the contralateral–ipsilateral difference was larger for right (7.6 nAm) than for left (1.7 nAm) stimulation, but this interaction did not reach statistical significance ($F(1,9)=4.68$, $p>0.05$). While in MEG SIIc amplitudes were larger after right versus left stimulation, the opposite was true for SIIi (compare Table 3.3). Amplitude asymmetries concerning left versus right stimulation have been reported from SI before [14]. The data extended these findings to SII. In the projected source waveforms

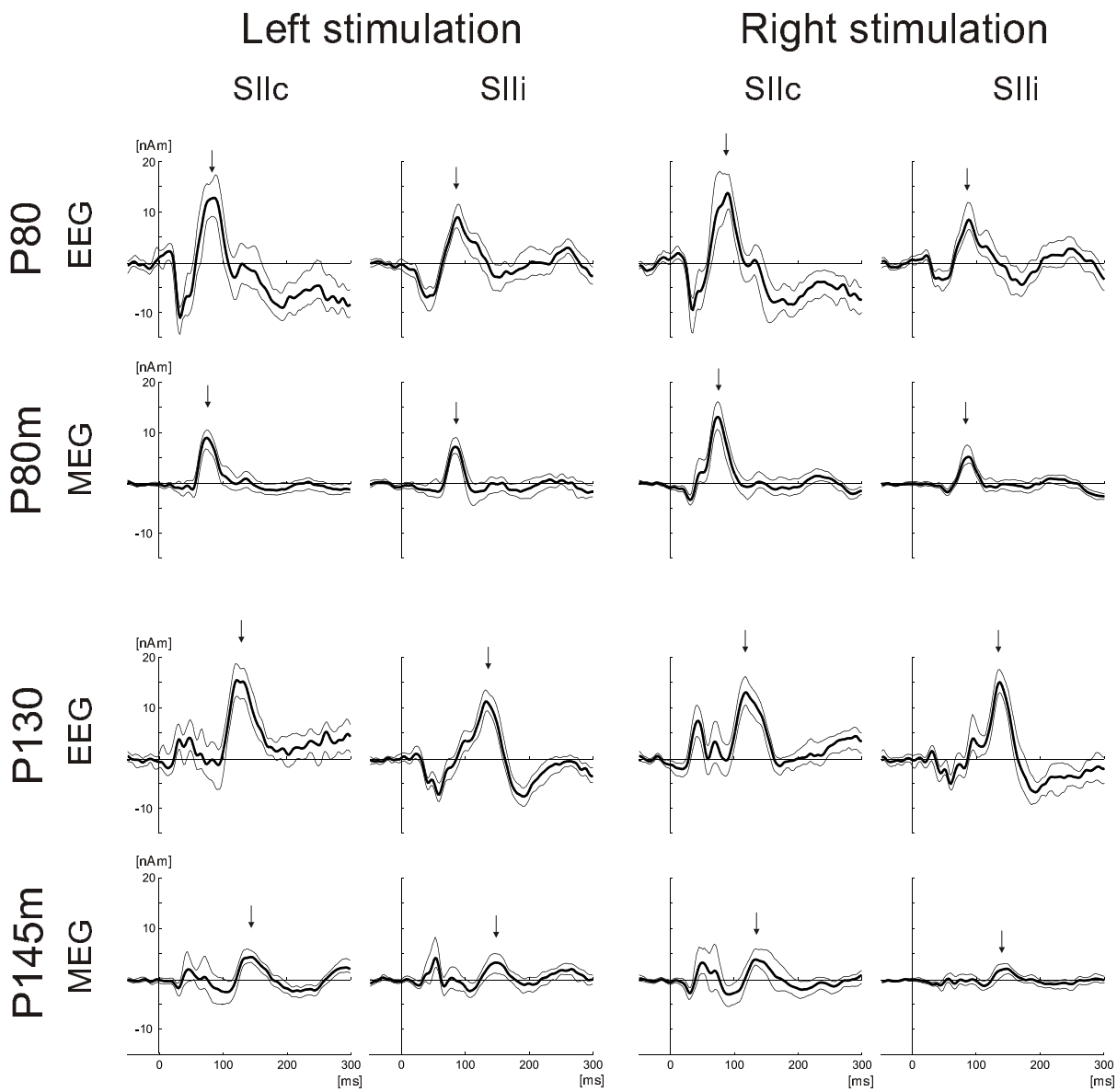

Figure 3.7: *Source waveforms of the P80 and P135 components. They were obtained from the oblique projection of the regional source activities onto the orientation vectors determined at the latencies that are indicated with the arrow for each component.*

a peak of opposite polarity preceding the P80/P80m peak occurred in EEG and MEG. In EEG, this earlier activity might be related to some extent to interference with SI activity as discussed above. However, it was present also at the ipsilateral hemisphere and in the MEG data. This suggests generation of a small component with latency around 50 ms (N50m) in SII.

Waveform morphologies were less consistent for the P130/P145m component. Again EEG

waveforms suffered from background noise activity. For this component previous studies employing electric stimulation reported significantly higher activity contralaterally [139, 147], but this result could be replicated here for left finger stimulation only. This might be an intrinsic property of tactile stimulus processing, but it is also possible that the effect was just not revealed due to the low signals produced by the tactile pressure pulse when compared to an electric median nerve stimulus. However, it should be stressed again that in EEG recordings small variations in the number, position and orientation of the model sources lead to substantial changes in peak amplitudes and latencies as demonstrated in Fig. 3.3. This can easily lead to contradicting effects. MEG P145m amplitudes were all less than 5 nAm (cf. also Table 3.3). Nevertheless the presence of a significant peak was evidenced by the 90 % confidence intervals exceeding the zero baseline.

3.4 Conclusion

This study employed simultaneous EEG and MEG recordings to image evoked activity in the secondary somatosensory cortex. The results provided answers to the two questions asked at the beginning of this chapter:

1. **Differences in localization accuracy between EEG and MEG:**
   EEG recordings suffered from disturbing contamination with background brain activity, mainly slow cortical rhythms like α-activity and possibly evoked signals from contralateral primary areas 1 and 2. This made it difficult to perform reliable source modeling with individual data sets. In addition, contralateral SII amplitudes and latencies were extremely sensitive to details of the chosen dipole model. Tactile evoked MEG responses, on the other hand, were characterized by a smooth and well defined morphology. Low noise contaminations made it possible to fit three sources individually to each data set. The higher localization accuracy of MEG can be attributed partly to the larger number of channels (in this study 122 versus 61) that provide more spatial information.

2. **Generators of SII components:**
   The study revealed the presence of two major components in SII with different orientations:

   A component peaking around 80 ms, the **P80/P80m**, occurred in EEG and MEG. The tangential projection of its orientation predominantly pointed in the inferior–superior direction. EEG measurements suggested a nearly tangential orientation ipsilaterally and a possibly more radial orientation at the contralateral hemisphere. However, the potential interference with unmodeled contralateral activity prevented

a reliable conclusion concerning the orientation contralaterally. A small **N50/ N50m** component preceded the P80/P80m peak. It probably corresponded to activity in the same region.

The dominant orientation in the tangential plane of the **P130/P145m** components in EEG and MEG was the anterior–posterior direction. Like for the P80/P80m, EEG orientations differed between SIIc and SIIi, the former having a small component pointing superior, the latter a component pointing inferior. In MEG no evidence for a difference between ipsi- and contralateral orientation was found. MEG P145m latency was significantly longer than that of the P130 in EEG. This suggested that MEG data recorded another component in the SII area with tangential orientation that was probably contained in the EEG signal but not discernible from the large more radial activity dominating the P130 peak.

The P145m amplitudes were extremely small in MEG recordings. Therefore, if SII activity at latencies larger than 100 ms is to be observed, EEG has advantages over MEG. However, higher signal-to-noise ratio and more reliable source localization was obtained using the P80m component in MEG. For this reason the following studies employed MEG as the more robust method and concentrated on the analysis of the P80m component.

Chapter 4

Effect of attention on tactile evoked responses

4.1 Introduction

4.1.1 Attention

Of all physical and biological systems, the brain's status is unique, being the stage where physical (i. e. physiological, neuronal) processes induce conscious experiences. Our impression of a 'free will' gives us the feeling to be able to take command of ourselves by actively influencing our brain processes in a seemingly undetermined way. The search for an integration of the concept of mind and physical processes is still ongoing and debated from very different point of views, in physics, biology, psychology or philosophy [98, 136]. Objective scientific results about processes at the interface between the cognitive and the physiological level are needed for a fruitful discussion of such issues. A small contribution is the study of the effects of voluntary attention on neuronal activity.

More than a century ago, William James, one of the pioneers in the integration of biology and psychology, defined attention as follows:

> [Attention] is the taking possession by the mind, in clear and vivid form, of one out of what seem several simultaneously possible objects or trains of thought. Focalization, concentration, of consciousness are of its essence. It implies withdrawal from some things in order to deal effectively with others. [80]

Since then more accurate definitions of different categories of attention have been made. The purpose of attention might be to give preference to the attended external elements

that compete with others for a common neural resource of limited capacity. This can be achieved by selected faster processing or lower thresholds for the attended external features [121]. It is also likely that non-attended stimuli are selectively suppressed [68], whereas the response amplitudes of the attended stimuli are enhanced [21]. Meanwhile neuroscience has at hand a multitude of methods to physically measure attentional effects on neuronal activity. The extracranial detection of neuromagnetic fields by means of MEG allows for noninvasive studies in humans with high temporal resolution. The common method is to look for changes in the neuronal response when attention is focused on a stimulus as compared to the unattended stimulus.

Multiple unit recordings in monkeys during vibratory stimulation documented only a minor dependence of neurons in the primary somatosensory cortex on the state of attention [73, 120]. These results are in contrast to a study employing a spatial form processing task that showed an enhancement of the discharge rate of 50 % of all SI neurons when the stimulus was attended [69]. In the same study, 80 % of all SII neurons were affected. The majority (52 %) reacted with an increase, 28 % with a decrease in the firing rate. The larger effect of attention on SII activity when compared to SI was also confirmed by other animal studies [21, 120]. It was shown that different SII neurons behave in a specific manner: when attending a vibratory stimulus, neurons with exclusively contralateral receptive fields showed a significantly weaker attentional enhancement than those with bilateral receptive fields [120].

Besides these reports on monkey responses, several studies on the role of attention have been carried out in humans as well. In most of them EEG activity was recorded during stimulation of the median nerve. As far as early somatosensory evoked potentials up to 60 ms are concerned, findings have been diverging. Whereas some studies found no evidence for attention-induced changes of these components that are generated mainly in SI [148, 149], amplitude enhancement of P30 and P40 components was reported in another [29]. A positive shift at 27 ms post-stimulus was reported when the stimulus contralateral to the recording site was attended [44]. In MEG measurements, no significant change in early SI activity could be detected [56, 105, 109]. Recent PET [19] and fMRI [82] investigations observed attentional enhancement of the recorded activity in SI that was smaller [19] or of the same magnitude [82] as that observed in SII.

Previous studies agreed on the fact that the influence of attention was largest on components later than 60 ms. However, different answers were given to the question whether attentional effects occur only when the focus of attention is the stimulus contralateral to the evoked activity [149] or also when an ipsilateral stimulation site is attended [44]. Divergent interpretations have been reported of the generators of the late components affected by attention. In a SEP study it was suggested that a N120 component generated in SII was not influenced by attention whereas a novel N140 component emerged in the

vicinity of SII during the attend condition [44, 45]. Another study reported invocation of a P100 and N140 component by attention due to interaction between the PPC area and the prefrontal cortex [29]. Previous MEG studies mainly used electrical stimuli presented in oddball paradigms (i. e. standard stimuli were interspersed pseudo-randomly with rare deviant stimuli) with either stimulus site [56, 105] or intensity [109] being varied. The reported results of attentional effects in SII have been diverging. Hari *et al.* found a small but not significant enhancement [56] in SII. Mauguière *et al.* reported no amplitude change in SII for short and regular interstimulus intervals of 1.2 s, but significant attentional enhancement when only the rare deviant stimuli in the oddball paradigm were presented without intervening standards. This is to be contrasted with the findings of Mima *et al.*, who documented enhanced activity in SII following deviant stimuli using an oddball paradigm with an interstimulus interval of 0.5 s [109]. The partly diverging results of these previous studies on evoked activity in humans have been attributed to differences in the recording method (EEG versus MEG) [105, 109] or the different stimulus properties that were varied in the oddball paradigm (location versus intensity) [109].

The first part of the present study had two objectives:

1. The hypothesis that the task properties influence attentional enhancement effects was tested. It was to be clarified whether attention to stimulus intensity and stimulus location have different effects on the evoked activity in SII.

2. So far attentional effects on somatosensory evoked fields have been studied mainly in response to electrical stimuli. As discussed before in section 3.3.2, the dominant components in SII source waveforms might differ from those generated by tactile pressure pulses that resemble natural stimuli more adequately. By monitoring the time course of attention-induced waveform changes, specific effects on the different tactile evoked components identified in chapter 3 were analyzed.

4.1.2 Habituation

After identification of the source components that were affected by the presence of attention, the question of the underlying mechanisms needed to be investigated. In this study focus was directed to the phenomenon of habituation. Here the term is used in the sense of response decrement over time during repeated stimulation. The goal was to clarify whether attention leads to an altered habituation behavior of the affected components. The hypothesis to be tested was whether reduced habituation could account for the effect of attentional amplitude enhancement.

Response decrement over stimulation time can have several causes. Adaptation of the stimulus-receiving sensors, in this case mechanoreceptors in the skin, is one of them. Another is fatigue of the subjects with increasing measurement duration, possibly leading to diminished brain response amplitudes. One of the most likely mechanism causing response decrement is refractivity of cortical and subcortical neurons: after a neuron has been activated, it remains insensitive to further excitation for a certain time period. Originally, the term 'habituation' was not applied to neuronal activity, but generally described a decrement of responses following repeated stimulation, like for example spinal reflexes [123, 137]. When applying it to evoked neuronal activity, it was unclear whether effects of refractivity were to be included in the phenomenon of habituation [24] or whether this term should be used to account for response decrements that can not attributed to one of the above-mentioned causes. Thompson and Spencer [144] determined exact response features that unambiguously defined this interpretation of habituation. In the present study, the term is used in the general meaning of a decrement of the evoked activity over time. Underlying mechanisms and contributions of the different causes mentioned above will be discussed at the end of the chapter.

Much information on habituation of somatosensory evoked potentials has been obtained from studies performed with cats. In a report by McGowan–Sass and Eidelberg [107], electrical stimuli were delivered at interstimulus intervals between 1 and 3 seconds and evoked potentials recorded at different sites along the afferent pathway. Significant habituation occurred in the sensory cortex, and also in the pyramidal tract, the ventroposterolateral nucleus of the thalamus and the medial lemniscus, but not in the dorsal column. The habituation level in the cortex was about 60 %. The authors suggested that habituation was characteristic of each neuronal group rather than being attributed to any specific ascending pathway. In addition to response decrement over time, the effect of active restoration of the evoked signal was demonstrated in order to fulfill one requirement given by Thompson and Spencer [144] for the identification of habituation. A later cat study [25] discriminated between responses from primary and secondary somatosensory cortices and demonstrated significantly faster habituation in SII as compared to SI.

A previous evoked potential study in humans [145] indicated absence of response decrement in the earliest evoked responses, in particular the non-cortical P14 and the first cortical component, N20. This result showed that there was no receptor fatigue or refractivity up to the cortical stage. Later components between 25 and 50 ms showed significant habituation that depended on the interstimulus interval. In this study different habituation parameters of two overlapping components were interpreted as indicator for different generators. A study applying pairs of electric median nerve stimuli with different time delays [2] also documented different recovery times of somatosensory evoked components. Components with a latency of around 80 ms, possibly corresponding to activity in SII,

were shown to have recovery times of at least 1 s. Angel *et al.* [6] measured response recovery following wrist extension as a function of the interstimulus interval (ISI). They found that the amount of response recovery y was best fitted by a function of the form $y[\%] = 100 - 84\,e^{-0.22 \cdot \mathrm{ISI[s]}}$. Interstimulus dependence of somatosensory evoked responses is closely connected to the response decrement behavior over time. MEG [60, 105] and fMRI [74] studies documented strong SII amplitude dependence on ISI with higher SII responses at longer ISIs. SEFs in SII were shown to not recover completely even at ISIs as long as 8 s [60].

In the present study the habituation of tactile evoked brain activity in SI and SII at an ISI of 1 s is analyzed. Focus of interest was the behavior of the secondary somatosensory area and possible effects of attention to stimulus location and intensity on the response decrement with stimulation time.

4.2 Materials and Methods

4.2.1 Stimulation paradigm

Tactile evoked magnetic fields were recorded in 10 healthy adults (aged 27-37 years, five male, nine right-handed). Measurements were approved by the local ethics committee and conducted with the informed consent of each subject. In two oddball paradigms, standard (80%) and deviant (20%) tactile stimuli (cf. section 1.4.3) were interspersed pseudo-randomly at a constant interstimulus interval of 1.03 s. In a spatial discrimination paradigm, deviants were delivered to the first, standards to the second phalanx of the left index finger. Here stimulus intensities of standards and deviants were equal. In an intensity discrimination paradigm, the deviant was a pressure pulse with an intensity three times as high as the standard. Both stimuli were delivered to the tip of the left index finger. The intensity variation was technically achieved by interposing a coupling device (a perspex block with drilled holes) between the end of the polyurethane tubes and the finger clip allowing four valves to supply air pressure pulses to the finger clip independently (Fig. 4.1). The strong (deviant) stimulus in the intensity paradigm was produced by opening all four valves simultaneously, whereas activation of valve 3 alone generated the weak stimulus.

Each paradigm was run in an attend and an ignore condition of 12 minutes duration each. Similar to previous studies [29, 109], visual distraction was used in the ignore condition when subjects were asked to concentrate on watching a video of their choice. In the attend condition, subjects had to count deviants silently while fixating the screen without video and, therefore, had to focus attention actively towards the stimuli. The mean ratio of

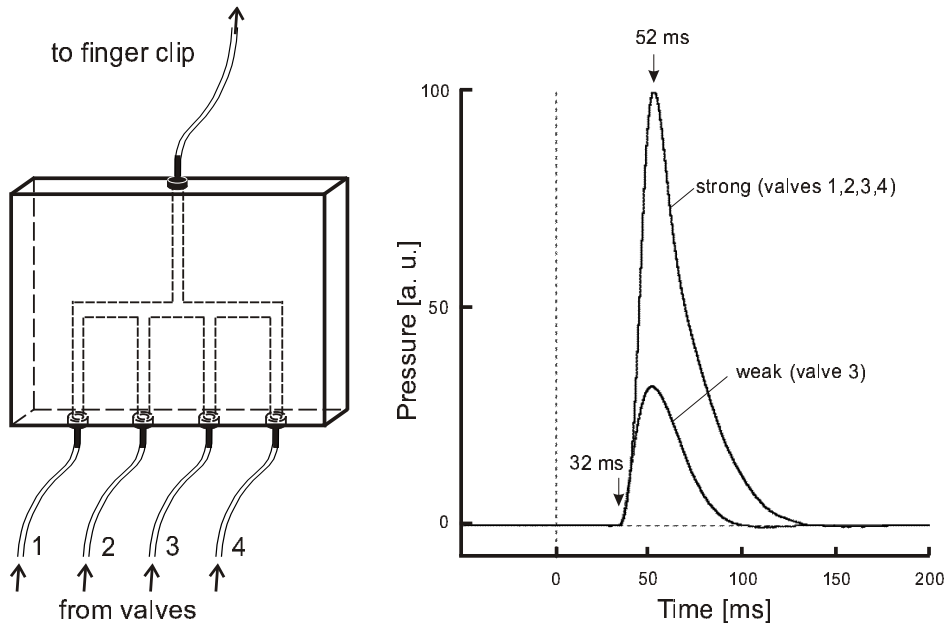

Figure 4.1: *Generation of the strong and weak stimuli in the intensity discrimination paradigm. Left: Coupling device made of perspex. Input is received from four air pressure valves and output passed to the finger clip. Right: Time courses of the resulting strong and weak stimuli.*

counted to presented deviants was 0.95 ± 0.09 in the intensity and 1.01 ± 0.09 in the spatial discrimination task, indicating both sufficient discriminability of the stimuli and good compliance of the subjects.

4.2.2 Data Recording and Source Modeling

Data were bandpass-filtered (0.03–200 Hz) during acquisition and sampled at 769 Hz. For final source analysis, digital zero-phase filters were applied offline (high–pass 0.3 Hz, slope 6 dB/oct; low–pass 70 Hz, 12 dB/oct). About 150 artifact-free deviant and 600 standard responses were averaged in each condition. Simultaneous recording of electrocardiogram (ECG) and electrooculogram (EOG) allowed for identification of heartbeat and eye-blink artifacts. The MEG head coordinate system was matched with individual anatomic T1–weighted magnetic resonance images (Picker Edge 1.5 T).

Dipole fits were performed for each averaged data set, i. e. for responses to standard and deviant stimuli, in both the attend and the ignore condition of each paradigm. For each subject, the average of the fitted source coordinates of all stable solutions was calculated and considered the optimum source model for this individual.

In all subjects, equivalent dipoles could be fitted to the contralateral SI (fit interval: 20–

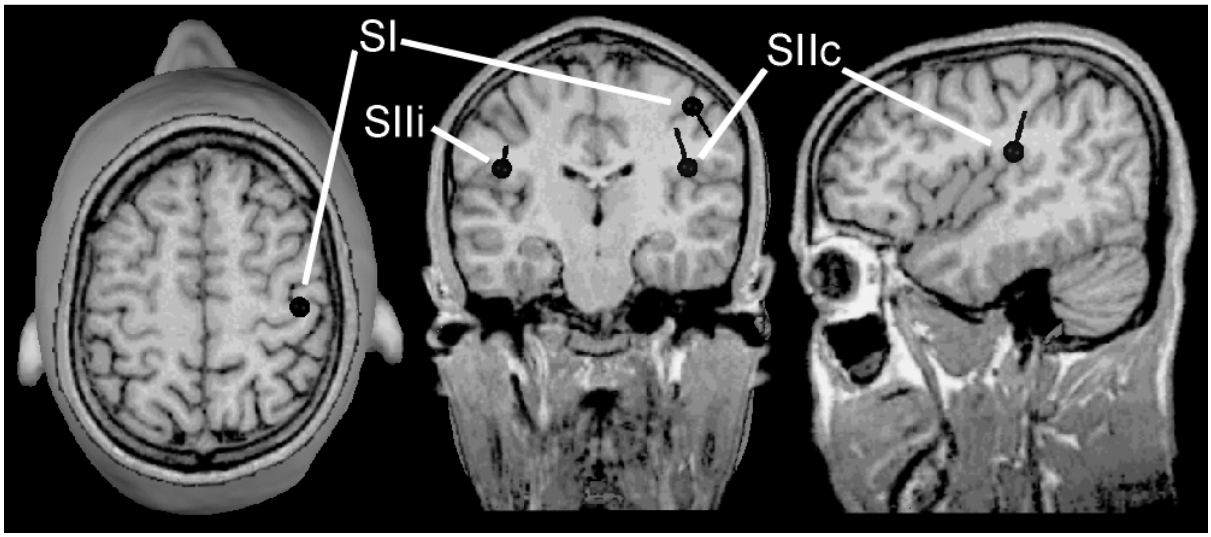

Figure 4.2: *Mean locations of SI and SII dipoles. Sources have been transformed back from the Talairach space onto an individual MRI.*

50 ms). Explanation of the later variance in the SEF required bilateral dipoles that fitted in the upper bank of the Sylvian fissure in the parietal operculum, consistent with the location of SII. In all subjects, stable dipole fits could be obtained in at least one condition for the activity in the ipsilateral parietal operculum (SIIi, fit interval 75–100 ms). Stable dipole fits in the contralateral parietal operculum (SIIc, 65–90 ms) could not be obtained in 3 of 10 subjects. For quantitative comparison of source activities in all subjects, SII source locations were seeded from the individual magnetic resonance images according to the analysis procedure for group data developed in section 2.4. After fitting dipole orientations to the individual MEG data, a fixed 3-dipole model was obtained for final analysis of dipole source waveforms (Fig. 4.2). This model showed bilateral SII activities in all subjects and allowed for robust estimation and comparison of source amplitudes and latencies across conditions. For each source and stimulus, the difference between the attend and the ignore condition was calculated in order to obtain a measure for the attention-related changes in brain activity.

4.2.3 Study of habituation

In order to study the evolution of the evoked responses over stimulation time, the data were divided into subsets of 1 minute duration each. Averages were taken as described above for each subset. The model obtained from the whole data was used to map SI and SII source waveforms in each 1 minute interval. Amplitudes of the main SII component were determined from the grand averages. The time evolution of its dipole moment Q

was modeled by a least squares fit of an exponential function of the form

$$Q(t) = Q_\infty + (Q_0 - Q_\infty) \cdot e^{-\frac{t}{\tau}} \tag{4.1}$$

to the data. Q_0 and Q_∞ are the dipole moments at $t = 0$ and $t = \infty$, respectively. τ is the time constant of the exponential response decrement.

4.2.4 Statistical analysis

The bootstrap BC_a-method [32] (800 samples, MATLAB® 5.2) was used to assess differences between conditions by calculating 90% confidence intervals from the Grand Average source waveforms. The effect of attention was considered significant on the 5 % confidence level where this interval did not include the baseline. Additionally, a multivariate analysis of variance (MANOVA) was performed (GLM procedure, SAS® 6.12) on individually determined peak latencies and amplitudes in both tasks independently. Tested factors were stimulus (standard/deviant), task (attend/ignore) and hemisphere (SIIc/SIIi).

4.3 Results

4.3.1 Waveform morphology

In agreement with previous reports [62, 109], source modeling localized SI at the anterior wall of the contralateral postcentral gyrus and SII deep in the parietal operculum bilaterally (Fig. 4.2). The mean Talairach coordinates of the fitted sources are given in Table 4.1. The three equivalent dipoles separated SI and bilateral SII source waveforms with very similar patterns across all subjects.

The outcome of the source analysis in an individual subject is illustrated in Fig. 4.3. The earliest MEG activity could be attributed to the primary somatosensory cortex with its dominant anterior-posterior orientation that agrees with a presumed location in the posterior wall of the central sulcus. The N20m and a P40m/P60m complex was mapped consistently in all conditions. Small differences between responses to attended (thick lines) and unattended stimuli (thin lines) were visible. In the intensity paradigm a small decline in P40m/P60m amplitude was observed. SII sources fitted nearly symmetrically in both hemispheres with dominant inferior–superior orientation (compare Fig. 2.6: bilateral symmetry in SII is a common feature observed in most subjects. However, orientations differ between individuals). In this subject SII amplitudes exceeded those of SI. SIIc showed substantially larger components and was activated earlier in all conditions than

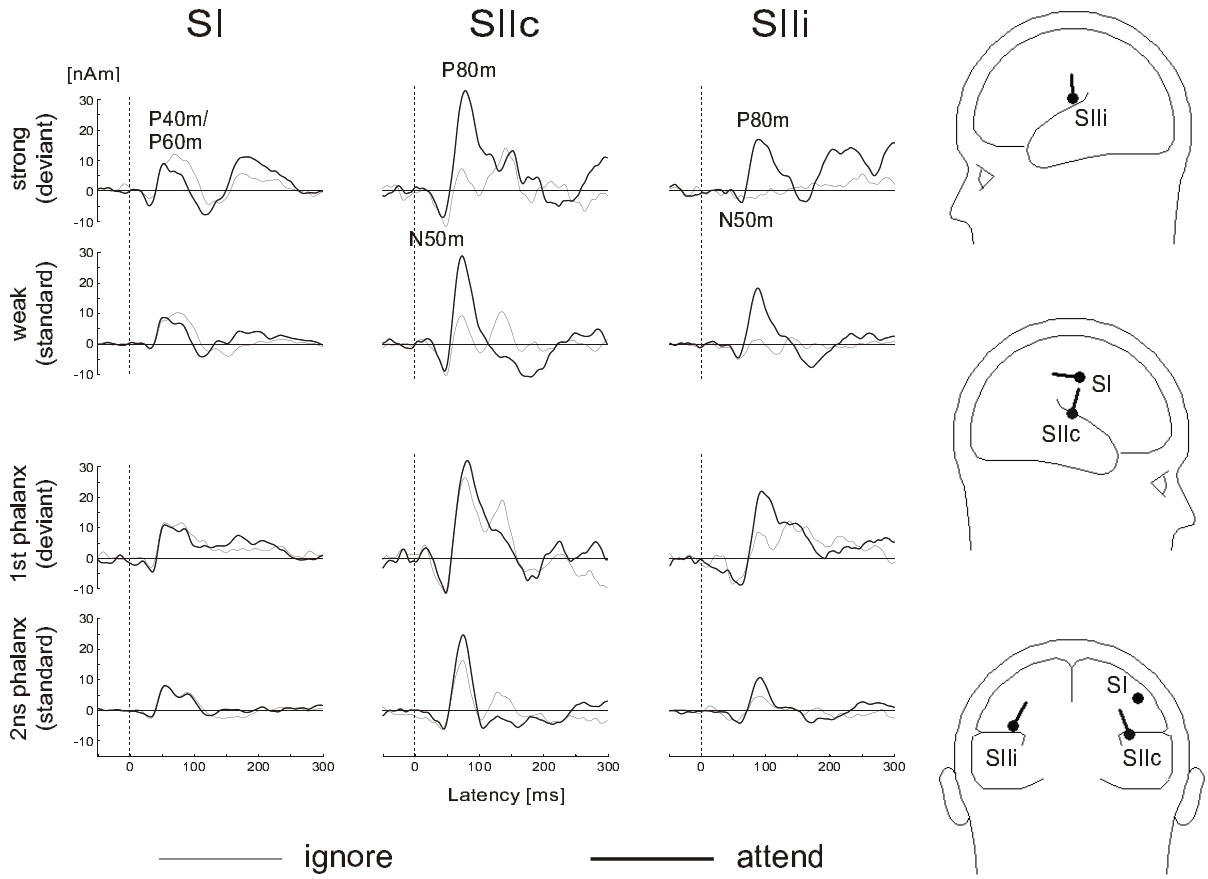

Figure 4.3: *Individual source waveforms of one subject in the different conditions. Responses of the attend and ignore conditions are superimposed.*

its ipsilateral counterpart. In response to strong and weak unattended stimuli, even no ipsilateral SII component could be defined due to low amplitudes. The prominent finding in this subject was a clear enhancement of P80m activity in the attended conditions, whereas N50m seemed to be unaltered. Another component was observed contralaterally at about 130 ms that appeared to be attenuated under attention. Statements about the significance of such individual findings, however, can be made only under consideration of the results of all 10 subjects in order to take into account inter-subject variability in waveform morphologies and effect sizes. Therefore, grand averages over all subjects were calculated for the responses of SI, SIIc and SIIi in each condition. Results are shown in Fig. 4.4.

	x	y	z
SI	42.4 ± 3.6	-20.0 ± 5.0	52.0 ± 4.6
SIIc	42.4 ± 3.4	-18.5 ± 4.6	24.5 ± 3.6
SIIi	-39.7 ± 2.3	-21.8 ± 2.2	24.9 ± 2.2

Table 4.1: *Fitted source locations in Talairach coordinates (mean $\pm$ s.d.)*

Primary somatosensory cortex

SI grand averages showed a small N20m and a large P40m peak (Tables 4.2, 4.3). The P60m component was discernible only as a shoulder superimposed on the P40m. Neither the N20m nor the P40m/P60m peaks were significantly enhanced by attention, as indicated by the flat difference waveforms in Fig. 4.4. Small deviances of the 90 % confidence intervals from the baseline around 80 ms (observed for example in the response to weak stimuli) were probably due to SII activity that interfered with SI and was falsely mapped to the SI waveforms. This interpretation is supported by the fact this latency corresponded to that of the P80m peak in SIIc and not to any prominent SI component.

Secondary somatosensory cortex

In the grand average responses SIIc/SIIi source activity exhibited a small negative peak around 50 ms (N50m) and a large positive peak around 80 ms (P80m). A smaller later component was observed inconsistently and predominantly in the ignore condition. In response to the strong stimulus, for example, this component was less clearly discernable in the attend conditions (cf. Fig. 4.4). SII source waveforms were very similar in both hemispheres with shorter latencies (on average ~ 7 ms) and larger amplitudes contralaterally (Fig. 4.4, Table 4.2).

No significant change in N50m amplitude was observed in any condition. In parallel with the N50m-P80m transient, however, an attentional enhancement of SII activity occurred, resulting in significantly enlarged P80m amplitudes in the attend conditions in both tasks (Fig. 4.4, Table 4.3), as observed best in the difference waveforms. The attention-related amplitude change of the N50m-P80m transient in SII was of similar proportion and duration in both the spatial (mean enhancement 52 %) and the intensity (64 %) discrimination task. Furthermore, no significant difference in time course and amplitude of the effect was detectable between responses to the rare deviant (44 %) stimuli that served as targets of the mental counting task, and the more frequent standard (72 %) pulses.

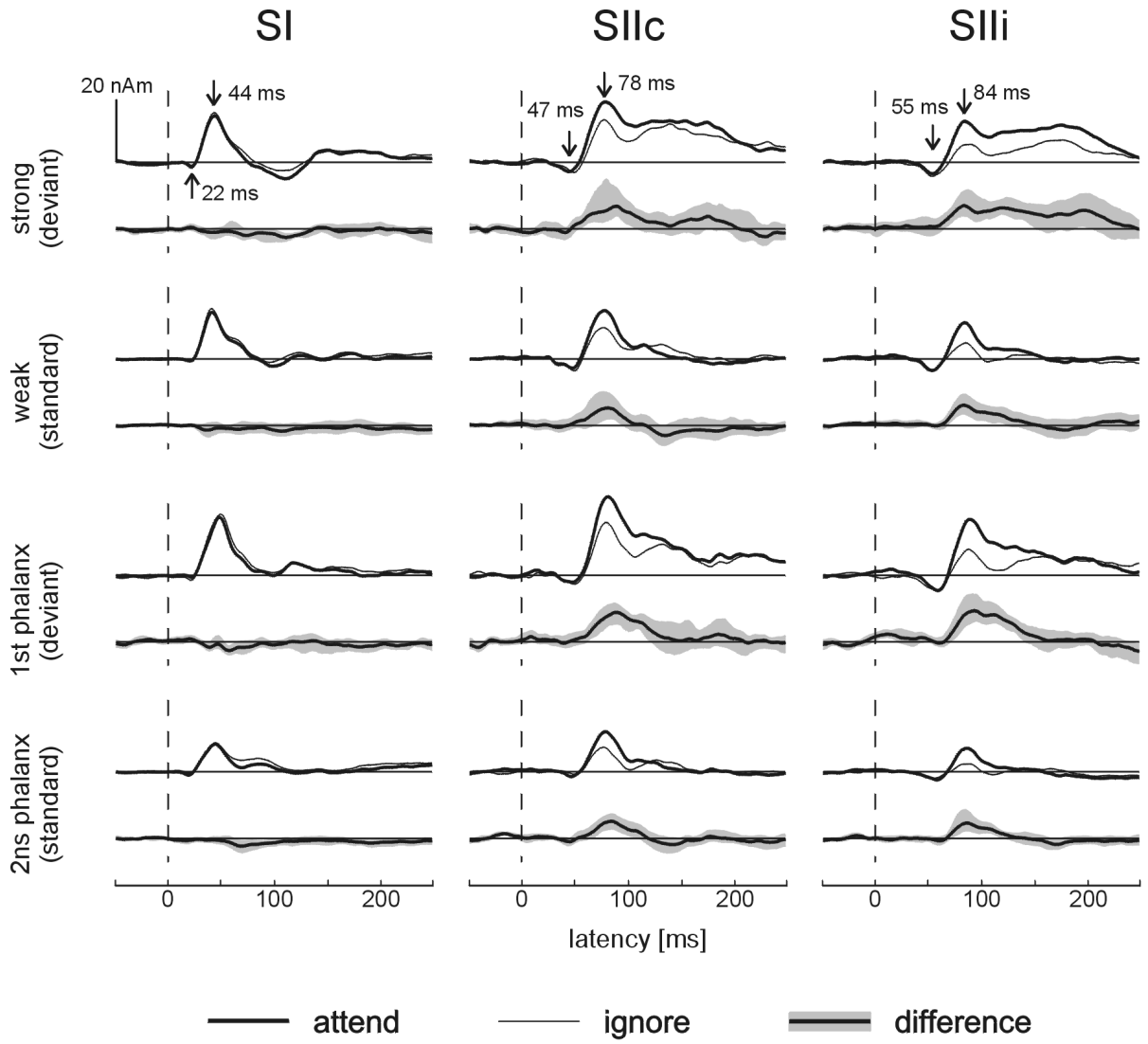

Figure 4.4: *Grand average source waveforms of SI, SIIc and SIIi. Responses of the attend and ignore conditions are superimposed. The curves at the bottom of each plot show the difference between attend and ignore grand averages. The shaded area indicates the 90 % confidence interval. While SI activation did not change under attention, SII showed an attentional enhancement of similar proportion in both tasks (intensity: weak-strong; location: 2nd-1st phalanx) and for both the standard (weak; 2nd phalanx) and deviant (strong; 1st phalanx) stimuli in the time interval of 55-130 ms.*

Separate MANOVAs of the N50m-P80m amplitude differences revealed a significant main effect of attention for both the spatial ($F(1,9) = 6.16$, $p < 0.05$) and intensity ($F(1,9) = 17.13$, $p < 0.01$) discrimination task. SII responses to the first phalanx (deviant in the spatial task) were significantly larger ($F(1,9) = 6.63$, $p < 0.05$) than to

the second phalanx (standard). In the intensity discrimination paradigm, amplitude differences between standard (weak) and deviant (strong) responses were significant ($F(1,9)=90.94$, $p<0.001$) and indicated the strong influence of stimulus intensity on SI and SII amplitudes [109]. There was also an ordinal interaction between stimulus and task in the intensity discrimination paradigm ($F(1,9)=6.12$, $p<0.05$), indicating that the absolute attentional enhancement effect was slightly larger in the response to the strong as compared to the weak stimuli (Fig. 4.5, left).

The N50m-P80m amplitude was significantly larger in contralateral as compared to ipsilateral SII ($F(1,9)=5.37$, $p<0.05$ in the spatial and $F(1,9)=12.35$, $p<0.01$ in the intensity paradigm). This observation is consistent with previously reported dipole moment differences of SIIc and SIIi [60, 105]. This hemispheric difference interacted ($F(1,9)=8.86$, $p<0.05$) with the type of stimulus (strong/weak) in the intensity task and was larger for the strong (deviant) as compared to the weak (standard) stimuli (Fig. 4.5, right). In the spatial discrimination paradigm, however, there was only a tendency towards an interaction between stimulus frequency and hemisphere.

4.3.2 Habituation

Primary somatosensory cortex

Figure 4.6 illustrates the evolution of the SI source waveforms during the 12 minutes of repeated stimulation. Grand average responses to the standard stimuli of the two discrimination paradigms are shown in both the attend and the ignore condition. At first glance no response decrement or increment at any latency was evident from the source waveforms. The peak amplitude of the major component around 40 ms was analyzed and plotted in Fig. 4.7 for standards and deviants. Here a small tendency towards decreasing response amplitudes over measurement time became visible. However, the effect was weak, indicating that habituation played only a minor role in SI. This statement holds both for the attend and the ignore conditions, which did not differ from each other, as was expected from the finding that attention did not alter SI source waveform morphologies significantly.

Secondary somatosensory cortex

As opposed to SI, the waveform plots in Fig. 4.8 document strong dependence of SII amplitudes on measurement time. The plot depicts the responses of contra- and ipsilateral hemisphere to the standard stimuli in the two paradigms. The most obvious change over

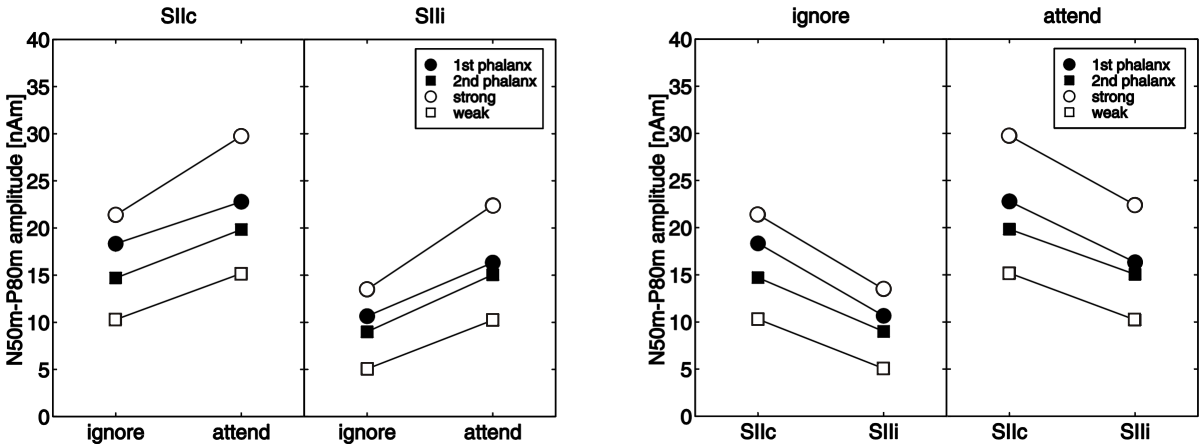

Figure 4.5: *Interaction diagrams of the SII amplitudes.*

	SI		SIIc		SIIi	
	N20m	P40m	N50m	P80m	N50m	P80m
1st ph., att.	21.2 ± 5.8	44.2 ± 4.7	46.8 ± 6.0	78.5 ± 6.2	55.1 ± 4.6	83.6 ± 2.7
1st ph., ign.	22.8 ± 2.8	44.0 ± 4.6	50.8 ± 4.8	78.0 ± 6.0	56.7 ± 4.3	83.5 ± 5.4
2nd ph., att.	21.8 ± 3.8	41.3 ± 5.2	46.8 ± 6.6	76.2 ± 5.8	54.4 ± 4.1	84.7 ± 3.0
2nd ph., ign.	21.7 ± 3.9	42.3 ± 5.5	49.5 ± 3.3	74.1 ± 5.1	55.5 ± 6.4	83.0 ± 5.5
strong, att.	21.0 ± 5.8	44.6 ± 6.3	49.7 ± 7.2	79.9 ± 5.0	57.3 ± 3.7	88.0 ± 3.9
strong, ign.	21.1 ± 4.2	44.6 ± 6.8	50.6 ± 6.9	78.6 ± 7.9	54.1 ± 4.7	85.4 ± 5.8
weak, att.	20.7 ± 4.5	45.0 ± 5.3	51.4 ± 5.3	81.8 ± 5.1	60.0 ± 6.2	88.5 ± 4.2
weak, ign.	19.8 ± 5.2	45.1 ± 5.9	51.5 ± 7.0	79.8 ± 7.2	56.4 ± 6.5	87.7 ± 5.7

Table 4.2: *Latencies [ms] of SI and SII components in the different conditions (mean $\pm$ s.d.).*

	SI		SIIc	SIIi
	N20m	P40m	N50m-P80m	N50m-P80m
1st ph., att.	-2.1 ± 1.8	17.0 ± 5.7	22.8 ± 11.3	16.3 ± 8.0
1st ph., ign.	-2.3 ± 1.1	16.9 ± 5.0	18.3 ± 7.7	10.7 ± 6.6
2nd ph., att.	-1.1 ± 0.9	15.5 ± 6.1	19.8 ± 9.6	15.1 ± 7.1
2nd ph., ign.	-1.3 ± 0.9	17.3 ± 5.3	14.7 ± 6.0	9.0 ± 4.6
strong, att.	-1.4 ± 1.4	19.5 ± 9.1	29.7 ± 7.9	22.4 ± 9.5
strong, ign.	-2.0 ± 1.4	20.4 ± 9.3	21.4 ± 9.0	13.5 ± 7.1
weak, att.	-1.2 ± 1.3	9.9 ± 3.2	15.2 ± 6.7	10.2 ± 7.0
weak, ign.	-0.8 ± 1.0	10.5 ± 3.0	10.3 ± 5.6	5.1 ± 3.1

Table 4.3: *Amplitudes [nAm] of SI and SII components in the different conditions (mean $\pm$ s.d.).*

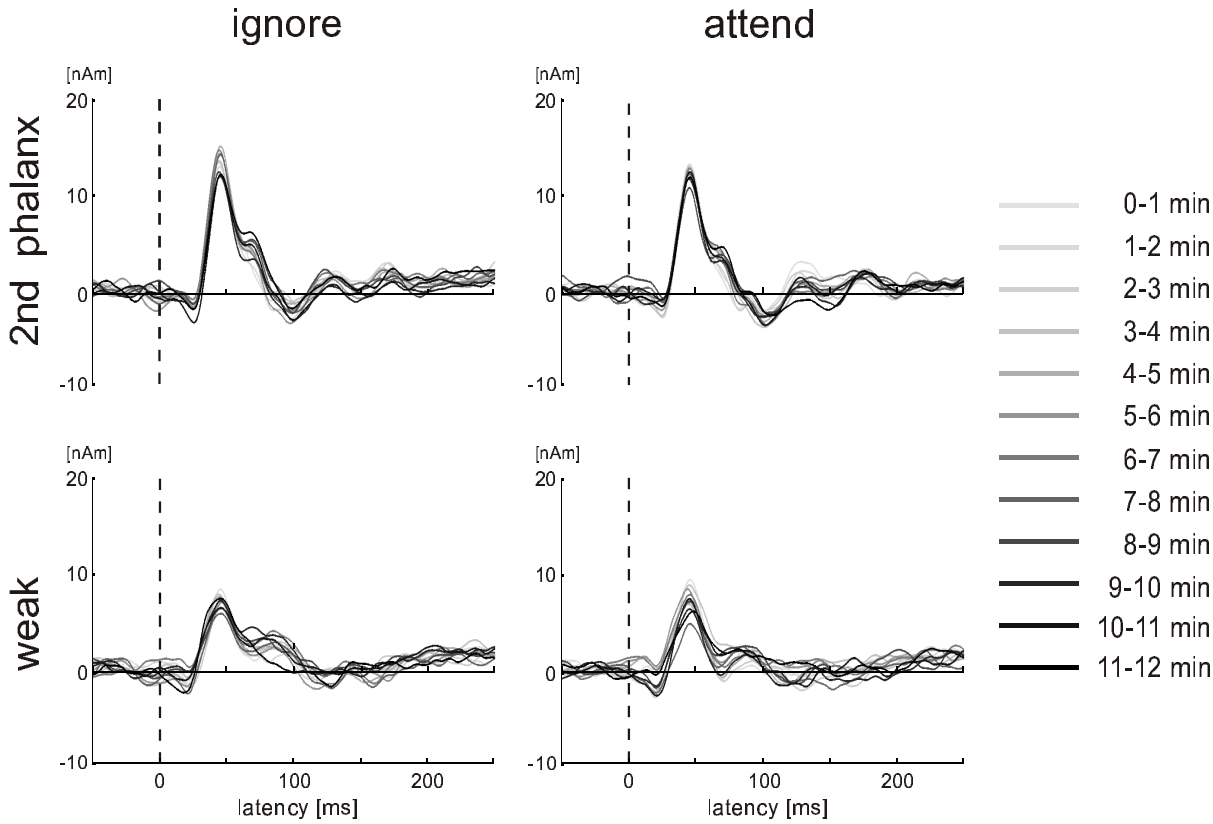

Figure 4.6: *Dependence of SI source waveforms on stimulation time. Shown are the grand averages of the 10 subjects taken over one minute intervals.*

time was an amplitude decrement of the P80m component that occurred consistently in all conditions with and without attention being directed towards the stimulus. In this respect the behavior of the P80m is decoupled from the other components. Although a small decrement of the P50m amplitude could be observed in this figure, the signal-to-noise ratio for this component was too low to obtain statistically meaningful results. A slight change in waveform morphology over time at a latency of around 170 ms was observed that was most prominent in the attend conditions. Here SII dipole moments, being in the negative range early in the measurement, changed towards positive values at later times. This effect, however, was weaker than the habituation effect observed for the P80m.

Habituation of the P80m was investigated in detail by analyzing the changes of its latency and amplitude over time. Latency evolution is illustrated in Fig. 4.9. The P80m amplitude decreased with continued stimulation, but latency was not affected. Attended

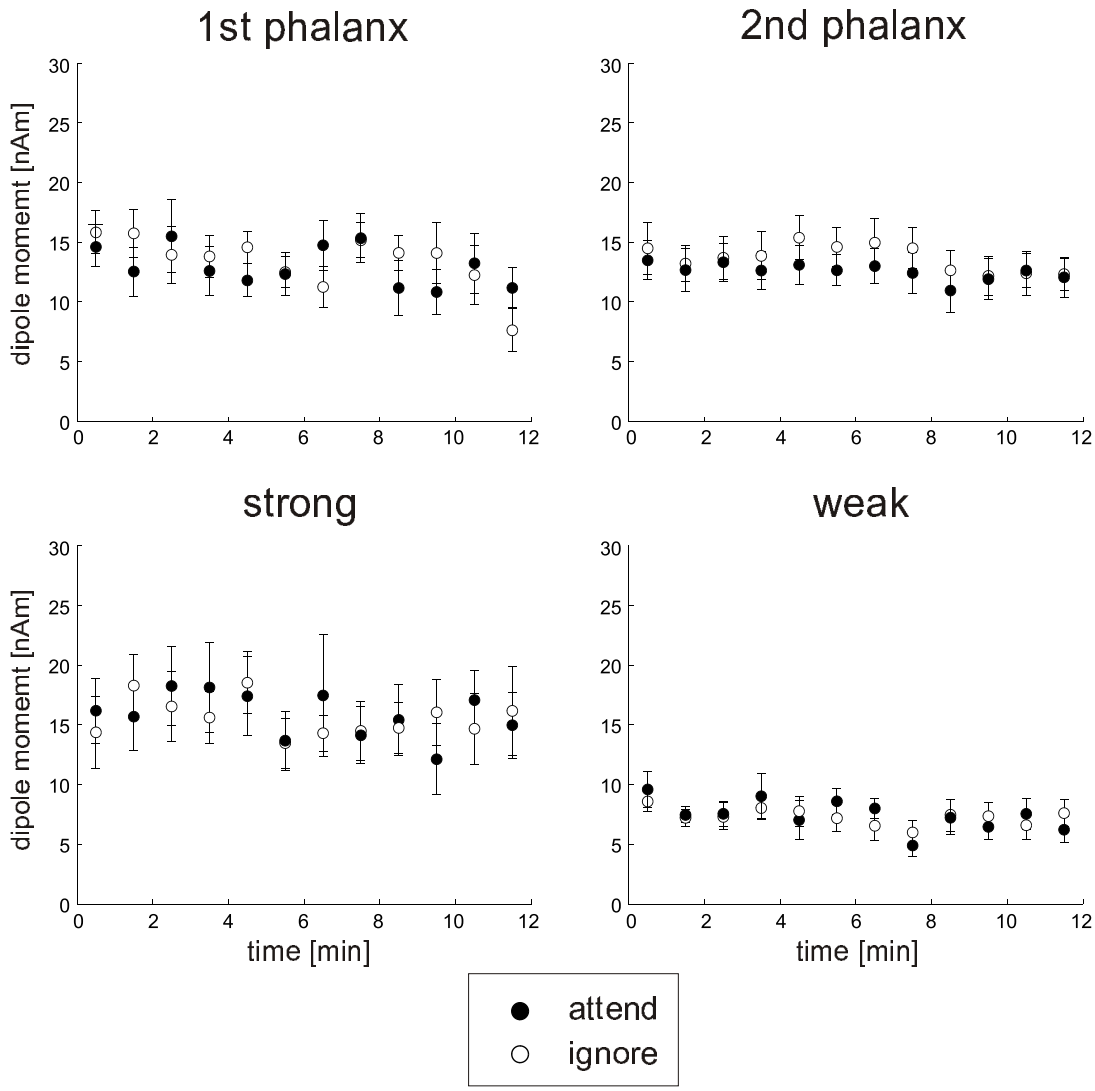

Figure 4.7: *Habituation of the P40m as determined from the the grand average SI source waveforms. Error bars indicate the standard error of the mean amplitude.*

and ignored stimuli peaked at the same latency, indicating that the attentional amplitude enhancement was not caused by the genesis of a novel component overlapping with the P80m.

For a quantitative analysis of the P80m amplitude habituation, exponential functions in the form of equation 4.1 were fitted to plots of the P80m dipole moment over measurement time (Fig. 4.10). In some attend conditions it was necessary to constrain the lower limit of Q_∞ to the value of the corresponding ignore condition, otherwise fits would have produced negative values due to the slow decrease of the data points in the observed time window between 0 and 12 minutes. These conditions are marked with an asterisk

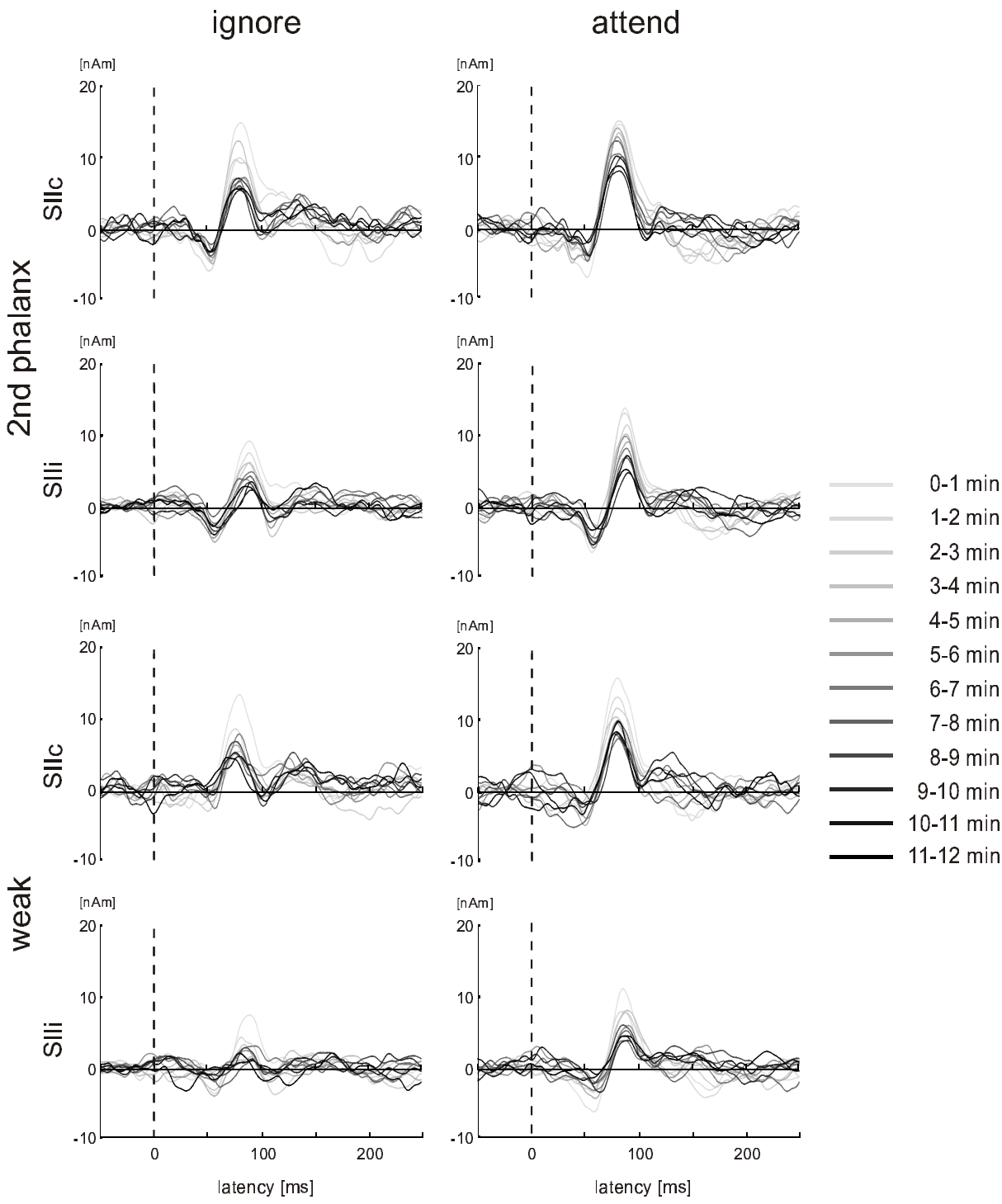

Figure 4.8: *Evolution of SII source waveforms during repeated stimulation. Shown are the grand averages of the 10 subjects taken over one minute intervals. There was substantial decrement of SII amplitudes over measurement time in all conditions, predominantly in the P80m component.*

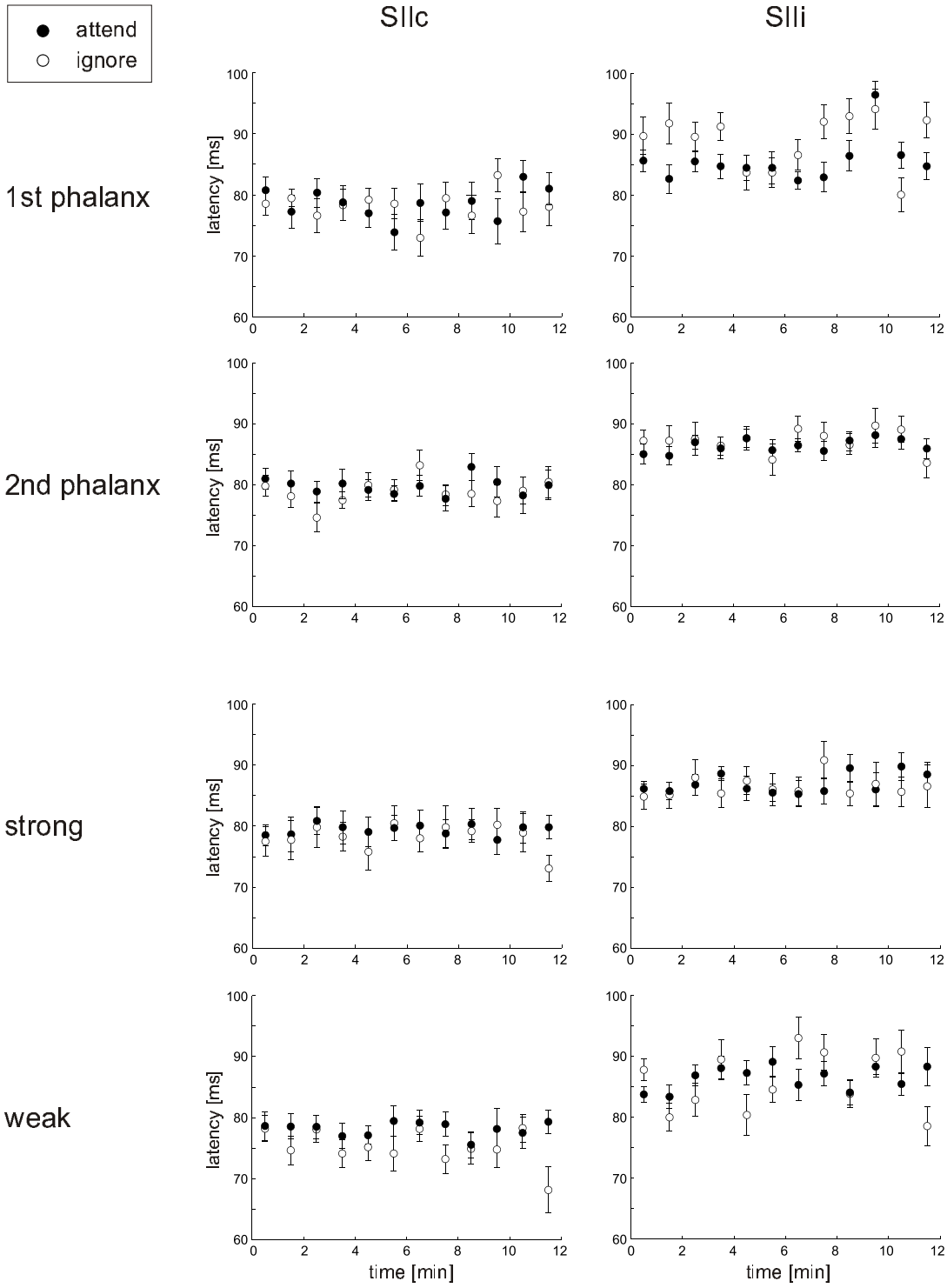

Figure 4.9: *P80m latency as a function of stimulation time as determined from the grand average source waveforms. Error bars indicate the standard error of the mean latency. No significant latency shift was induced by attention.*

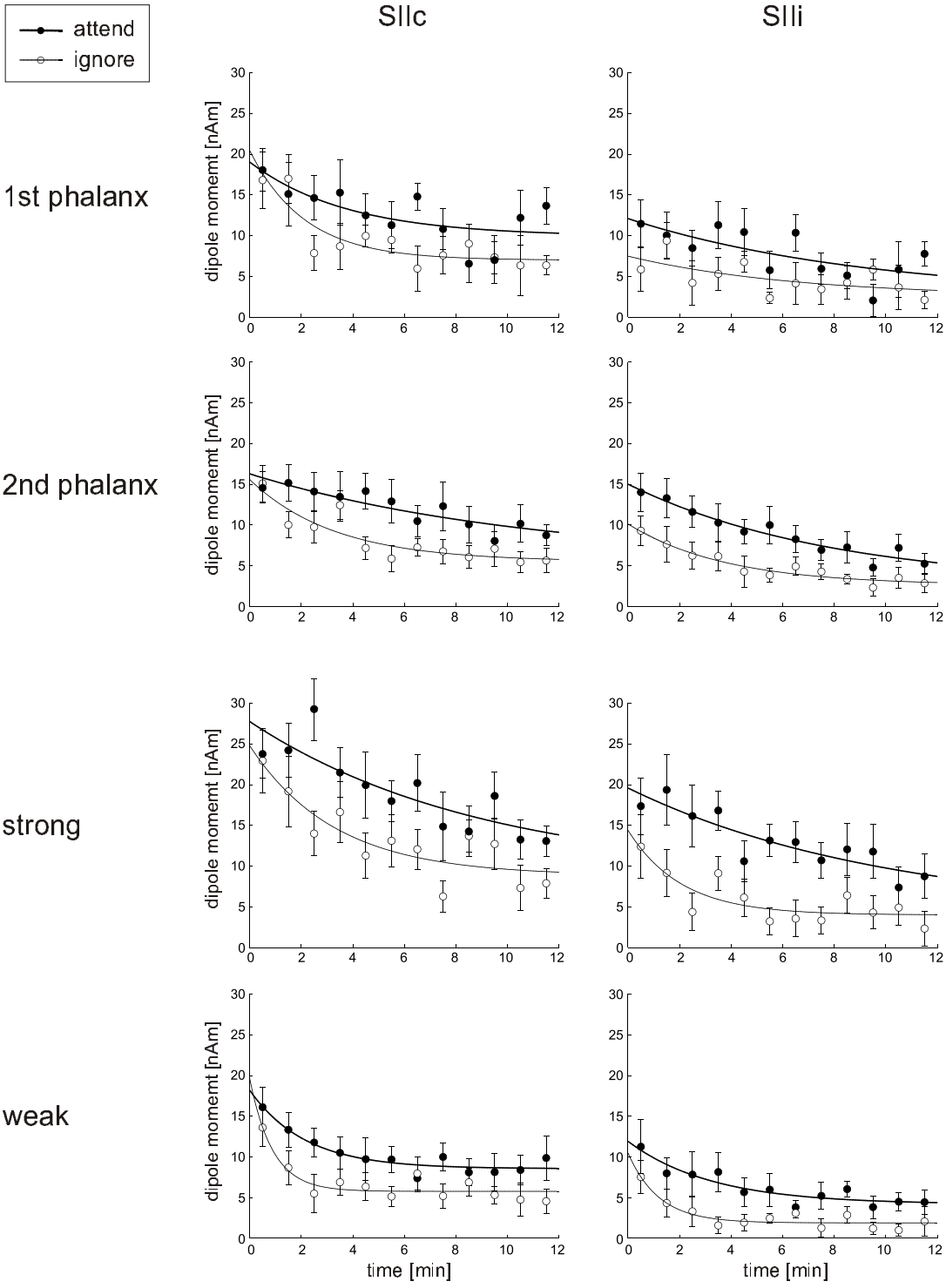

Figure 4.10: *Habituation of contra- and ipsilateral P80m as determined from the grand average SII source waveforms. An exponential decrement over time was fitted to the measured data. Error bars indicate the standard error of the mean amplitude.*

		ignore			attend		
		τ [min]	Q_0 [nAm]	Q_∞ [nAm]	τ [min]	Q_0 [nAm]	Q_∞ [nAm]
1st phalanx	SIIc	2.1	20.5	7.0	3.9	19.0	9.9
	SIIi	6.5	7.5	2.5	9.4	12.1	2.5 *
2nd phalanx	SIIc	3.3	15.6	5.5	10.9	16.3	5.5 *
	SIIi	3.8	10.1	2.6	7.9	15.0	2.6 *
strong	SIIc	3.3	24.8	8.8	9.0	27.8	8.8 *
	SIIi	2.1	14.4	4.0	10.0	19.6	4.0 *
weak	SIIc	0.9	19.6	5.8	2.1	18.2	8.6
	SIIi	1.2	10.5	1.9	3.3	16.4	5.3

Table 4.4: *Parameters of the exponential fit to the habituation data. An asterisk (*) indicates failure to determine Q_∞ to positive values in the attend condition without setting the lower limit to Q_∞ of the corresponding ignore condition.*

in Table 4.4, which lists the obtained fit parameters. Habituation time constants τ of SII activity ranged from 0.9 min to 6.5 min in the ignore conditions and from 2.1 min to 10.9 min with attention directed towards the stimuli. For more exact determination of τ, more averages and an extension of the measurement time would have been needed. However, relative differences in the response behavior to attended and ignored stimuli could well be obtained from the present data.

Figure 4.10 shows that the habituation of P80m amplitude developed in a different manner in the attend and the ignore conditions. With attention focused to the stimulated body site, response decrement was slower than in the ignore conditions. As a consequence, the amplitude differences between attend and ignore responses were at maximum after approximately 3 minutes on average. The larger values of the habituation time constant τ in response to attended as compared to ignored stimuli is the quantitative manifestation of this effect (cf. Table 4.4). It is illustrated in Figure 4.11, where the time constants of attend and ignore responses are directly contrasted for each stimulus in both hemispheres.

Hence decelerated habituation of the P80m amplitude under attention played a crucial role in the observed attentional enhancement. However, the effect cannot be attributed to this phenomenon exclusively, since even at $t=0$ responses to attended stimuli tended to be larger than those to ignored pressure pulses, as indicated by the exponential decay curves in Fig. 4.8 and the fitted values of Q_0 given in Table 4.4. Therefore, attentional enhancement observed in the averaged waveforms (Fig. 4.4) was a combined effect of instantaneous attentional enhancement and decelerated habituation.

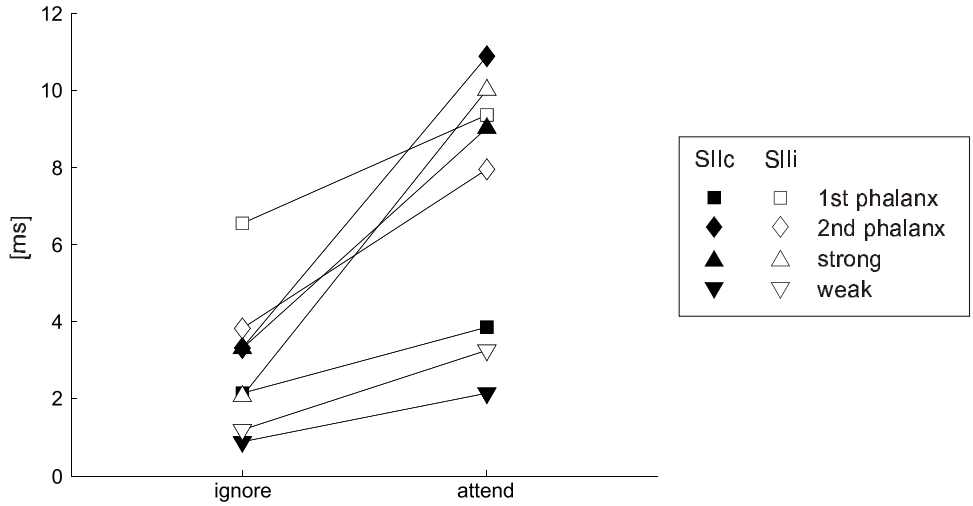

Figure 4.11: *Habituation time constants in the attend and ignore conditions. Habituation is markedly decelerated in the attend conditions.*

4.4 Discussion

The 3–dipole model used in this analysis separated the earlier SI activity (20–70 ms) from the later SII activity (45–150 ms). The use of the combined fitting and seeding technique by applying the transformations to Talairach coordinates (section 2.4) corrected for noise-induced depth localization errors and proved valuable to provide robust source waveforms across individuals, even for the 3 subjects in whom noise prohibited fitting of contralateral SII.

Visual distraction as used in this report has been commonly applied as a control condition in other attention-related studies [29, 109]. It proved convenient for the subjects and assisted the 'neglect' of the somatosensory stimulus [29]. Whether continuous visual input, e. g. reading [29] or video [109], affects somatosensory evoked activity independently of attention is still under debate [95].

4.4.1 Waveform morphology

Primary somatosensory cortex

None of the early SI components were significantly altered by attention. This is in agreement with previous SEF [56, 105, 109] and SEP [148, 149] results, but in contradiction to some other SEP [29, 44], positron emission tomography (PET) [19] and functional magnetic resonance imaging (fMRI) [82] studies. Weaker effects of attention on the

activity in SI as compared to SII have been observed in intracranial recordings in animals [21, 69, 120] showing a significantly larger fraction of neurons in SII influenced by attention when compared to SI. The emergence of new components around 140 ms as reported in an evoked potential study [44] was not observed.

As Mauguière et al. [105] suggested, these discrepancies may result from the insensitivity of MEG measurements to radial activity in SI. Neuronal activity in area 1 of the primary somatosensory cortex is scarcely recorded in MEG measurements (cf. Fig. 1.14). Also it should be considered that in some individuals early attention-related effects in SI might occur, as was documented by Fig. 4.3. However, the absence of an enhancement in the grand average waveforms indicated that such effects are not a common feature. If one was to assume attentional effects in area 1, an interindividual difference in the exact orientation of this region could be an explanation. Regarding recent evidence for attentional enhancement in SI from PET [19] and fMRI [82] studies is concerned, it should be emphasized that these methods measure different indirect correlates of neuronal activity with very limited time resolution and are in particular sensitive to activity in primary areas 1 and 2. On the basis of the presented results, however, it can be concluded that there are no significant attention-related changes in tangential SI activity up to a latency of 300 ms.

Secondary somatosensory cortex

Within the MEG localization accuracy, fitted SII locations agreed well with the anatomical regions known to comprise the secondary somatosensory cortex [119]. Waveform morphologies were very similar for contra– and ipsilateral SII with an average contralateral lead of 7 ms that had also been observed in previous studies [60, 105] (compare section 3.3.2).

The most striking result of the present study was the presence and similarity of attentional effects in all conditions. Activity enhancement occurred during the same post-stimulus time period ($\sim$ 55–130 ms) in all conditions. The relative magnitude of the effect and its temporal evolution did not vary substantially between contra– and ipsilateral hemisphere, between deviant (target) and standard stimuli, and between spatial and intensity discrimination paradigms. Thus the present findings extend the previously observed attention-related enhancement of SII activity following rare [105] and deviant [109] electrical median nerve stimuli to standard as well as deviant tactile stimuli in two different oddball paradigms.

The parallel behavior of the two hemispheres underpins the close connectivity of SIIc and SIIi. No hemispheric specialization occurred concerning attentive stimulus processing.

This similarity might be due to transcallosal fiber connections from the contralateral hemisphere to SIIi. Transcallosal signal conduction is also in agreement with the observed latency delay of SIIi with respect to SIIc. Therefore, it seems reasonable that attentional effects on contralateral SII activity directly map onto the corresponding components in the ipsilateral counterpart.

In contrast to previous suggestions [109], the attentional enhancement of SII did not depend on the target attribute (intensity or location) of the stimulus in our data. Nor did the enhancement reflect the process of target recognition, as was suggested in a previous study [105], since attention enhanced target and non-target responses similarly. Rather, the mere process of focusing attention towards the stimulated body part appeared to enhance neuronal activity in SII. The paradigm design with its close proximity of all stimuli at the left index finger was such that even though only deviants had to be counted, the subjects were forced to focus attention to both deviant and standard stimuli. Hence the task itself merely served to invoke attention but had no direct specific correlate in the evoked responses.

Consistent with the proposal of Garcia-Larrea *et al.* [44] that attention leads to the priming of any input coming from the attended body region, our results might reflect this priming effect in SII for target and non-target stimuli in the post-stimulus time period of 55 to 130 ms. This notion is in line with the results of single cell recordings [21], in which neuronal firing rates in SII were altered when attention was drawn to a body region within the neuron's receptive field. In addition, neurons exist in SII which are sensitive to *changes* in tactile input [81]. Thus, the purpose of attention-related increase of SII activity might be to facilitate the process of feature extraction that is necessary for tactile discrimination. However, this process, which is different for intensity and spatial discrimination, is likely to occur at a cortical stage beyond SII that is not mapped in standard somatosensory evoked fields due to sparse neuronal synchronization.

In the intensity task, statistical analysis revealed an interaction between attention and stimulus type (strong versus weak) that was not present in the spatial paradigm. This interaction may reflect a special significance of deviancy during intensity discrimination. The lack of an interaction in the spatial task, however, could rather indicate a general dependence of the attentional enhancement effect on stimulus intensity.

Regarding the latency dependence of the attentional enhancement, it is worth noting that not all SII components were affected in the same way. The early N50m was not altered significantly by attention in any condition, whereas the enhancement was largest in the latency range of the P80m. This indicates that these components behave differently and, therefore, should not be considered as representing one uniform biphasic activity. Later SII activity was considerably less enhanced, which supports the notion of distinct

generators of SII components P80m and P145m that has been derived in chapter 3. The emergence of a new N140 component that was observed in previous studies [44, 45] could not be replicated. On the contrary, the enhancement of the P80m tended to make later components less discernible in the attend conditions (cf. Fig. 4.4).

Divergent reports on component latencies and their sensitivity towards the state of attention can be attributed to several differences in the applied paradigms and recording methods. On one hand, the differences between EEG and MEG findings that have already been discussed above for SI are likely to account also for varying SII results. On the other hand, in some SEP studies no source analysis was performed but rather the waveform of individual recording channels or scalp topographies were examined [29, 44, 45, 148, 149]. Over the contralateral hemisphere, however, strong spatial and temporal overlapping of EEG activity (cf. discussion in chapter 3) prevents separation of activities in SI and SIIc. Therefore, the assignment of attentional effects to a confined brain area is difficult in these cases. A notable difference to previous work is the employment of tactile as opposed to electrical stimuli. Only the former represent an adequate way to simulate natural sensory input. Activated sources in the somatosensory system might slightly differ between the two methods, which may also account for the divergent findings mentioned above.

4.4.2 Habituation

This MEG study can not give an answer to the question about the mechanisms through which attentional enhancement is initiated, since only the effects on the obligatory sensory evoked activity could be observed. Active attention likely activates a multitude of brain regions. In a PET study, involvement of the frontal cortex, the anterior cingulate gyrus and bilateral parietal regions was observed [19]. A cued visual attention task monitored by fMRI activated a network consisting of superior frontal, inferior parietal and superior temporal cortex [67]. The study of habituation presented here provided insight into the temporal evolution of the enhancement effect and suggested that two independent processes participate in the phenomenon.

Primary somatosensory cortex

SI differed from SII not only with respect to the influence of attention on the source waveform morphology, but also regarding the habituation behavior. At most a weak response decrement over measurement time in SI was observed in this study. Although some previous results documented habituational effects in the primary somatosensory cortex [145], the present findings are in line with reports on much weaker response decrements in SI when compared to SII [25]. The fact that habituation is very closely linked to

the interstimulus time [6] is probably an explanation for differences to formerly published studies.

The results raised the question whether the absence of habituation and of attentional effects on SI source waveform are in any direct causal connection to each other. this would be the case if decelerated response decrement was the main cause for overall attentional enhancement effects. However, the attentional enhancement in SII already occurred during the first averaged time interval in the habituation study (Fig. 4.8). Hence an attentional enhancement mechanism independent of habituation behavior must be active.

The lack of habituation in SI has a very important consequence for the interpretation of the data obtained from the secondary somatosensory cortex. It can be excluded that receptor fatigue or substantial response decrement in the primary ascending pathways were the major cause for the habituation observed in the cortical projection areas. Otherwise already primary cortical responses that directly rely on afferent thalamo-cortical input should have shown significantly habituating responses.

Secondary somatosensory cortex

The presented results documented significant amplitude decrement of the P80m component as a function of measurement time in both the attend and ignore conditions and a small waveform change around 170 ms in the response to attended stimuli. P80m habituation could be fitted with an exponential decay function. Thereby the corresponding time constants could be quantified to be on the order of several minutes. The fact that SII amplitude declined over time is consistent with previous studies on habituation [60, 150] and ISI dependence of SII recovery [105]. However, in those studies electric stimulation was applied, which did not necessarily evoke the same response behavior as tactile pressure pulses.

More accurate quantitative data analysis could be obtained by using a larger number of subjects and a longer stimulation time in order to stabilize the fits of the exponential decline curves to the data. However, subject compliance and ability to focus attention to the stimulus is limited, which places constraints on the overall measurement time. The parameters chosen in this study were sufficient to allow a relative comparison of attend and ignore conditions.

Several mechanisms can account for the decrement of the SII response over time. Fatigue of the mechanoreceptors and other processes in the ascending pathway can be excluded in the present case, since, as discussed above, the early cortical components in SI habituated only marginally. Other suggested physiological mechanisms include the long

recovery times of SII neurons following excitation [105] and GABAergic inhibition in SII [74]. Declining vigilance of the subjects might also contribute to decreasing response amplitudes in SII [150]. However, this effect holds both for attend and ignore conditions and does not prevent a relative comparison of the two. The difference in the habituation time constants in the two conditions are unlikely due to a faster decline of vigilance in the ignore condition. Rather, some subjects reported it more tiresome to perform the monotonous counting task and focus attention to the stimuli than watching the movie that attracted their attention in the ignore condition. Therefore, the slower response decline to attended stimuli can be attributed to an active effect of attention rather than a passive side-effect. In addition attention to the stimulus tends to decrease towards the end of the mental counting paradigm. This should lead to a response decline with increasing time towards the amplitude values in the ignore condition, which would result in a seemingly faster habituation. Therefore, it is likely that the time constants determined for the attended stimuli would have been even higher if the subjects' attention could have been kept at a constant level.

Therefore, the attentional enhancement effect that was found in the source waveforms averaged over the whole measurement epoch could be assigned to two distinct mechanisms. As was to be expected, attention produced an initial enhancement of the P80m response amplitude in most conditions. However, after stimulation of the first phalanx and after weak stimuli the fitted initial dipole moments Q_0 were even slightly larger in the ignore condition in the contralateral hemisphere. Therefore, initial amplitude enhancement does not appear to play the major role in the observed overall dipole moment increase in SII under attention. As a second effect, decelerated habituation due to attention caused the difference towards the ignore condition to be at maximum after 2–5 minutes of stimulation. Thereafter the difference became smaller again. Subject fatigue and accordingly waning attention towards the end of the stimulation found its correlate in values of Q_∞ that were on average only slightly higher with than without attention directed towards the stimulated site. Data from longer stimulation times than 12 minutes would be necessary to model the long term development of habituation with higher accuracy.

The finding of an altered response decrement with stimulation time as mechanism underlying the attentional enhancement effect sheds a new light on diverging results in previous studies. The duration of the individual measurement sessions should have an influence on the magnitude of the observed overall attentional enhancement effects. Since in our study the largest difference between attend and ignore conditions occurred between 2 and 5 minutes, averaging over longer stimulation times would rather attenuate the overall attentional effects. Different stimulation times in previous studies on the effects of attention therefore make it difficult to directly compare the published results. In addition, the known dependence of habituation on the interstimulus interval makes it likely

that the attentional enhancement is similarly sensitive to the chosen ISI. Interstimulus time may thus be a crucial parameter in the study of attention. These considerations merit future investigations that could contribute to a quantification of these qualitative statements.

4.5 Conclusion

The 3-dipole model consisting of contralateral SI and bilateral SII sources was appropriate for mapping attention-induced activity changes in these brain regions. The combined anatomy-based fitting and seeding technique developed in chapter 2 allowed for consistent waveform mapping across all subjects. A reliable comparison of conditions could be performed by determining Grand Averages of the difference waveforms between attend and ignore conditions and calculating confidence intervals by means of bootstrapping.

The applied paradigm proved appropriate to determine functional differences between the SII components identified in chapter 3. Attention-induced activity modifications were not equal for those components. Enhancement was largest for the P80m component and significantly weaker for later SII activity. The early N50m component was not influenced by attention at all.

The presented MEG results document the strong influence of attention on the processing of tactile information in SII, whereas no effects were observed in SI. The attention-related increase of the P80m component in SII was present during spatial and intensity discrimination tasks, both for deviant and standard tactile stimuli. Therefore, the observed attentional enhancement in electrical source activity does not seem to represent the process of feature extraction itself. Rather the results indicate that attention exerts a general control on neuronal activation in SII and that the unknown mechanisms underlying the enhancement effect are initiated merely by focusing attention towards the stimulated body region.

The analysis of SII response decrement during stimulation revealed that the observed attentional enhancement was composed of two separate effects. Apart from a general enhancement of the P80m activity in SII, also its decrement over measurement time was altered by focusing attention towards the stimulation site. The decelerated amplitude decrease caused the difference between attend and ignore conditions to reach a maximum after several minutes of stimulation. Future investigations focusing on this dual effect of attention might contribute to a better understanding of the underlying mechanisms and contributing brain areas. Promising results can be expected for example from fMRI measurements with their good spatial resolution and a time resolution that, although

inferior to MEG measurements, should be sufficient to study the attention-related effects on habituation of tactile evoked SII activity.

Chapter 5

Interaction of simultaneous tactile stimuli

5.1 Introduction

Magnetic fields evoked by tactile stimulation of a single body site allow to image the time course of tactile evoked brain activity in SI and SII. The fit of the equivalent dipole location provides information about the center of the corresponding activity. However, the size of the receptive fields of the activated neurons cannot be estimated by single site stimulation, and no information about convergence of input from different body parts at the cortical level can be obtained. In order to study these processes, stimuli need to be delivered to several body sites and their mutual interaction must be evaluated. The different sites can be stimulated in an alternating fashion or simultaneously. In either case, the effects of the presence of the second stimulus on the evoked activity produced by the first contain valuable information about the convergence of information from different body sites at the various cortical levels. Interaction of two stimuli indicates that they are not processed independently. Interactions can be dissociated as suppressive and facilitating. In the former case, the presence of the second stimulus leads to a reduction of activity, in the latter case to an enhanced response.

The majority of the previous reports on interaction of somatosensory stimuli focused on the primary somatosensory cortex. Suppressive interaction of input to fingers at the same hand has been observed in SEP and SEF studies. Response amplitudes were reduced when interfering stimuli occurred simultaneously [10, 70, 76]. Additional facilitating effects in SI have been reported for weak and non-simultaneous stimulation in evoked response studies [42, 71, 86] and in single cell recordings [90]. Bilateral interaction has

been observed in one SEF study [134]. The effect was facilitating, tactile stimuli to one hand increased the SEF evoked by median nerve stimulation at the opposite hand. The stage at which the interaction of different stimuli occurs has not yet been determined. However, single neuron recordings in cats [23] have suggested interactions already at subcortical levels. Suppressive interaction is commonly interpreted in terms of receptive fields. When the receptive fields of the activated cortical neurons contain both stimulation sites, a preceding stimulus tends to reduce the neuronal response due to habituation. SI neurons in area 2 partly possess receptive fields that can comprise several fingers, while those of area 3b neurons are rather discrete and have much smaller spatial overlap [78]. Magnetoencephalographic measurements mainly detect the activity in the tangentially oriented primary area 3b (cf. Fig 1.15).

Animal studies employing fluorescent tracers [20] and microelectrode recordings [93, 151] agree in the finding of a rough somatotopic organization in SII. At least two mirror symmetrical maps of the body exist in SII and the adjacent parietal ventral area (PV) in the macaque monkey [93, 151]. This has been shown to be true for humans as well in a recent fMRI study [30]. Correlates of a rough somatotopic organization of SII were also found in magnetoencephalography (MEG) experiments [56, 60, 100]. In the latter studies, separate representation of the fingers in SII was suggested.

SII might play an important role in integrating somatosensory information from both sides of the body, especially during coordinated actions of both hands, because this cortical area is known to respond substantially both to contralateral and ipsilateral input. Input to contralateral SII is mainly transmitted via SI as well as via direct thalamic connections [83, 85]. Pathways activating ipsilateral SII might originate from the ventral postero-inferior nucleus of the thalamus [17, 37, 85] or from contralateral SI or SII via transcallosal connections [34, 84, 117]. Intracranial recordings in monkeys have shown that on the average receptive fields of SII neurons are larger than those of SI neurons [124]. Also, many SII neurons receive input from both sides of the body, mainly from homologous locations [151]. In SII, a strong decrease of activity was found in a recent MEG study using electrical stimulation of the median nerve [138] when a stimulus occurred 300 ms previously at the opposite hand. This interaction was interpreted as a correlate of bilateral receptive fields of SII neurons.

The present study was performed to investigate the temporal dynamics of the source activity evoked in SI and SII by simultaneous tactile input to fingers of one and both hands. Reference tactile stimuli were applied to the tip of the left thumb. These were combined with stimuli at four sites assumed to have cortical projection areas that were increasingly distant from that of the reference stimulus [108]: the second phalanx of the left thumb, the tip of the left little finger and the tips of digits 1 & 5 of the right hand. SEF source activity of SI and SII was compared for separate and simultaneous stimulation

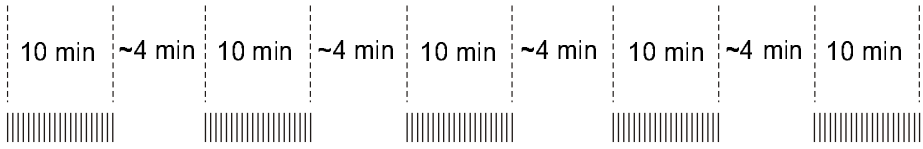

1st measurement:	D1 left, 2nd ph.	D1 left & D1 left, 2nd ph.	D1 left	D1 left & D5 left	D5 left
2nd measurement:	D1 right	D1 left & D1 right	D1 left	D1 left & D5 right	D5 right

Figure 5.1: *Sketch of the paradigm consisting of two measurements for each subject. In five blocks of 10 minutes duration each, one or two fingers were stimulated. D1 left, 2^{nd} phalanx and D5 left as well as D1 right and D5 right were exchanged randomly between subjects.*

at these sites. Interaction was investigated by comparing the sum of the source waveforms following separate stimulation with the brain activity following simultaneous stimulation. Independent processing of the simultaneous input should result in the summation of the brain activities following separate stimulation. Interaction was expected to affect simultaneous response amplitudes and/or latencies.

5.2 Materials and Methods

5.2.1 Stimulation paradigm

Tactile evoked fields were recorded in 10 healthy adults (aged 27-37 years, six male, nine right-handed). Measurements were approved by the local ethics committee and conducted with the informed consent of each subject. Each subject participated in two measurement sessions, each consisting of five blocks. In each block, tactile stimuli (section 1.4.3) were presented for ten minutes. The subjects did not perform any attention-focusing task in order to prevent effects on source waveform amplitudes caused by varying attention (cf. chapter 4). To compensate for the smaller SII amplitude that was to be expected due to the lack of attentional enhancement, the interstimulus interval was set to 1.6 s, longer than that used in the studies presented in the previous chapters. SII activity has been reported to be stronger at large interstimulus intervals [105]. However, a low stimulus rate leads to a reduction of the number of averaged epochs and hence to increased background noise. The value of 1.6 s has been chosen as an estimate of the value providing the highest signal–to–noise ratio. The stimulation paradigm is illustrated in Fig 5.1. The stimulated area was either the tip of the left thumb or a control site or both simultaneously. In

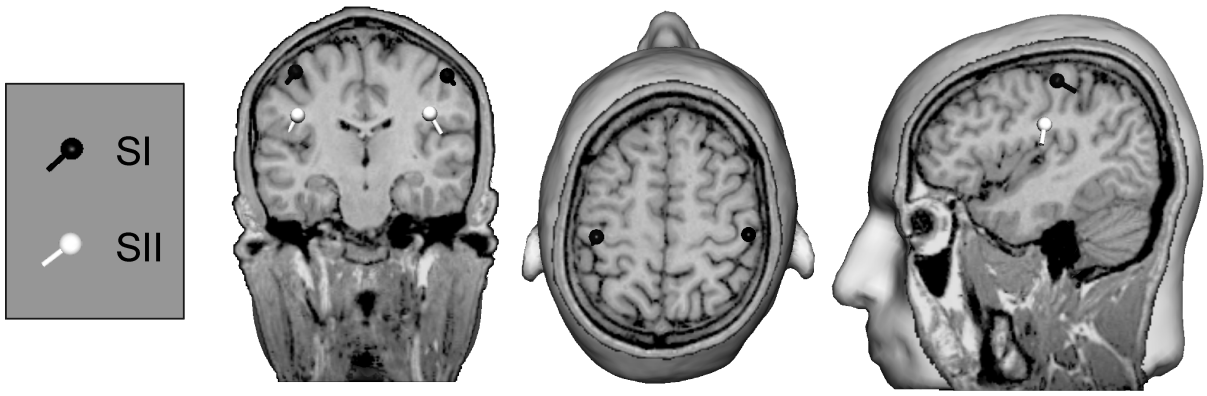

Figure 5.2: *Source model with SII equivalent dipoles seeded from Talairach space in subject 1, showing the model for data of the simultaneous stimulation of left digit 1 and right digit 5.*

session 1, contralateral interaction was studied with the tip of the right thumb (D1) and digit 5 (D5) as control sites. In session 2, ipsilateral interaction was tested with the tip of the left little finger and the second phalanx of the left thumb ($D1_2$). Between blocks, one finger clip had to be added or removed. The sequence of stimulation was designed such that clips at one stimulation site did not have to be attached twice in order to prevent amplitude differences due to slightly altered clip positions. The temporal order of the two control sites within one measurement block was randomized between subjects.

5.2.2 Data Recording and Source Modeling

Data were bandpass-filtered between 0.03 Hz and 200 Hz during recording and sampled at 769 Hz. For final analysis digital offline filtering was performed with a high-pass filter of 0.3 Hz (zero-phase, slope 6 dB/oct) and a low-pass of 70 Hz (zero-phase, 12 dB/oct). Simultaneous recording of ECG and EOG allowed for identification of heartbeat and eye artifacts. Approximately 375 artifact-free responses were averaged in each condition. MEG coordinate systems were matched with individual T1 weighted magnetic resonance images (Picker Edge 1.5 T).

Equivalent current dipoles in SI and SII were used to analyze the interaction of the left thumb with the four control sites (Fig. 5.2). To investigate bilateral interaction in SI, one equivalent dipole in each hemisphere was fitted to the separate measurements of each finger site over an interval of 20-60 ms. In the unilateral measurements a single dipole was fitted over the same interval to each of the two simultaneous SEF data sets to determine one equivalent center of SI. The closeness of the SI representations of the two stimulated finger sites of the same hand necessitated and allowed this simplification.

To separate the activities of SII and to investigate interaction in these brain areas, two additional equivalent dipoles were placed into the left and right parietal operculum according to the procedure for the analysis of group data that was developed in section 2.4. The resulting equivalent dipoles (three for unilateral, four for bilateral stimulation) were held fixed to calculate the source activity waveforms in SI and SII in the separate and simultaneous conditions (Table 5.1, Fig. 5.2). For each condition, an interaction waveform was derived by subtracting the response to simultaneous stimulation from the sum of the responses to separate stimulation. In the resulting interaction waveforms flat signals indicated the absence of interaction while deviations having the same polarity as the separate signals indicated suppressive interaction and deviations of opposite polarity indicated facilitation.

5.2.3 Statistical Analysis

Peak intensities and latencies were determined for the source waveforms and compared using the two-tailed Student's t-test for correlated observations. Grand averages of the data of all subjects were calculated. The 90 % confidence interval to the grand average of the interaction waveform was determined using the bootstrap-BC_a-method [32] with 1000 randomly drawn bootstrap samples of the data (MATLAB® 6.0). Like in chapter 4, the effect was considered significant on the 5 % confidence level where this confidence interval did not include the baseline.

5.3 Results

Fig. 5.3 illustrates typical features of the individual source waveforms. Modeled waveforms in all stimulation conditions are shown for one subject. In each condition, the earliest cortical activity was generated at the primary somatosensory cortex. During stimulation of right digits 1 and 5, no activity in the ipsilateral, right SI was observed, as was to be expected on the basis of previous MEG studies [87, 106]. SII waveforms were very similar across conditions. However, in response to separate stimulation of digits 5 on both sides amplitudes of right SII were small and no distinct components could be determined. Fig. 5.3 gives an impression of the intra-subject variability and the background noise activity contained in the source waveforms. Therefore, for further analysis the confidence intervals of the grand averages were used to allow for the assessment of statistically significant effects.

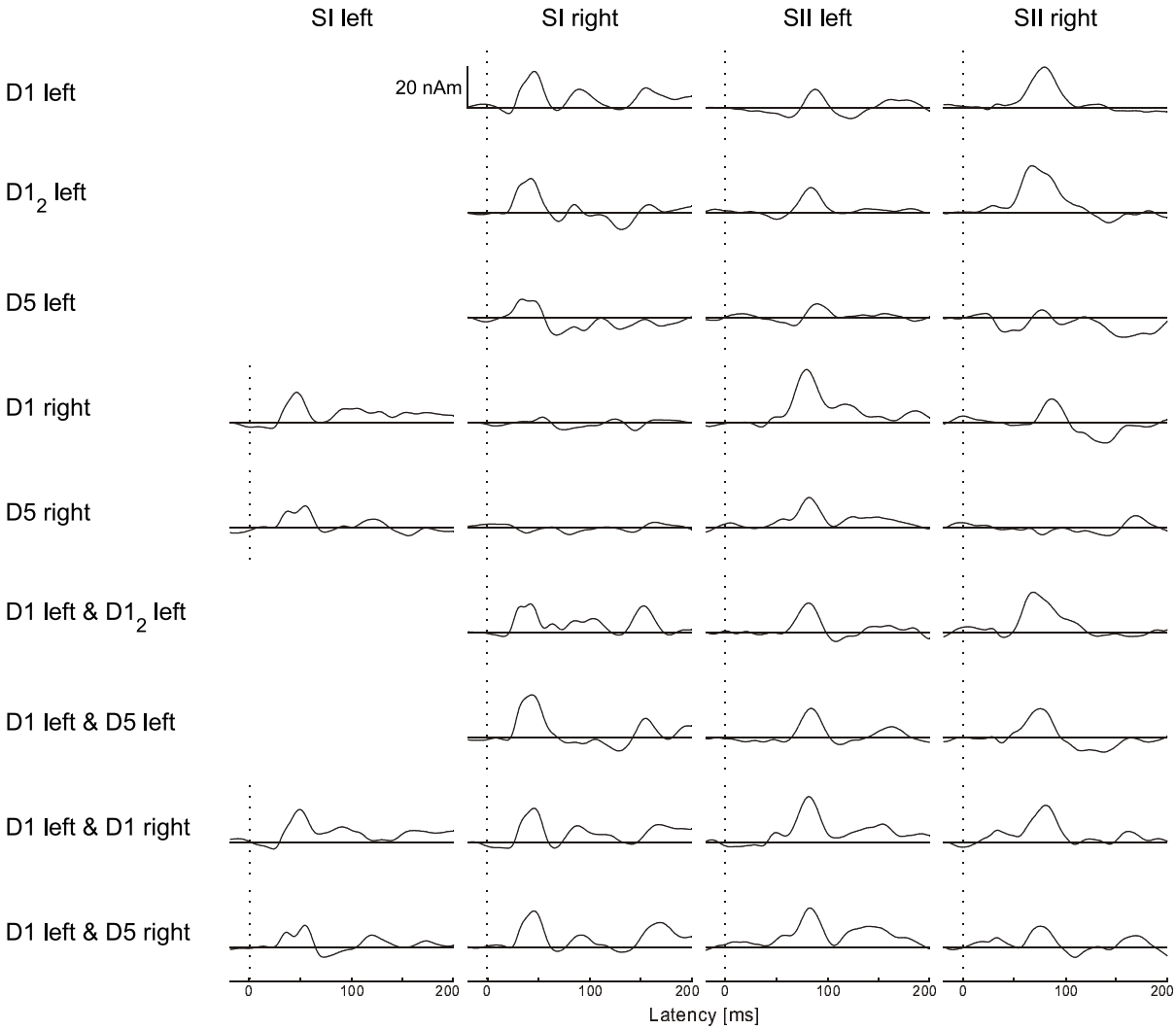

Figure 5.3: *SI and SII source waveforms of all measurements of one subject. Each row shows the responses to the stimulation of one or two digits as indicated on the left.*

5.3.1 Primary somatosensory cortex

The fitted equivalent current dipoles related to the early activity in SI (20–60 ms) were located at the anterior wall of the postcentral gyrus contralateral to the stimulus (Fig. 5.2, Table 5.1). Location, latency and orientation were consistent with activity in the hand region (area 3b) of the somatotopically organized primary somatosensory cortex [4, 62, 88]. The SI source waveforms showed a small N20m and a large P40m/P60m complex with comparable latencies across all conditions. Fig. 5.4 illustrates the evoked responses averaged over all subjects.

SI interaction waveforms in Fig. 5.4 showed interaction of unilateral but not of bilateral

	x	y	z
SI right (D1 left)	46.1±5.5	-19.8±5.9	50.0±3.1
SI right ($D1_2$ left & D1 left)	42.8±4.8	-22.5±6.7	52.0±5.3
SI right (D5 left & D1 left)	44.7±3.4	-20.8±6.9	52.9±4.7
SI right (D1 right)	-44.2±4.8	-20.1±5.2	46.4±4.8
SI right (D5 right)	-43.1±3.8	-21.3±5.3	53.0±3.7
SII right	40.1±4.3	-19.3±6.3	29.3±4.4
SII left	-42.9±6.1	-17.4±6.1	28.4±4.6

Table 5.1: *Fitted source locations in Talairach coordinates (mean ± s.d.).*

simultaneous input (Fig. 3). Simultaneous stimulation of the left thumb and digit 5 resulted in significantly enhanced SI activity (mean enhancement 4.3 ± 2.4 nAm, $t(9) = 5.66$, $p < 0.001$), but the response was significantly smaller than the sum of the separate responses. Unilateral interaction increased considerably when the immediately adjacent first and second phalanges of the left thumb were stimulated. The simultaneous response was almost identical to the response following separate stimulation of the second phalanx (Fig. 5.4, Table 5.2). During bilateral stimulation, however, SI responses showed near to flat interaction waveforms and, thus, did not interact significantly (Fig. 5.4). Apparently, this was a result of the non-activation of SI by ipsilateral input during the early interval (20–60 ms).

5.3.2 Secondary somatosensory cortex

Bilateral sources could be localized in seven subjects during the interval of 70–100 ms in the parietal operculum above the Sylvian fissure (Table 5.1, Figure 5.2), the region known to comprise SII [62, 119]. The fitted source locations agreed well with those obtained in section 4. The morphology of the SII source waveforms was consistent with previous studies [39, 41, 65] (compare also section 3.3.2) and showed a small negative component around 50 ms (N50m) followed by a prominent positive peak around 80 ms (P80m). SII responses also exhibited a late deflection around 120 ms superimposed on the downslope of the P80m (Fig. 5.5), in agreement with former EEG studies [45, 147] and intracranial recordings [41]. However, this second positivity did not occur consistently over all subjects and conditions and was, therefore, not analyzed in detail. Contralateral source activity was significantly larger and earlier as compared to ipsilateral activity. P80m amplitudes were 95 % larger in SIIc (Table 5.2) and peaked 8.5 ms earlier (Fig. 5.6) when averaging over all separate stimulation conditions and subjects.

SII source waveforms did not show summation when comparing simultaneous to separate

	SI right (P40m/P60m)	SII left (P80m)	SII right (P80m)
Separate			
D1 left	14.5 ± 5.0	10.1 ± 3.8	20.0 ± 7.2
$D1_2$ left	16.1 ± 5.0	11.2 ± 5.9	21.2 ± 6.5
D5 left	11.4 ± 2.7	8.5 ± 6.5	16.3 ± 12.5
D1 right	–	22.3 ± 8.7	12.3 ± 6.5
D5 right	–	19.8 ± 7.4	9.2 ± 8.4
Simultaneous			
$D1_2$ left & D1 left	17.2 ± 6.1 n.s.	12.2 ± 5.8 n.s.	20.5 ± 4.9 n.s.
D5 left & D1 left	18.3 ± 4.4 ***	11.8 ± 4.6 n.s.	20.1 ± 10.0 n.s.
D1 right & D1 left	14.2 ± 5.5 n.s.	21.9 ± 7.2 **	23.5 ± 7.4 n.s.
D5 right & D1 left	15.1 ± 4.6 n.s.	19.2 ± 8.8 **	19.9 ± 9.1 n.s.
Interaction			
$D1_2$ left - D1 left	12.8 ± 4.4 ***	8.4 ± 5.3 ***	18.4 ± 8.9 ***
D5 left - D1 left	7.4 ± 2.7 ***	6.6 ± 4.8 **	15.7 ± 9.5 **
D1 right - D1 left	–	13.4 ± 6.0 ***	10.7 ± 5.7 ***
D5 right - D1 left	–	12.0 ± 6.8 **	9.0 ± 4.9 ***

Table 5.2: *Amplitudes of the main activity peaks in nAm (mean $\pm$ s.d.). Asterisks indicate different significance levels obtained from the paired two-tailed t-tests. Simultaneous responses were compared with separate stimulation of left digit 1, interaction amplitudes were tested versus zero (n.s.: not significant, *: $p<0.05$, **: $p<0.01$, ***: $p<0.001$).*

responses. In both hemispheres, interaction waveforms were large and of similar size as one of the separate responses (Fig. 5.5). In the bilateral stimulation condition, the simultaneous source waveform of each hemisphere was almost identical to the source waveform elicited by stimulation of the corresponding contralateral side alone. Hence, the bilateral interaction waveforms in Fig. 5.5 closely resembled the response to separate ipsilateral stimulation which did not contribute to the simultaneous response. This effect was observed throughout the SII response interval of about 50–200 ms and was supported by the statistical comparison of the individual latencies: P80m latency of the bilateral interaction waveforms was significantly longer (on average 10.6 ± 7.2 ms, $t(34) = 8.73$, $p < 0.001$) than the response to contralateral finger stimulation but not significantly different (-1.9 ± 8.1 ms, $t(35) = 1.42$, $p > 0.05$) from the response to ipsilateral finger stimulation (Fig. 5.6).

Also in the unilateral stimulation condition, one stimulation site appeared to dominate the response to simultaneous stimulation. The P80m latency of the separate response to the first phalanx of left digit 1 was significantly longer than that of the response to

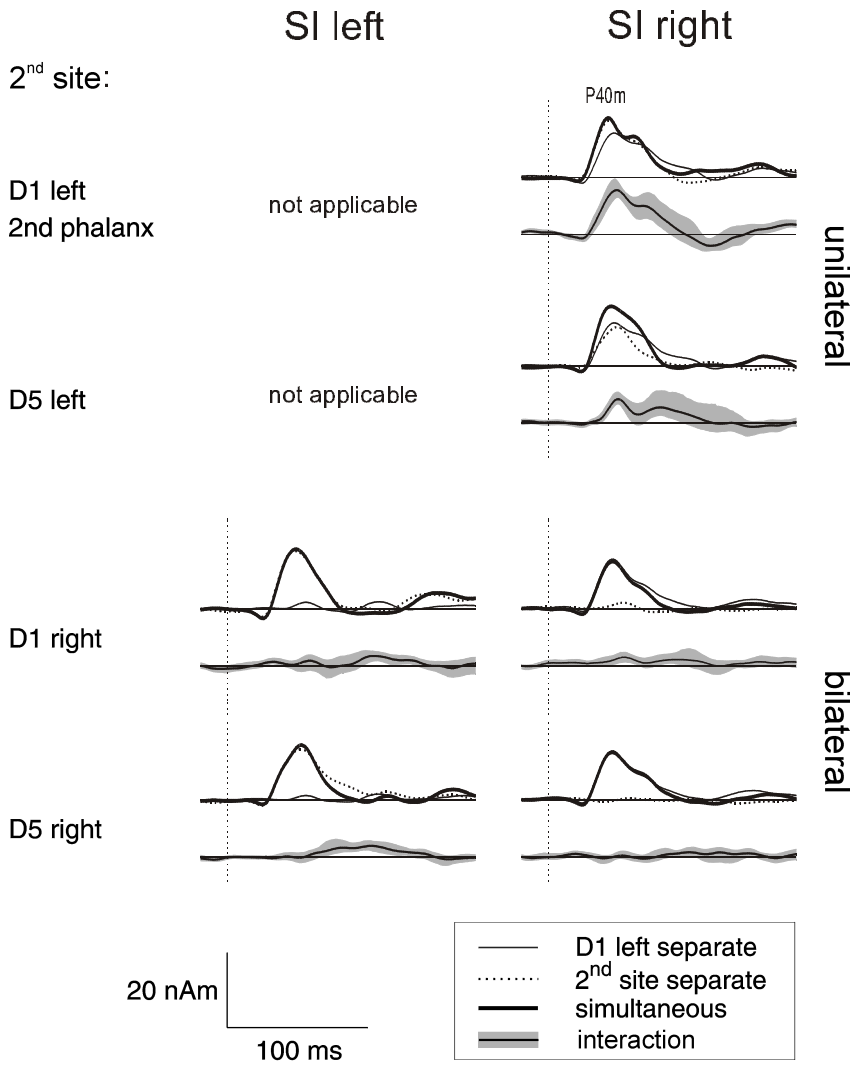

Figure 5.4: *Grand average source waveforms of the responses in SI. In each row, the interaction of left digit 1 with one of four control fingers (second site) is shown. The vertical dashed line indicates the stimulus onset. The interaction waveform was calculated as the difference between the summed responses to separate finger stimulation and the response to simultaneous stimulation. The shaded area is the 90 % confidence interval for this curve as determined with the bootstrap BC_a method. For analysis of the unilateral stimulation, left SI was not modeled.*

the second phalanx in the left hemisphere (2.6 ± 1.8 ms, $t(9) = 2.50$, $p < 0.01$). Left digit 1 latency was significantly shorter than that of left digit 5 in the left (2.7 ± 2.0 ms, $t(9) = 4.97$, $p < 0.01$) and the right (3.3 ± 3.2 ms, $t(6) = 3.82$, $p < 0.05$) hemisphere. In both conditions, the input that evoked activity at earlier latencies dominated the simultaneous response and the interaction waveform peaked at the same latency as the later input (Figs. 5.5, 5.6).

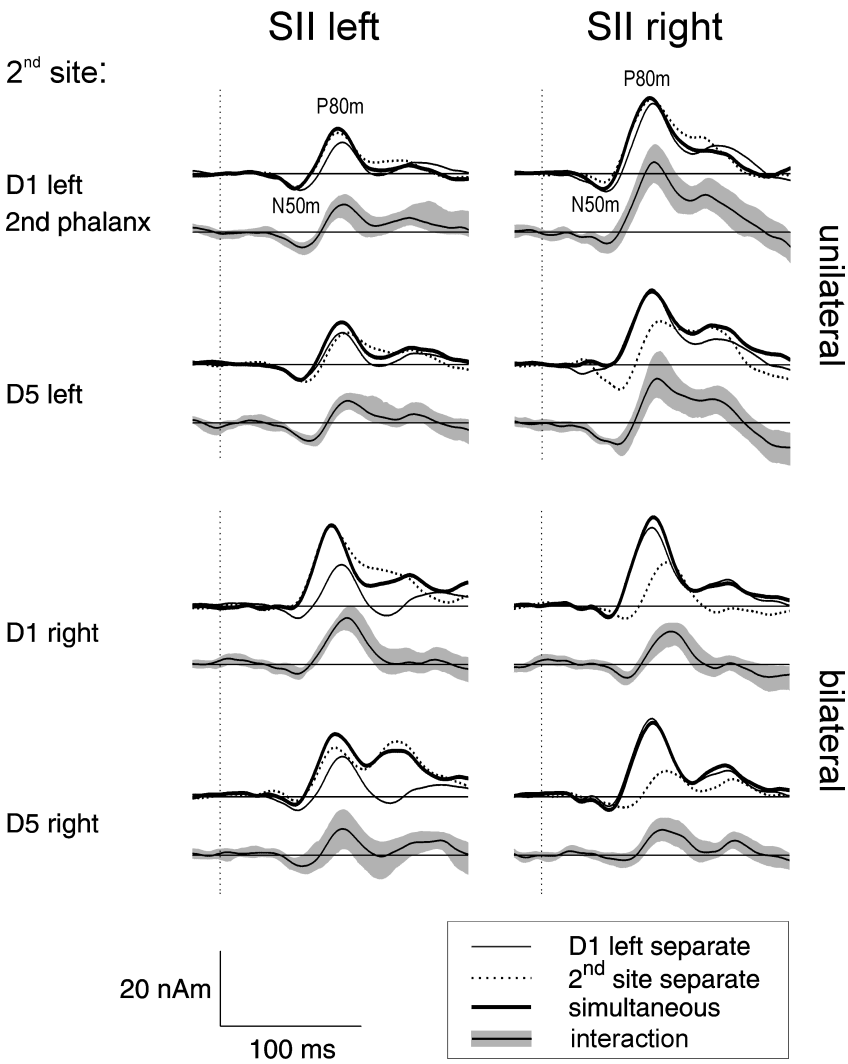

Figure 5.5: *Grand average source waveforms of the responses in SII. In each row, the interaction of left digit 1 with one of four control fingers (second site) is shown. The vertical dashed line indicates the stimulus onset. The interaction waveform was calculated as the difference between the summed responses to separate finger stimulation and the response to simultaneous stimulation. The shaded area is the 90 % confidence interval for this curve as determined with the bootstrap BC_a method.*

5.4 Discussion

5.4.1 Primary somatosensory cortex

Our results on the interaction in SI following simultaneous stimulation of two finger sites at the contralateral hand confirm findings of former studies [10, 70, 76]. The unilateral

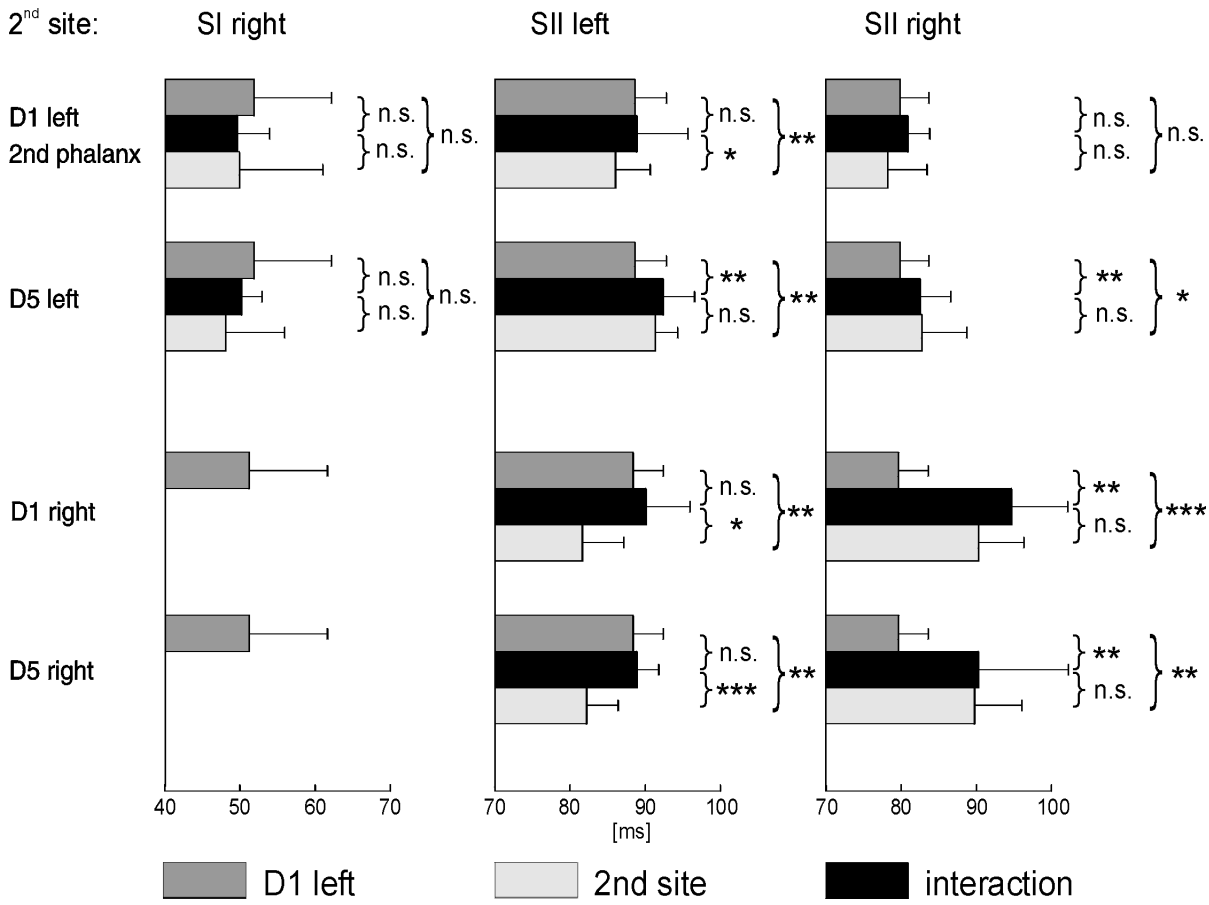

Figure 5.6: *Latencies (mean and standard deviation) of the main peaks of the source waveforms of right SI and bilateral SII. The responses to separate finger stimulation as well as the corresponding interaction curves were evaluated. For SI, latencies were determined for the P40m/P60m complex, SII latencies refer to the P80m peak. Asterisks behind the brackets indicate different significance levels of the paired, two-tailed t-test (n.s. = not significant, * = $p < 0.05$, ** = $p < 0.01$, *** = $p < 0.001$).*

interaction was largest for phalanges 1 & 2 of the left thumb and, in this case of immediately adjacent sites, simultaneous stimulation did not lead to a significant enhancement of the SI response when compared to separate stimulation. Interaction was still present but decreased for the two more distant sites, digits 1 & 5. Thus, the interaction of unilateral input to SI appears to be related to the amount of convergence of the two inputs along the somatosensory pathway [71].

The interactions in SI observed in our study were suppressive in all conditions in agreement with previous studies [48, 138]. The observed suppressive interaction is probably not due to occlusion along the somatosensory pathway, because the stimulus intensity used in this study was in a range in which SI as well as SII activity have previously

shown strong intensity dependence (cf. chapter 4). Therefore, inhibition is the more likely cause for the observed interaction in SI. At which level in the afferent pathway this interaction occurs cannot be determined from our data because MEG predominantly measures cortical currents. One possible explanation might be mutual lateral inhibition of the adjacent and partially overlapping cortical projection areas of the digits. However, unilateral interaction could also occur at the thalamic level as suggested by Okajima et al. [116].

We did not observe any significant activation in SI following ipsilateral stimulation nor any interaction due to bilateral stimulation. Based on a model with four equivalent dipoles located bilaterally in SI and SII, a near to complete separation of the source activities of both hemispheres and both areas was achieved as evidenced by the flat SI source waveforms following separate ipsilateral stimulation. Previous studies have reported SI activity due to ipsilateral input only at longer latencies above 80 ms [4, 92]. Bilateral interaction was observed with input of different modalities in a SEF study by Schnitzler et al. [134] in which SI activity due to contralateral electrical median nerve stimulation was significantly enhanced by concurrent ipsilateral tactile stimulation. Our findings, however, rule out a significant bilateral interaction of simultaneous brief tactile stimuli at an early processing stage up to 80 ms. This lack of bilateral interaction in SI is consistent with the observation that the receptive fields of SI neurons are almost exclusively unilateral [108].

5.4.2 Secondary somatosensory cortex

The observed differences between contra- and ipsilateral activity in SII agree with previous studies: the latency lag of ipsilateral SII of 8.5 ms has been shown previously in MEG [37, 65] and intracortical studies [41] and might reflect polysynaptic transmission from the contralateral hemisphere via corpus callosum [34]. Our P80m amplitudes were higher in contralateral than ipsilateral SII, also consistent with former MEG [65, 138] and intracranial measurements [18]. Previous findings of a hemispheric difference of the two SII areas in anterior-posterior direction [138, 150] were not replicated.

The responses to simultaneous bilateral finger stimulation had the same amplitudes, latencies and waveforms as the responses to separate stimulation of the contralateral finger. The later input from the corresponding ipsilateral finger appeared to be suppressed. This conclusion is not fully stringent, since neuromagnetic fields record the compound activity of all neuronal assemblies in one area and cannot dissociate the contributions arriving via different pathways. However, the striking similarity of the responses to separate contralateral and simultaneous finger stimulation during the whole period of SII activity

(50–200 ms post-stimulus, Fig. 5.5) strongly favors the above interpretation. This resemblance might be caused by the earlier arrival of the contralateral input in SII and inhibitory or refractory effects on the ipsilateral input arriving consecutively with a delay of about 8 ms. The results for unilateral interaction support this interpretation. In both unilateral conditions, simultaneous waveforms resembled the separate response arriving a few milliseconds earlier and the interaction waveforms peaked at a latency corresponding to the slightly later input (Fig. 5.6).

The interactions in SI and SII were very different. SI showed only unilateral interactions decreasing with distance between the stimulated sites, thus suggesting moderate overlap of the related receptive fields in SI. In contrast, complete interaction was observed in SII even for bilateral stimulation. This might be interpreted in terms of largely overlapping, bilateral receptive fields in SII, as found in animal studies [93, 151], or an additional mechanism involving inhibitory and/or refractory effects. The interactions cannot be explained by an exclusively hierarchical processing of the input from SI in the same hemisphere, since SII responded to separate ipsilateral input either via contralateral SI and transcallosal connections and/or via thalamic connections. Connections from both the ipsilateral and contralateral SI to SII [83, 84] as well as direct connections from the thalamus [17, 37, 85] have been documented in the literature. However, the latency delay in SII observed in our and previous studies [60, 138] following separate ipsilateral stimulation suggests activation from the contralateral SI via transcallosal fibers. Transcallosal fibres are also involved in transmitting signals between the SII areas of both hemispheres [34, 84, 117]. Hence one could expect at least a partial dependence of SII activity in one hemisphere on that in the other. However, the suppression of the ipsilateral input in SII during simultaneous stimulation suggests that the transmission of information between both hemispheres is either not reflected in the evoked response or not necessary for the processing of simple tactile stimuli presented synchronously to both hands.

In consideration of the identification of several SII components presumably having distinct generators and functional properties (cf. chapters 3 and 4), it is noteworthy that interaction occurred for all of these components. The interaction waveforms in Fig 5.5 nearly equaled the corresponding later separate waveform (i. e. ipsilateral in the case of bilateral stimulation) over the whole observed time interval of SII activity. No specific behavior of N50m, P80m and the late components was observed. This finding could be interpreted as manifestation of the dependence of the late SII activity on the earlier components, i. e. a serial signal transmission within the generators of the different components in SII. Any suppressive effect in the N50m would then propagate to all later components. However, the fact that attention appeared to affect the P80m much more than later SII activity (cf. chapter 4) contradicts this simple interpretation. Rather it appears that a

common mechanism acting independently on the different SII components underlies the interaction.

5.5 Conclusion

The reported congruent findings of unilateral and bilateral interaction in SII suggest a mechanism leading to the selection of the earlier input in SII for further processing and the complete suppression of any other input arriving up to several milliseconds later. In the case of bilateral interaction, this mechanism seems to provide a basis for hemispheric specialization to the contralateral sensory space. In a report on median nerve SEFs using paired stimuli with an asynchrony of 300 ms, Simões and Hari [138] found unilateral and bilateral interactions with only partially reduced response amplitude to the second stimulus. How long and how effectively the suggested interaction mechanism sustains suppression of ipsilateral input needs to be studied further using asynchronous bilateral input with smaller time disparities.

Summary and outlook

In the presented work the secondary somatosensory cortex has been studied by means of magnetoencephalographic measurements and spatio-temporal source imaging of the recorded data. Tactile pressure pulses were applied in order to elicit somatosensory evoked activity in the primary and secondary somatosensory cortex. An appropriate technique for imaging tactile evoked activity in SII and for the statistical evaluation of group studies has been developed. The results have been applied to identify and characterize different components in SII. The dominant SEF activity in SII, the P80m peak, has been analyzed in detail with respect to its dependence on the subject's state of attention and its response when stimuli at two different body sites are delivered simultaneously.

As a first step in the examination of the secondary somatosensory cortex, different modeling techniques have been tested with respect to their feasibility to image activity in SII. Interpolated data maps, distributed source models and the MUSIC approach, a discrete modeling technique based on the principal component analysis, proved not adequate, since they did not allow for a separation of SII responses from the overlapping SI activity. Instead, sequential fits of equivalent current dipoles not only allowed for source separation of SI and bilateral SII, but also provided the possibility to identify characteristic components in the source waveforms and thereby enabled the quantitative analysis of SII source activity. With this result as a basis, a fitting and seeding technique was developed for the combined analysis of data obtained from several subjects. The method employs coregistration of MEG data and magnetic resonance images in order to combine the localization capacities of spatio-temporal dipole modeling and Talairach coordinates as a standardized brain reference system.

A study that combined EEG and MEG was performed in order to elaborate differences and common features of the electric and magnetic correlates of neuronal activity in SII and to characterize orientations and latencies of its generators. Two major contributions to SII activity could be identified. Both EEG and MEG showed activity in SII around a latency of 80 ms with a dominant inferior–superior orientation, preceded by a small component around 50 ms of opposite polarity. Later activity around 135 ms was produced

by a generator with posterior–anterior orientation in the tangential plane that was dominant in EEG but small in MEG data. EEG and MEG results were compatible in source orientations, whereas the latencies of the late component were slightly different. It was concluded that at least two distinct generators in or near the SII area contribute to the activity that can be mapped in spatio-temporal source analysis of both EEG and MEG data. Evoked EEG data was much more contaminated by background brain activity and suffered from localization inaccuracies more than its magnetic counterpart. The sensitivity towards radial components and the active role of volume currents in the generation of extracranial potentials accounted for these disadvantages. Due to this observation, it was concluded that for functional mapping of SII it is most appropriate to employ magnetoencephalography and focus attention on the P80m component.

Using these methods, the influence of attention on SII activity evoked by tactile finger stimulation was studied. Two oddball paradigms with stimuli varying in location and intensity, respectively, were applied. One objective was to test for differences in the effects of the corresponding discrimination tasks on SII amplitudes. P80m amplitudes were enhanced in both paradigms, both contra- and ipsilaterally to the stimulated left index finger. Responses to deviant and standard stimuli were similarly affected. Evidence was found for specific behavior of the different identified components in SII. Attention selectively enhanced the P80m, but not the N50m and later components. SI waveforms were not altered by attention. By taking subaverages of the evoked data over one-minute intervals it was shown that the attentional enhancement was partly due to an altered response decrement with stimulation duration. The determination of habituation time constants by means of exponential fits to the P80m amplitude over time revealed significantly slower response decay following attended compared to ignored stimuli. This led to a maximum difference between the responses to attended and ignored stimuli in the time range between 2 and 5 minutes after onset of the stimulation. Under consideration of the sensitivity of habituation to the interstimulus interval, it was suggested that diverging results in former attention studies might be due to differences in this parameter. The effect of decelerated habituation when attention is focused towards the stimulated body site should be quantified in future studies by extending the number of measurements and stimulation duration. A study employing varying interstimulus intervals should clarify the relative contribution of this effect to the observed overall attentional enhancement of the P80m component. It is suggested that with increasing interstimulus interval the role of habituation vanishes and the original attentional enhancement effect can be observed in separation.

By comparison of source waveforms in response to separate and simultaneous stimulation of two fingers, interaction in the primary and secondary somatosensory cortex was studied. The analysis revealed hemispheric specialization in this cortical area during bilateral

stimulation. In each hemisphere predominantly the input delivered to the corresponding contralateral finger was processed. Since input from the contralateral body side reaches SII earlier than ipsilateral signals, refractory effects were the most likely explanation for the observed effect. The finding of hemispheric specialization of SII during simultaneous bilateral stimulation sheds new light on the current notion of SII as being in charge for the integration of the two body halves. MEG measurements applying stimulus pairs with varying interstimulus interval could clarify to which amount this effect is due to the earlier arrival of the contralateral afferent signals in SII.

From a medical point of view it is interesting to determine whether the observed behavior of SII responses to tactile stimulation can be transferred to painful stimuli that stimulate SII via nociceptive skin receptors. This question could be answered by experiments analogous to those presented here with application of painful stimuli that can be generated for example by infrared laser pulses.

Hence while providing new insights into the functionality of the secondary somatosensory cortex, the current work also raises new questions that merit further investigation. MEG proved powerful to analyze the cortical spatio-temporal activity distribution evoked by tactile stimulation. Based on the current results it can be expected that MEG will continue to contribute to our understanding of somatosensory processing in the human brain in the future research.

Bibliography

[1] A. I. Ahonen, M. S. Hämäläinen, M. J. Kajola, M. E. T. Knuutila, J. P. Laine, O. V. Lounasmaa, L. T. Parkkonen, J. T. Simalo, and C. D. Tesche. 122-channel SQUID instrument for investigating the magnetic signals from the human brain. *Phys. Scripta*, T49:198–205, 1993.

[2] T. Allison. Recovery functions of somatosensory evoked responses in man. *Electroencephalography & Clinical Neurophysiology*, 14:331–343, 1962.

[3] T. Allison, G. McCarthy, and C. C. Wood. The relationship between human long–latency somatosensory evoked potentials recorded from the cortical surface and from the scalp. *Electroencephalography & Clinical Neurophysiology*, 84(4):301–314, 1992.

[4] T. Allison, G. McCarthy, C. C. Wood, T. M. Darcey, D. D. Spencer, and P. D. Williamson. Human cortical potentials evoked by stimulation of the median nerve. I. Cytoarchitectonic areas generating short–latency activity. *Journal of Neurophysiology*, 62(3):694–710, 1989.

[5] T. Allison, G. McCarthy, C. C. Wood, P. D. Williamson, and D. D. Spencer. Human cortical potentials evoked by stimulation of the median nerve. II. Cytoarchitectonic areas generating long–latency activity. *Journal of Neurophysiology*, 62(3):711–722, 1989.

[6] R. W. Angel, W. M. Quick, C. C. Boylls, M. Weinrich, and R. L. Rodnitzky. Decrement of somatosensory evoked potentials during repetitive stimulation. *Electroencephalography & Clinical Neurophysiology*, 60(4):335–342, 1985.

[7] P. Berg and M. Scherg. A fast method for forward computation of multiple-shell spherical head models. *Electroencephalography & Clinical Neurophysiology*, 90:58–64, 1994.

[8] P. Berg and M. Scherg. A multiple source approach to the correction of eye artifacts. *Electroencephalography & Clinical Neurophysiology*, 90:229–241, 1994.

[9] R. Beucker and H. A. Schlitt. On minimal Lp-norm solutions of the biomagnetic inverse problem. *Technical Report KFA-ZAM-IB-9614, Forschungszentrum Jülich*, 1996.

[10] K. Biermann, F. Schmitz, O. W. Witte, J. Konczak, H. J. Freund, and A. Schnitzler. Interaction of finger representation in the human first somatosensory cortex: a neuromagnetic study. *Neuroscience Letters*, 251(1):13–16, 1998.

[11] K. Brodmann. *Vergleichende Lokalisationslehre der Großhirnrinde in ihren Prinzipien dargestellt auf Grund des Zellenbaus.* Barth, Leipzig, 1909.

[12] H. Buchner, L. Adams, A. Knepper, R. Ruger, G. Laborde, J. M. Gilsbach, I. Ludwig, J. Reul, and M. Scherg. Preoperative localization of the central sulcus by dipole source analysis of early somatosensory evoked potentials and three–dimensional magnetic resonance imaging. *Journal of Neurosurgery*, 80(5):849–856, 1994.

[13] H. Buchner, L. Adams, A. Muller, I. Ludwig, A. Knepper, A. Thron, and M. Niemann K. Scherg. Somatotopy of human hand somatosensory cortex revealed by dipole source analysis of early somatosensory evoked potentials and 3d–nmr tomography. *Electroencephalography & Clinical Neurophysiology*, 96(2):121–134, 1995.

[14] H. Buchner, I. Ludwig, T. Waberski, K. Wilmes, and A. Ferbert. Hemispheric asymmetries of early cortical somatosensory evoked potentials revealed by topographic analysis. *Electromyography & Clinical Neurophysiology*, 35(4):207–215, 1995.

[15] H. Buchner and M. Scherg. Analyse der generatoren fruher kortikaler somatosensibel evozierter potentiale (n. medianus) mit der dipolquellenanalyse: Erste ergebnisse. *EEG-EMG Zeitschrift fur Elektroenzephalographie Elektromyographie und Verwandte Gebiete*, 22(2):62–69, 1991.

[16] H. Buchner, T. D. Waberski, M. Fuchs, R. Drenckhahn, M. Wagner, and M. Wischmann. Postcentral origin of P22: evidence from source reconstruction in a realistically shaped head model and from a patient with a postcentral lesion. *Electroencephalography & Clinical Neurophysiology*, 100:332–342, 1996.

[17] H. Burton. Corticothalamic connections from the second somatosensory area and neighboring regions in the lateral sulcus of macaque monkeys. *Brain Research*, 309(2):368–372, 1984.

[18] H. Burton. Second somatosensory cortex and related areas. In E. Jones and A. Peters, editors, *Cerebral cortex*, pages 31–97. Plenum, New York, 1986.

[19] H. Burton, N. S. Abend, A. M. MacLeod, R. J. Sinclair, A. Z. Snyder, and M. E. Raichle. Tactile attention tasks enhance activation in somatosensory regions of parietal cortex: a positron emission tomography study. *Cerebral Cortex*, 9(7):662–674, 1999.

[20] H. Burton, M. Fabri, and K. Alloway. Cortical areas within the lateral sulcus connected to cutaneous representations in areas 3b and 1: a revised interpretation of the second somatosensory area in macaque monkeys. *Journal of Comparative Neurology*, 355(4):539–562, 1995.

[21] H. Burton, R. J. Sinclair, S. Y. Hong, J. Pruett Jr., and K. C. Whang. Tactile–spatial and cross–modal attention effects in the second somatosensory and 7b cortical areas of rhesus monkeys. *Somatosensory & Motor Research*, 14(4):237–267, 1997.

[22] H. Burton, T. Videen, and M. Raichle. Tactile-vibration-activated foci in insular and parietal-opercular cortex studied with positron emission tomography: mapping the second somatosensory area in humans. *Somatosensory & Motor Research*, 10:297–308, 1993.

[23] E. Bystrzycka, B. S. Nail, and M. Rowe. Inhibition of cuneate neurones: its afferent source and influence on dynamically sensitive "tactile" neurones. *Journal of Physiology*, 268(1):251–270, 1977.

[24] E. Callaway. Habituation of averaged evoked potentials in man. In H. V. S. Peeke and M. J. Herz, editors, *Habituation*, volume 2, pages 153–171. Academic Press, New York, 1973.

[25] V. N. Chernigovskii, S. S. Musyashchikova, and A. A. Mokrushin. Dynamics of habituation in different cortical regions of tha cat brain. *Biology Bulletin of the Academy of Sciences of the USSR*, 6(1):1–7, 1979.

[26] D. Cohen. Magnetoencephalography: detection of the brain's electrical activity with a superconducting magnetometer. *Science*, 175:664–666, 1972.

[27] D. Cohen, B. N. Cuffin, K. Yunokuchi, R. Maniewski, C. Purcell, J. Cosgrove GR. Ives, J. G. Kennedy, and D. L. Schomer. MEG versus EEG localization test using implanted sources in the human brain. *Annals of Neurology*, 28(6):811–817, 1990.

[28] A. M. Dale and M. I. Sereno. Improved localization of cortical activity by combining EEG and MEG with cortical surface reconstruction: A linear approach. *Journal of Cognitive Neuroscience*, 52:162–176, 1993.

[29] J. E. Desmedt and C. Tomberg. Mapping early somatosensory evoked potentials in selective attention: critical evaluation of control conditions used for titrating by difference the cognitive P30, P40, P100 and N140. *Electroencephalography & Clinical Neurophysiology*, 74(5):321–346, 1989.

[30] E. Disbrow, T. Roberts, and L. Krubitzer. Somatotopic organization of cortical fields in the lateral sulcus of *homo sapiens*: evidence for SII and PV. *Journal of Comparative Neurology*, 418(1):1–21, 2000.

[31] K. Drüen. *Prächirurgische Diagnostik mittels MEG im Rahmen der Strahlentherapieplanung und vor chirurgischen Eingriffen.* PhD thesis, University of Heidelberg, 2000.

[32] B. Efron and R. J. Tibshirani. *An introduction to the bootstrap.* Chapman and Hall, New York, 1993.

[33] M. Elton, M. Scherg, and D. von Cramon. Effects of high–pass filter frequency and slope on BAEP amplitude, latency and wave form. *Electroencephalography & Clinical Neurophysiology*, 57(5):490–494, 1984.

[34] M. Fabri, G. Polonara, A. Quattrini, U. Salvolini, M. Del Pesce, and T. Manzoni. Role of the corpus callosum in the somatosensory activation of the ipsilateral cerebral cortex: an fMRI study of callosotomized patients. *European Journal of Neuroscience*, 11(11):3983–3994, 1999.

[35] H. Flor, W. Mühlnickel, A. Karl, C. Denke, S. Grüsser, and E. Taub. A neural substrate for nonpainful phantom limb phenomena. *Society of Neuroscience Abstracts*, 24(249.16):636, 1998.

[36] N. Forss, R. Hari, R. Salmelin, A. Ahonen, M. Hamalainen M. Kajola, J. Knuutila, and J. Simola. Activation of the human posterior parietal cortex by median nerve stimulation. *Experimental Brain Research*, 99(2):309–315, 1994.

[37] N. Forss, M. Hietanen, O. Salonen, and R. Hari. Modified activation of somatosensory cortical network in patients with right–hemisphere stroke. *Brain*, 122:1889–1899, 1999.

[38] N. Forss and V. Jousmäki. Sensorimotor integration in human primary and secondary somatosensory cortices. *Brain Research*, 781:259–267, 1998.

[39] N. Forss, I. Merlet, S. Vanni, M. Hämäläinen, F. Mauguiere, and R. Hari. Activation of human mesial cortex during somatosensory target detection task. *Brain Research*, 734(1-2):229–235, 1996.

[40] N. Forss, R. Salmelin, and R. Hari. Comparison of somatosensory evoked fields to airpuff and electric stimuli. *Electroencephalography & Clinical Neurophysiology*, 92(6):510–517, 1994.

[41] M. Frot and F. Mauguière. Timing and spatial distribution of somatosensory responses recorded in the upper bank of the sylvian fissure (SII area) in humans. *Cerebral Cortex*, 9(8):854–863, 1999.

[42] S. C. Gandevia, D. Burke, and B. B. McKeon. Convergence in the somatosensory pathway between cutaneous afferents from the index and middle fingers in man. *Experimental Brain Research*, 50(2-3):415–425, 1983.

[43] H. S. Garcha and G. Ettlinger. The effects of unilateral or bilateral removals of the second somatosensory cortex (area SII): a profound tactile disorder in monkeys. *Cortex*, 14(3):319–326, 1978.

[44] L. Garcia–Larrea, H. Bastuji, and F. Mauguiere. Mapping study of somatosensory evoked potentials during selective spatial attention. *Electroencephalography & Clinical Neurophysiology*, 80(3):201–214, 1991.

[45] L. Garcia-Larrea, A. C. Lukaszewicz, and F. Mauguière. Somatosensory responses during selective spatial attention: The N120-to-N140 transition. *Psychophysiology*, 32:526–537, 1995.

[46] D. E. Goldberg. *Genetic Algorithms.* Addison and Wesley, Cambridge, 1989.

[47] D. E. Goldman. Potential, impedance, and rectification in membranes. *Journal of general physiology*, 27:37–60, 1943.

[48] P. M. Greenwood and W. R. Goff. Modification of median nerve somatic evoked potentials by prior median nerve, peroneal nerve, and auditory stimulation. *Electroencephalography & Clinical Neurophysiology*, 68(4):295–302, 1987.

[49] H. Hämäläinen, J. Kekoni, M. Sams, K. Reinikainen, and R. Naatanen. Human somatosensory evoked potentials to mechanical pulses and vibration: contributions of SI and SII somatosensory cortices to P50 and P100 components. *Electroencephalography & Clinical Neurophysiology*, 75(2):13–21, 1990.

[50] M. Hämäläinen, R. Hari, R. J. Ilmoniemi, J. Knuutila, and O. V. Lounasmaa. Magnetoencephylography – theory, instrumentation, and applications to noninvasive studies of the working human brain. *Reviews of Modern Physics*, 65(2):413–497, 1993.

[51] M. S. Hämäläinen and R. J. Ilmoniemi. Interpreting magnetic fields of the brain: minimum norm estimates. *Medical & Biomedical Engineering & Computing*, 32(1):35–42, 1994.

[52] H. O. Handwerker. Somatosensorik. In R. F. Schmidt, editor, *Neuro- und Sinnesphysiologie*, pages 221–247. Springer, Berlin, 2nd edition, 1995.

[53] R. Hari. MEG in the study of human cortical functions. *Electroencephalography & Clinical Neurophysiology Supplement*, 47:47–54, 1994.

[54] R. Hari and N. Forss. Magnetoencephalography in the study of human somatosensory cortical processing. *Philosophical Transactions of the Royal Society London B*, 354:1145–1154, 1999.

[55] R. Hari, J. Hallstrom, J. Tiihonen, and S. L. Joutsiniemi. Multichannel detection of magnetic compound action fields of median and ulnar nerves. *Electroencephalography & Clinical Neurophysiology*, 72(3):277–280, 1989.

[56] R. Hari, H. Hämäläinen, M. Hämäläinen, J. Kekoni, M. Sams, and J. Tiihonen. Separate finger representations at the human second somatosensory cortex. *Neuroscience*, 37(1):245–249, 1990.

[57] R. Hari, M. Hämäläinen, R. Ilmoniemi, and O. V. Lounasmaa. MEG versus EEG localization test. *Annals of Neurology*, 30(2):222–224, 1991.

[58] R. Hari, M. Hamalainen, E. Kaukoranta, K. Reinikainen, and D. Teszner. Neuromagnetic responses from the second somatosensory cortex in man. *Acta Neurologica Scandinavica*, 68(4):207–212, 1983.

[59] R. Hari, R. Hänninen, T. Mäkinen, V. Jousmäki, N. Forss, M. Seppä, and O. Salonen. Three hands: fragmentation of bodily awareness. *Neuroscience Letters*, 240:131–134, 1998.

[60] R. Hari, J. Karhu, M. Hamalainen, J. Knuutila, O. Salonen, M. Sams, and V. Vilkman. Functional organization of the human first and second somatosensory cortices: a neuromagnetic study. *European Journal of Neuroscience*, 5(6):724–734, 1993.

[61] R. Hari, E. Kaukoranta, K. Reinikainen, T. Huopaniemie, and J. Mauno. Neuromagnetic localization of cortical activity evoked by painful dental stimulation in man. *Neuroscience Letters*, 42(1):77–82, 1983.

[62] R. Hari, K. Reinikainen, E. Kaukoranta, M. Hamalainen, R. Ilmoniemi, A. Penttinen, J. Salminen, and D. Teszner. Somatosensory evoked cerebral magnetic

fields from SI and SII in man. *Electroencephalography & Clinical Neurophysiology*, 57(3):254–263, 1984.

[63] H. L. F. von Helmholtz. Über einige Gesetze der Vertheilung elektrischer Ströme in körperlichen Leitern, mit Anwendung auf die thierisch-elektrischen Versuche. *Ann. Phys. Chem.*, 89:211–233, 353–377, 1853.

[64] K. Hoechstetter, A. Rupp, H.-M. Meinck, C. Stippich, and M. Scherg. Early cortical processing of tactile input: magnetic source imaging of enhanced SII activation by selective attention to stimulus intensity and location. *Neuroimage*, 11(5):18, 2000.

[65] K. Hoechstetter, A. Rupp, H.-M. Meinck, D. Weckesser, H. Bornfleth, C. Stippich, P. Berg, and M. Scherg. Magnetic souce imaging of tactile input shows task-independent attention effects in SII. *Neuroreport*, 11(11):2461–2465, 2000.

[66] K. Hoechstetter, A. Rupp, A. Stančák, H.-M. Meinck, C. Stippich, P. Berg, and M. Scherg. Interaction of tactile input in the human primary and secondary somatosensory cortex - a magnetoencephalographic study. *Neuroimage*, 2001, in press.

[67] J. B. Hopfinger, M. H. Buonocore, and G. R. Mangun. The neural mechanisms of top–down attentional control. *Nature Neuroscience*, 3(3):284–291, 2000.

[68] G. Houghton and S. P. Tipper. Inhibitory mechanisms of neural and cognitive control: applications to selective attention and sequential action. *Brain and cognition*, 30:20–43, 1996.

[69] S. S. Hsiao, D. M. O'Shaughnessy, and K. O. Johnson. Effects of selective attention on spatial form processing in monkey primary and secondary somatosensory cortex. *Journal of Neurophysiology*, 70(1):444–447, 1993.

[70] C. L. Hsieh, F. Shima, S. Tobimatsu, S. J. Sun, and M. Kato. The interaction of the somatosensory evoked potentials to simultaneous finger stimuli in the human central nervous system. a study using direct recordings. *Electroencephalography & Clinical Neurophysiology*, 96(2):135–142, 1995.

[71] J. Huttunen, S. Ahlfors, and R. Hari. Interaction of afferent impulses in the human primary sensorimotor cortex. *Electroencephalography & Clinical Neurophysiology*, 82(3):176–181, 1992.

[72] J. Huttunen, H. Wikstrom, A. Korvenoja, A. M. Seppalainen, and R. J. Aronen H. Ilmoniemi. Significance of the second somatosensory cortex in sensorimotor integration: enhancement of sensory responses during finger movements. *Neuroreport*, 7(5):1009–1012, 1996.

[73] J. Hyvärinen, A. Poranen, and Y. Jokinen. Influence of attentive behavior on neuronal responses to vibration in primary somatosensory cortex of the monkey. *Journal of Neurophysiology*, 43(4):870–882, 1980.

[74] V. Ibañez, M. P. Deiber, N. Sadatao, C. Toro, J. Grissom, R. P. Woods, J. C. Mazziotta, and M. Hallett. Effects of stimulus rate on regional cerebral blood flow after median nerve stimulation. *Brain*, 118:1339–1351, 1995.

[75] R. J. Ilmoniemi, M. S. Hämäläinen, and J. Knuutila. The forward and inverse problems in the spherical model. In H. Weinberg, G. Stroink, and T. Katila, editors, *Biomagnetism: Applications & Theory*, pages 278–282. Pergamon, New York, 1985.

[76] H. Ishibashi, S. Tobimatsu, H. Shigeto, T. Morioka, T. Yamamoto, and M. Fukui. Differential interaction of somatosensory inputs in the human primary sensory cortex: a magnetoencephalographic study. *Clinical Neurophysiology*, 111(6):1095–1102, 2000.

[77] K. Itomi, R. Kakigi, K. Maeda, and M. Hoshiyama. Dermatome versus homunculus; detailed topography of the primary somatosensory cortex following trunk stimulation. *Clinical Neurophysiology*, 111(3):405–412, 2000.

[78] Y. Iwamura, M. Tanaka, and O. Hikosaka. Overlapping representation of fingers in the somatosensory cortex (area 2) of the conscious monkey. *Brain Research*, 197(2):516–520, 1980.

[79] G. P. Jacobson. Magnetoencephalographic studies of auditory systemm function. *Journal of Clinical Neurophysiology*, 11(3):343–364, 1994.

[80] W. James. *The principles of psychology*, volume 1. MacMillan, London, 1891.

[81] W. Jiang, F. Tremblay, and C. E. Chapman. Neuronal encoding of texture changes in the primary and the secondary somatosensory cortical areas of monkeys during passive texture discrimination. *Journal of Neurophysiology*, 77(3):1656–1662, 1997.

[82] H. Johansen–Berg, V. Christensen, M. Woolrich, and P. M. Matthews. Attention to touch modulates activity in both primary and secondary somatosensory areas. *Neuroreport*, 11(6):1237–1241, 2000.

[83] E. G. Jones and T. P. Powell. Connexions of the somatic sensory cortex of the rhesus monkey. I. Ipsilateral cortical connexions. *Brain*, 92(3):477–502, 1969.

[84] E. G. Jones and T. P. Powell. Connexions of the somatic sensory cortex of the rhesus monkey. II. Contralateral cortical connexions. *Brain*, 92(4):717–730, 1969.

[85] E. G. Jones and T. P. Powell. Connexions of the somatic sensory cortex of the rhesus monkey. III. thalamic connexions. *Brain*, 93(1):37–56, 1970.

[86] S. J. Jones and C. N. Power. Scalp topography of human somatosensory evoked potentials: the effect of interfering tactile stimulation applied to the hand. *Electroencephalography & Clinical Neurophysiology*, 58(1):25–36, 1984.

[87] R. Kakigi. Somatosensory evoked magnetic fields following median nerve stimulation. *Neuroscience Research*, 20(2):165–174, 1994.

[88] R. Kakigi, M. Hoshiyama, M. Shimojo, D. Naka, H. Yamasaki, J. Watanabe S. Xiang, K. Maeda, K. Lam, K. Itomi, and A. Nakamura. The somatosensory evoked magnetic fields. *Progress in Neurobiology*, 61(5):495–523, 2000.

[89] R. Kakigi, S. Koyama, M. Hoshiyama, Y. Kitamura, M. Shimojo, and S. Watanabe. Pain-related magnetic fields following painful CO_2 laser stimulation in man. *Neuroscience Letters*, 192:45–48, 1995.

[90] R. Kang, D. Herman, M. MacGillis, and P. Zarzecki. Convergence of sensory inputs in somatosensory cortex: interactions from separate afferent sources. *Experimental Brain Research*, 57(2):271–278, 1985.

[91] A. Korvenoja, J. Huttunen, E. Salli, H. Pohjonen, S. Martinkauppi, J. M. Palva, L. Lauronen, J. Virtanen, R. J. Ilmoniemi, and H. J. Aronen. Activation of multiple cortical areas in response to somatosensory stimulation: combined magnetoencephalographic and functional magnetic resonance imaging. *Human Brain Mapping*, 8:13–27, 1999.

[92] A. Korvenoja, H. Wikstrom, J. Huttunen, J. Virtanan, P. Laine, A. M. Aronen HJ. Seppalainen, and R. J. Ilmoniemi. Activation of ipsilateral primary sensorimotor cortex by median nerve stimulation. *Neuroreport*, 6(18):2589–2593, 1995.

[93] L. Krubitzer, J. Clarey, R. Tweedale, G. Elston, and M. Calford. A redefinition of somatosensory areas in the lateral sulcus of macaque monkeys. *Journal of Neuroscience*, 15(5s):3821–3839, 1995.

[94] V. Kunde and R. D. Treede. Topography of middle–latency somatosensory evoked potentials following painful laser stimuli and non–painful electrical stimuli. *Electroencephalography & Clinical Neurophysiology*, 88(4):280–289, 1993.

[95] K. Lam, R. Kakigi, Y. Kaneoke, D. Naka, K. Maeda, and H. Suzuki. Effects of visual and auditory stimulation on somatosensory evoked magnetic fields. *Clinical Neurophysiology*, 110:295–304, 1999.

[96] R. M. Leahy, J. C. Mosher, M. E. Spencer, M. X. Huang, and J. D. Lewine. A study of dipole localization accuracy for MEG and EEG using a human skull phantom. *Electroencephalography & Clinical Neurophysiology*, 107:159–173, 1998.

[97] Y. Y. Lin, C. Simões, N. Forss, and R. Hari. Differential effects of muscle contraction from various body parts on neuromagnetic somatosensory responses. *Neuroimage*, 11(4):334–340, 2000.

[98] P. B. Lloyd. Is the mind physical? Dissecting conscious brain tissue. *Philosophy Now*, 6, 1993.

[99] P. J. Maccabee, E. I. Pinkhasov, and R. Q. Cracco. Short latency somatosensory evoked potentials to median nerve stimulation: effect of low frequency filter. *Electroencephalography & Clinical Neurophysiology*, 55(1):34–44, 1983.

[100] K. Maeda, R. Kakigi, M. Hoshiyama, and S. Koyama. Topography of the secondary somatosensory cortex in humans: a magnetoencephalographic study. *Neuroreport*, 10(2):301–306, 1999.

[101] J. H. Martin. Anatomical substrates for somatic sensation. In E. R. Kandel and J. H. Schwartz, editors, *Principles of neural science*, pages 301–315. Elsevier, New York, 2nd edition, 1985.

[102] J. H. Martin. Receptor physiology and submodality coding in the somatic sensory system. In E. R. Kandel and J. H. Schwartz, editors, *Principles of neural science*, pages 287–300. Elsevier, New York, 2nd edition, 1985.

[103] K. Matsuura and Y. Okabe. Selective minimum-norm solution of the biomagnetic inverse problem. *IEEE Transactions on Biomedical Engineering*, 42(6):608–615, 1995.

[104] F. Mauguière. A consensus statement on relative merits of EEG and MEG. *Electroencephalography & Clinical Neurophysiology*, 82(5):317–319, 1992.

[105] F. Mauguière, I. Merlet, N. Forss, S. Vanni, V. Jousmäki, P. Adeleine, and R. Hari. Activation of a distributed somatosensory cortical network in the human brain. a dipole modelling study of magnetic fields evoked by median nerve stimulation. Part II: Effects of stimulus rate, attention and stimulus detection. *Electroencephalography & Clinical Neurophysiology*, 104(4):290–295, 1997.

[106] F. Mauguière, I. Merlet, N. Forss, S. Vanni, V. Jousmäki, P. Adeleine, and R. Hari. Activation of a distributed somatosensory cortical network in the human brain. a dipole modelling study of magnetic fields evoked by median nerve stimulation. Part

I: Location and activation timing of SEF sources. *Electroencephalography & Clinical Neurophysiology*, 104(4):281–289, 1997.

[107] B. K. McGowan–Sass and E. Eidelberg. Habituation of somatosensory evoked potentials in the lemniscal system of the cat. *Electroencephalography & Clinical Neurophysiology*, 32(4):373–381, 1972.

[108] M. M. Merzenich, R. J. Nelson, J. H. Kaas, M. P. Stryker, W. M. Jenkins, M. S. Zook JM. Cynader, and A. Schoppmann. Variability in hand surface representations in areas 3b and 1 in adult owl and squirrel monkeys. *Journal of Comparative Neurology*, 258(2):281–296, 1987.

[109] T. Mima, T. Nagamine, K. Nakamura, and H. Shibasaki. Attention modulates both primary and second somatosensory cortical activities in humans: a magnetoencephalographic study. *Journal of Neurophysiology*, 80(4):2215–2221, 1998.

[110] J. C. Mosher and R. M. Leahy. Recursive MUSIC: a framework for EEG and MEG source localization. *IEEE Transactions on Biomedical Engineering*, 45(11):1342–1354, 1998.

[111] J. C. Mosher, P. S. Lewis, and R. M. Leahy. Multiple dipole modeling and localization from spatio-temporal MEG data. *IEEE transactions on biomedical engineering*, 39(6):541–557, 1992.

[112] V. B. Mountcastle, J. C. Lynch, A. Georgopoulos, H. Sakata, and C. Acuna. Posterior parietal association cortex of the monkey: command functions for operations within extrapersonal space. *Journal of Neurophysiology*, 38:871–908, 1975.

[113] E. Murray and M. Mishkin. Relative contributions of SII and area 5 to tactile discrimination in monkeys. *Behavioral Brain Research*, 11:67–83, 1984.

[114] A. Nakamura, T. Yamada, A. Goto, T. Kato, K. Ito, T. Abe Y. Kachi, and R. Kakigi. Somatosensory homunculus as drawn by MEG. *Neuroimage*, 7(4):377–386, 1998.

[115] Y. C. Okada, J. Wu, and S. Kyuhou. Genesis of MEG signals in a mammalian cns structure. *Electroencephalography & Clinical Neurophysiology*, 103:474–485, 1997.

[116] Y. Okajima, N. Chino, E. Saitoh, and A. Kimura. Interactions of somatosensory evoked potentials: simultaneous stimulation of two nerves. *Electroencephalography & Clinical Neurophysiology*, 80(1):26–31, 1991.

[117] D. N. Pandya and L. A. Vignolo. Interhemispheric projections of the parietal lobe in the rhesus monkey. *Brain Research*, 15(1):49–65, 1969.

[118] W. Penfield and E. Boldrey. Somatic motor and sensory representation in the cerebral cortex of man as studied by electrical stimulation. *Brain*, 60:389–443, 1937.

[119] W. Penfield and T. Rasmussen. *The cerebral cortex of man.* MacMillan, New York, 1950.

[120] A. Poranen and J. Hyvarinen. Effects of attention on multiunit responses to vibration in the somatosensory regions of the monkey's brain. *Electroencephalography & Clinical Neurophysiology*, 53(5):525–537, 1982.

[121] M. I. Posner and D. E. Presti. Selective attention and cognitive control. *Trends in Neurosciences*, 10:13–17, 1987.

[122] W. H. Press, A. Teukolsky, W. T. Vetterling, and B. P. Flannery. *Numerical Recipes in C.* Cambridge University Press, Cambridge, 2nd edition, 1994.

[123] C. L. Prosser and W. S. Hunter. The extinction of startle responses and spinal reflexes in the white rat. *American Jouirnal of Physiology*, 117:609–618, 1936.

[124] C. J. Robinson and H. Burton. Somatotopographic organization in the second somatosensory area of m. fascicularis. *Journal of Comparative Neurology*, 192(1):43–67, 1980.

[125] J. Sarvas. Basic mathematical and electromagnetic concepts of the biomagnetic inverse problem. *Physics in Medicine & Biology*, 32(1):11–22, 1987.

[126] M. Scherg. Distortion of the middle latency auditory response produced by analog filtering. *Scand Audiol*, 11:57–60, 1982.

[127] M. Scherg. *Akustisch evozierte Potentiale.* Kohlhammer, Stuttgart, 1991.

[128] M. Scherg. Functional imaging and localization of electromagnetic brain activity. *Brain Topography*, 5(2):103–111, 1992.

[129] M. Scherg. *Biomagnetismus. Skriptum zur Weiterbildung Medizinische Physik.* Akademie für Weiterbildung an den Universitäten Heidelberg und Mannheim e. V., 1997.

[130] M. Scherg and P. Berg. New concepts of brain source imaging and localization. *Electroencephalography & Clinical Neurophysiology, Supplement*, 46:127–137, 1996.

[131] M. Scherg and J. S. Ebersole. Models of brain sources. *Brain Topography*, 5(4):419–423, 1993.

[132] M. Scherg and T. W. Picton. Separation and identification of event–related potential components by brain electric source analysis. *Electroencephalography & Clinical Neurophysiology, Supplement.*, 42:24–37, 1991.

[133] M. Scherg and D. von Cramon. Evoked dipole source potentials of the human auditory cortex. *Electroencephalography & Clinical Neurophysiology*, 65(5):344–360, 1986.

[134] A. Schnitzler, R. Salmelin, S. Salenius, V. Jousmäki, and R. Hari. Tactile information from the human hand reaches the ipsilateral primary somatosensory cortex. *Neuroscience Letters*, 200(1):25–28, 1995.

[135] A. Schnitzler, J. Volkmann, P. Enck, T. Frieling, H.-J. Freund, and O. W. Witte. Different cortical organization of visceral and somatic sensations in humans. *European Journal of Neuroscience*, 11:305–315, 1998.

[136] J. R. Searle. How to study consciousness scientifically. *Brain Research Reviews*, 26(2-3):379–387, 1998.

[137] C. S. Sherrington. *The integrative action of the nervous system.* Yale University Press, New Haven, 1906.

[138] C. Simões and R. Hari. Relationship between responses to contra– and ipsilateral stimuli in the human second somatosensory cortex SII. *Neuroimage*, 10(4):408–416, 1999.

[139] A. Stančák, K. Hoechstetter, J. Tintěra, R. Rachmanová, J. Králík, and M. Scherg. Source activity in human second somatosensory cortex depends on the size of corpus callosum. *Brain Research*, 2001, submitted.

[140] C. Stippich, R. Hofmann, D. Kapfer, E. Hempel, S. Heiland, O. Jansen, and K. Sartor. Somatotopic mapping of the human primary somatosensory cortex by fully automated tactile stimulation using functional magnetic resonance imaging. *Neuroscience Letters*, 277(1):25–28, 1999.

[141] J. Suk, U. Ribary, J. Cappell, T. Yamamoto, and R. Llinas. Anatomical localization revealed by MEG recordings of the human somatosensory system. *Electroencephalography & Clinical Neurophysiology*, 78(3):185–196, 1991.

[142] J. Talairach and P. Tournoux. *Co-planar stereotaxic atlas of the human brain.* Thieme, New York, 1988.

[143] D. Teszner, R. Hari, P. Nicolas, and T. Varpula. Aomatosensory evoked magnetic fields: mapping and the influence of stimulus repetition rate. *Nuovo Cimento*, 2D:429–437, 1983.

[144] R. F. Thompson and W. A. Spencer. Habituation: A model phenomenon for the study of neuronal substrates of behavior. *Psychological Review*, 73(1):16–43, 1966.

[145] C. Tomberg, J. E. Desmedt, I. Ozaki, T. H. Nguyen, and V. Chalklin. Mapping somatosensory evoked potentials to finger stimulation at intervals of 450 to 4000 msec and the issue of habituation when assessing early cognitive components. *Electroencephalography & Clinical Neurophysiology*, 74(5):347–358, 1989.

[146] K. Uutela, M. Hämäläinen, and E. Somersalo. Visualization of magnetoencephalographic data using minimum current estimates. *Neuroimage*, 10(2):173–180, 1999.

[147] M. Valeriani, D. Le Pera, D. Niddam, L. Arendt–Nielsen, and A. C. Chen. Dipolar source modeling of somatosensory evoked potentials to painful and nonpainful median nerve stimulation. *Muscle & Nerve*, 23(8):1194–1203, 2000.

[148] M. Velasco and F. Velasco. Differential effect of task relevance on early and late components of cortical and subcortical somatic evoked potentials in man. *Electroencephalography & Clinical Neurophysiology*, 39(4):353–364, 1975.

[149] M. Velasco, F. Velasco, and A. Olvera. Effect of task relevance and selective attention on components of cortical and subcortical evoked potentials in man. *Electroencephalography & Clinical Neurophysiology*, 48(4):377–386, 1980.

[150] K. Wegner, N. Forss, and S. Salenius. Characteristics of the human contra– versus ipsilateral SII cortex. *Clinical Neurophysiology*, 111(5):894–900, 2000.

[151] B. L. Whitsel, L. M. Petrucelli, and G. Werner. Symmetry and connectivity in the map of the body surface in somatosensory area II of primates. *Journal of Neurophysiology*, 32:170–183, 1969.

[152] S. J. Williamson. MEG versus EEG localization test. *Annals of Neurology*, 30(2):222, 1991.

[153] S. J. Williamson and L. Kaufmann. Theory of neuroelectric and neuromagnetic fields. In F. Grandori, M. Hoke, and G. L. Romani, editors, *Auditory Evoked Magnetic Fields and Electric Potentials*, volume 6, pages 1–39. Karger, Basel, 1990.

[154] J. E. Zimmermann, P. Thiene, and J. T. Harding. Design and operation of stable rf-biased superconducting point-contact quantum devices and a note on the properties of perfectly clean metal contacts. *Journal of Applied Physics*, 41:1572–1580, 1970.

Acknowledgments

At the end of this thesis I would like to thank all colleagues and friends who supported me and contributed to this work in different ways.

I want to express my first thanks to Prof. Dr. Michael Scherg, who was my supervisor at the Section of Biomagnetism at the University Hospital of Heidelberg. My work profited a lot from his knowledge concerning technical questions and from his confidence and support for my work. He gave valuable advice in scientific questions and let me the freedom to make my own decisions on the coarse of my research.

I thank Prof. Dr. Karlheinz Meier from the Kirchhoff-Institut für Physik at the University of Heidelberg for refereeing this thesis. Thereby he made it possible for me to earn the doctorate at the Faculty of Physics in Heidelberg.

Rainer Roth was in charge for the maintenance of the technical devices and computer systems in the laboratory. He was the one to solve all urgent technical problems that were inexplicable to anyone else. Thereby he was the guarantee for a smooth performance of the experiments and data evaluation.

It would have been impossible to carry out the experiments without the help of the medical technical assistants of the laboratory. Esther Tauberschmidt, Barbara Burghardt, Annette Opgenorth and Uwe Gollner-Nohlen were responsible for subject preparation, measurement observation and data archiving and thereby were a valuable support for me in all performed studies.

I want to thank the team of MEGIS software GmbH. Dieter Weckesser, Dr. Harald Bornfleth, Nicole Ille, Dr. Roland Beucker, Ulrike Wehling and Dr. Patrick Berg were in charge for the data analysis software BESA® 2000. They were always willing to implement "special features" on demand of their users. I owe special thanks to Dr. Patrick Berg for proofreading my publications in English language.

Dr. André Rupp gave me valuable advice in questions of statistical data analysis and the design of efficient paradigms.

Dr. Christoph Stippich provided the magnetic resonance images that were used for MEG–MR coregistration.

The secretaries of the Section of Biomagnetism, Heike Wegener and Heide Rogatzki, were a big support by taking care of all organizational matters.

During the time of my work in Heidelberg I had the opportunity to work with researchers from other institutes. I thank Dr. Ulf Baumgartner from the Institut für Physiologie und Pathophysiologie, University of Mainz, for the cooperation in the combined EEG/MEG study, and Dr. Andrej Stančák from the Department of Normal, Pathological and Clinical Physiology at the Charles University in Prague for his cooperation and stimulating scientific discussions.

My years in Heidelberg would not have been the same without the relaxed and enjoyable atmosphere within our laboratory. Therefore I would like to thank all fellow PhD students and members of the Section of Biomagnetism, who became more than just colleagues over the years. Thanks to Regina Weißer, Miriam Röhrig, Dr. Peter Schneider, Dr. Kai Drüen, Caroline Achenbach, Dr. Alexander Gutschalk, Dr. Susanne Wildermuth, Lukas Alexa and Andreas Sparschuh.

I owe many thanks to all the volunteers, mainly members of the laboratory, who dared to serve as subjects for the different experiments. I know they are all relieved that eventually my plans to apply painful laser stimuli were not realized.

This work was funded by the Pain Research Programme of the University Hospital of Heidelberg. Prof. Dr. Hans-Michael Meinck was the head of the sub-project within which this thesis was performed.

At the end of my studies I would like to thank my parents. During the highs and lows that are part of each graduate study, they gave me all their support and thereby provided the ground for the realization of this thesis.